Principal Component Based System Identification and its Application to the Study of Cardiovascular Regulation

by

Xinshu Xiao

B.E. Precision Instrument and Mechanology
Tsinghua University, 1998

M.S. Mechanical Engineering
Massachusetts Institute of Technology, 2000

SUBMITTED TO THE HARVARD-MIT DIVISION OF HEALTH SCIENCES AND TECHNOLOGY
IN PARTIAL FULFILLMENT OF THE REQUIREMENTS FOR THE DEGREE OF

DOCTOR OF PHILOSOPHY IN BIOMEDICAL ENGINEERING
AT THE
MASSACHUSETTS INSTITUTE OF TECHNOLOGY

JUNE 2004

Signature of Author: _____
Harvard-MIT Division of Health Sciences and Technology
May 26, 2004

Certified by: _____
Richard J. Cohen, M.D., Ph.D.
Whitaker Professor of Biomedical Engineering
Harvard-MIT Division of Health Sciences and Technology
Thesis Supervisor

Accepted by: _____
Martha L. Gray, Ph.D.
Edward Hood Taplin Professor of Medical and Electrical Engineering
Co-Director, Harvard-MIT Division of Health Sciences and Technology

Principal Component Based System Identification and Its Application to the Study of Cardiovascular Regulation

by

Xinshu Xiao

Submitted to the Harvard-MIT Division of Heath Sciences and Technology
on May 26, 2004, in partial fulfillment of the requirement for the degree of
Doctor of Philosophy in Biomedical Engineering

ABSTRACT

System identification is an effective approach for the quantitative study of physiologic systems. It deals with the problem of building mathematical models based on observed data and enables a dynamical characterization of the underlying physiologic mechanisms specific to the individual being studied. In this thesis, we develop and validate a new linear time-invariant system identification approach which is based on a weighted-principal component regression (WPCR) method. An important feature of this approach is its asymptotic frequency-selective property in solving time-domain parametric system identification problems. Owing to this property, data-specific candidate models can be built by considering the dominant frequency components inherent in the input (and output) signals, which is advantageous when the signals are colored, as are most physiologic signals. The efficacy of this method in modeling open-loop and closed-loop systems is demonstrated with respect to simulated and experimental data.

In conjunction with the WPCR-based system identification approach, we propose new methods to noninvasively quantify cardiac autonomic control. Such quantification is important in understanding basic pathophysiological mechanisms or in patient monitoring, treatment design and follow-up. Our methods analyze the coupling between instantaneous lung volume and heart rate and, subsequently, derive representative indices of parasympathetic and sympathetic control based on physiological and experimental findings. The validity of each method is evaluated via experimental data collected following interventions with known effect on the parasympathetic or sympathetic control.

With the above techniques, this thesis explores an important topic in the field of space medicine: effects of simulated microgravity on cardiac autonomic control and orthostatic intolerance (OI). Experimental data from a prolonged bed rest study (simulation of microgravity condition) are analyzed and the conclusions are: 1) prolonged bed rest may impair autonomic control of heart rate; 2) orthostatic intolerance after bed rest is associated with impaired sympathetic responsiveness; 3) there may be a pre-bed rest predisposition to the development of OI after bed rest. These findings may have significance for studying Earth-bound orthostatic hypotension as well as for designing effective countermeasures to post-flight OI. In addition, they also indicate the efficacy of our proposed methods for autonomic function quantification.

Thesis Supervisor: Richard J. Cohen
Title: Whitaker Professor of Biomedical Engineering

Acknowledgements

Many people have been a part of my graduate education, as friends, teachers, and colleagues. This thesis would not have been possible without their support and encouragement.

I would like to start off by thanking my thesis advisor, Prof. Richard Cohen, for his academic guidance and financial support throughout my Ph.D. study. I am especially grateful to his concern about my professional development and the ample help he offered whenever needed.

Although it is impossible for me to thank him enough, I would like to take this opportunity to express my gratitude to Prof. Ramakrishna Mukkamala. Rama was the first person I met when I came to learn more about Dr. Cohen's laboratory in January, 2001. Ever since then, he has been helping me in every aspect of my graduate study, including curriculum design, research topics, paper writing and many more. I could not have achieved what I have done without his help. I particularly appreciate his serving on my thesis committee considering the tremendous responsibility he had in his new job at MSU.

I would like to thank the other members of my thesis committee, Prof. Roger Mark and Prof. George Verghese. Their participation, comments, and suggestions greatly enhanced the quality of this thesis. In addition, I thank Dr. Mark for his advice about my clinical preceptorship and my professional pursuit.

I owe many thanks to Prof. Roger Kamm, who has been my academic advisor since my arrival at MIT. I thank him as well for opening to me the world of cardiovascular research and for his constant encouragement and understanding during and after my Masters thesis.

I am grateful to all the members of Dr. Cohen's group, both past and present, for their scientific wisdom and friendship. Particularly, Dr. Antonis Armoundas has always been there whenever I had a question or I was confused about the future. Maya and Tamara offered the dearest friendship and made the seemingly dull days enjoyable. Dr. Yuri Chernyak and Dr. Evgeny Ter-Ovanesyan provided invaluable scientific insights to my current research and future improvement. Lastly and most importantly, Amy Donovan deserves my big thank-you for handling professionally all the confusing administrative matters and making my life much easier than what it could have been.

My gratitude also extends to our collaborators in the hospitals. I thank Dr. Gordon Williams, Dr. Natalie Sheynberg, Dr. Marlene Grenon, Mike Ehrman, Christine Kim and all the subjects who participated in the study for making available the bed rest database and for the various discussions about the study. Dr. Daniel Bloomfield helped me with the analysis of the bed rest leg compliance data and provided vast insights about orthostatic intolerance. I am also grateful to Dr. Roy Freeman and Dr. Marcelo Risk for providing the AGE database.

I would also like to thank members of Dr. Mark's laboratory. Wei Zong has been a close friend and offered an understanding ear at any time. He helped me retrieve the CRC data, among all other technical issues, and provided invaluable advice in many aspects of research and life. Thomas Heldt was always ready to help me with any questions and to kindly offer the necessary stimulus when I intended to sit back and be lazy. George Moody offered tremendous help in implementing the ECG-derived respiration algorithm and in related data analysis.

I would like to thank all the HST administrative staff for their professional and efficient hard work. I can not imagine how hard life would have been without Cathy, Ron, Domingo, Jennifer, Patty and many others. The various agencies and institutions that granted financial support during all these years deserve my thanks as well: NASA, NSBRI and Harvard-MIT HST.

I would also like to express my gratitude to those individuals who have given me their friendship during my study at MIT. All of you helped me through the difficult times and thanks for making my life colorful.

At this point, I come to those for whom appreciation is most overdue. I would like to express my deep gratitude and love for my husband, Zhuangli Liang. He has indulged me in endless love and support in our five years of marriage, shared with me all the successes and failures of my research, and patiently served as an impartial, honest critic to my work despite the furious, unfiltered reaction he got from time to time. To him, I have boundless love and respect.

Lastly, I wish to thank my sister, Xinjie, and my parents, Peizhi and Rongyin, to whom I dedicate this thesis. They instilled in me a desire to learn and a drive to excel. Their unconditional love, unlimited support and excellent guidance fostered the self-motivation and self-confidence in me, which are indispensable for a successful career. To them, I am forever in debt.

Table of Contents

List of Figures

List of Tables

Chapter 1

Introduction

System identification is a process of deducing mathematical models of dynamic systems from observed data of the system. It is a powerful experimental approach often referred to as inverse modeling, as opposed to forward modeling which utilizes basic laws from physics in formulating model equations. In the past few decades, ample applications of system identification have been established in almost every engineering discipline, ranging from the traditional field of mechanical engineering to emerging areas such as systems biology. As a typical attempt in science and engineering, this thesis work aims to explore one tree in the immense forest of system identification. Briefly, a new cardiovascular system identification method will be presented followed by its application in the study of cardiac autonomic control. In this chapter, we first provide a brief overview on several important aspects concerning the practical usage of system identification techniques. It should be noted that we intend to review some of the most frequently encountered problems, rather than present a complete coverage of system identification theory.

1.1 System Identification Overview

Normally, three basic steps are involved in the process of system identification: data generation, model determination and model validation [1, 2]. Among these steps, model determination is the most important and most difficult one. It involves the determination of model

structure, evaluation of model quality, and estimation of model parameters. In the remainder of this section, we provide an overview of the above aspects of system identification.

1.1.1 Data Generation

For the first step, data associated with the targeted system should be obtained either during specifically designed identification experiments or from the normal operation of the system. Such data normally include the input and output signals of the system. However, in some circumstances, the input data are not available or they are the variables being pursued through system identification. A special technique called blind system identification has been developed for such scenarios [3]. In this thesis, we focus on system identification methods involving both input and output data.

One objective of data generation is that the data should be maximally informative, subject to constraints that may be at hand [2]. Therefore, white noise is the ideal probe to the system being considered and it has been utilized frequently in the design of system identification experiments. However, in many circumstances, such as noninvasive monitoring of human physiological states, the input signal of the system may not be manipulated liberally. The user should choose appropriate input signals or a more informative signal may need to be derived based on the measured data to enable an accurate system identification (for an example, see [4]).

After data collection, it may be necessary to preprocess the data before the next identification step. This procedure usually involves data digitization, denoising using various filtering techniques, outlier detection, missing data compensation, or further computation for an input/output series based on measured data (e.g., derivation of heart rate from surface electrocardiogram).

1.1.2 Model Determination

The next important and most difficult step of the system identification process is the determination of the mathematical model. Both parametric and nonparametric methods have been employed. Examples of nonparametric methods include frequency-response analysis, correlation analysis, spectral analysis, *et al.* [2]. We focus on parametric methods in this section since they are closely relevant to the techniques involved in the other chapters of this thesis. Three main problems need to be tackled in parametric model determination. One is model structure determination, the second one is model parameter estimation, and the last one is model selection.

Model Structure and Parameter Estimation

To determine a candidate model structure, it is necessary to combine *a priori* knowledge and engineering principles and insights with formal properties of models [2]. It is very often that a number of assumptions and approximations need to be formulated based on the fundamental laws of physics that govern the system. The frequently exploited models in system identification belong to one or more of the following categories: time domain models, frequency domain models, linear models, nonlinear models, time-invariant models, time-varying models, *et al.* In this section, we focus on time domain models with time-invariant characteristics which are relevant to the intended scope of the thesis.

An essential task in model structure determination is to decide whether a process is linear or nonlinear based on input-output data. If it is possible to excite the system with specifically designed input signals (e.g., sinusoids, Gaussian signals), then various methods may be used to test the linearity of the system, as discussed in [5]. However, as aforementioned, the signals related to physiologic systems (the main interest of this thesis) are not often controllable by the user. In such cases, one frequently used approach is to compare the performance of both linear and nonlinear models in terms of their ability to account for the variability in the output signal (see, e.g. [6-8]). Note that this testing may be part of the model validation procedure to be discussed below. For time-invariant systems, another often used

measure of the quality of data and the LTI assumption is the coherence function [9, 10]. Ideally, it should have a value of unity over all frequencies given noiseless data and LTI system. Ref. [5] provides a thorough introduction of various methods for linearity testing.

Linear time-invariant (LTI) models are very frequently utilized in system identification applications due to their simplicity and effectiveness. Such models are justified when the variations in the signals are small enough so that a linearization is allowed and when the system is approximately stationary to be modeled as time-invariant. For example, at stable, resting conditions, LTI models have proved to be effective in representing the cardiovascular regulatory system [7, 10]. We next review some of the often-employed LTI model structures and their associated parameter estimation methods.

The two types of LTI model structures most intensively investigated are state-space models and transfer function models. A state-space model relates the input, noise and output signals through a system of difference equations involving an auxiliary state vector. Subspace methods are often used to estimate the parameters in a state-space model [2]. In Chapter 2, we will review this category in more detail in conjunction with the application of singular value decomposition. The system identification models to be focused on in the rest of this thesis belong to the family of transfer function models. A generalized model structure of a single-input single-output (SISO) system in this category is expressed as:

$$A(q)y(t) = \frac{B(q)}{F(q)}u(t) + \frac{C(q)}{D(q)}e(t) \tag{1.1}$$

where q is the shift operator [2]. A, B, C, D, and F represent finite-order polynomials whose parameters are unknown. $y(t)$ and $u(t)$ are the output and input signals respectively, while $e(t)$ is white noise typically with zero mean. In open-loop systems, the noise and the input data are normally assumed to be uncorrelated. In often-utilized model structures, one or more of the terms A, B, C, D or F are fixed to be one. Examples of such model structures are listed in Table 1-1. In the abbreviated names, MA refers to moving average model, AR refers to autoregressive model and X refers to exogenous input [2].

Table 1-1 Some common LTI model structures and parameter estimation methods

Model Structure	Terms	Parameter estimation
MA	B	Linear least squares estimation
ARX	$A\,B$	Linear least squares estimation
ARMAX	$A\,B\,C$	High-order ARX and model reduction [11], extended least squares [12]
ARMA	$A\,C$	AR modeling and instrumental variable method [13]
ARARX (GLS)	$A\,B\,D$	Repeated least squares [14], bilinear estimation [15],
ARARMAX	$A\,B\,C\,D$	Numerical search [2], ASYM [11]
OE (output error)	$B\,F$	Numerical search [2], ASYM [11], state-space method [16], recursive least squares [11]
BJ (Box-Jenkins)	$B\,F\,C\,D$	Numerical search [2], ASYM [11], recursive least squares [2]
Orthonormal basis expansion	B	Laguerre expansion [17], Kauz expansion [18], generalized basis functions [19]
State-space models		Subspace method [2, 20]

The MA and ARX models have been effectively applied in physiological system identification (see, e.g. [21-23]). Parameter estimation of these models can be generalized as a linear regression problem and thus can be solved analytically via linear least squares estimation [2]. The ARX structure allows a noise model in the form of $1/A(q)$ which, together with $B(q)$, also constitutes the system impulse response model. Although its noise model and impulse response model are not independent, the ARX structure is very effective in linear system modeling because it can be shown that a high-order ARX model is capable of approximating any linear system relatively well [16]. The output error structure has a fixed noise model and it is a natural choice if only the identification of system dynamics is desired. In contrast, the ARMAX, GLS (generalized least squares), ARMA, ARARMAX and BJ structures allow more comprehensive noise models. However, for these fairly complicated structures, linear regression generalization does not apply directly. The most basic approach for their respective parameter estimation is therefore based on iterative numerical search schemes [2]. Nevertheless, extensive research efforts have been devoted to develop alter-

ative techniques to rephrase the parameter estimation as a linear regression problem or a series of such problems. Table 1-1 lists some of the special techniques corresponding to specific model structures, a detailed discussion of which can be found in the relevant literature. Other popular parameter estimation methods not listed include the instrumental variable (IV) method and the maximum likelihood method [1, 2].

In Table 1-1, there is another important type of LTI modeling method, the orthonormal basis expansion method. This approach fits into the general moving average framework. However, the transfer function ($B(\cdot)$ in Equation (1.1)) is represented by a linear orthonormal basis expansion, instead of the shift operator. Employment of appropriate orthonormal bases can enable a compact or parsimonious representation of the system (with reduced model order). However, *a priori* knowledge about the system poles needs to be incorporated into the construction of basis functions. Refs. [17-19, 24] provide detailed presentations on the orthonormal basis expansion methods and their applications in automatic control.

In the category of nonlinear model structures, Hammerstein model and Wiener model are two often encountered types representing systems whose nonlinearity is static which only presents at the input and/or output (e.g., due to saturation). Nonlinear black-box models, another often-used model structure, may be thought of as a linear combination of some basis functions, e.g., the Volterra series, wavelets, Fourier series, etc, many of which can be graphically delineated by *networks* (including neural networks). Finally, fuzzy models, which are based on verbal and imprecise descriptions on the relationships between the measured signals in a system, are often employed when it is difficult to set up precise mathematical models. Refs. [2, 5] provide extensive coverage on nonlinear model structures and parameter estimation.

Model Selection

Once the model set is selected, the "best" model in the set should be determined guided by the data. The assessment of model quality is typically based on how the models perform

when they are used to reproduce a fresh set of measured data [2], i.e., to minimize the *prediction error*. This approach, which is commonly referred to as cross validation, is an effective option for model order selection. However, the trade-off is that a fresh data set has to be saved for this purpose and that not all of the measured data can be utilized for training the model. Thus, due to asymptotic arguments, the quality of the models to be selected from will not be as high as possible. One way to perform linear cross-validation while utilizing all the data to build the model is the leave-one-out cross-validation (LOOCV) approach [25]. This method is asymptotically equivalent to FPE and AIC (see below) and it is not consistent [25] in the following sense: the probability of selecting the true model which is included in the candidate model set does not converge to one asymptotically. In addition, the computational cost of LOOCV may be prohibitively large for practical applications when the data length is long.

To achieve a similar goal of linear model evaluation based on the cross-validation concept, model order selection criteria have been developed to estimate the prediction error by employing only *training* data. Such criteria are often categorized as cross-validation criteria in the literature [26]. They are usually utilized in model selection among a set of nesting structures where a model with a higher order is formed by adding extra terms to a lower order candidate model. Typical criteria in this vein include Akaike's Final Prediction Error (FPE) [27], Mallows' C_p criterion [28], the Generalized Cross-Validation (GCV) [29], Shibata's Model Selector (SMS) [30], and the VC theory-based Vapnik's Measure (VM) [31]. Note that prediction estimates provided by FPE, GCV and SMS are asymptotically equivalent. The recently developed Signal Prediction Error (SPE) [32] also belongs to the cross-validation category. It employed a similar rational in the derivation as that of C_p but without the assumption of a known noise variance. In addition, Chapelle *et al.* [33] proposed two criteria, the Direct Eigenvalue Estimator (DEE) and the Smallest Eigenvalue Bound (SEB) methods, appropriate for small sample regression based on an estimator of the ratio of the expected training error and the expected generalization error.

Another category of linear model order selection criteria is named information-based criteria by Gustafsson *et al.* [26]. This category includes Akaike's original AIC criterion [34].

It is based on the concept of the Kullback-Leibler distance between two probability density functions. The idea is to minimize the distance between the distribution of the estimated output and the true data distribution. AIC is asymptotically equivalent to FPE, GCV and SMS, all of which tend to overestimate the model order [2]. This disadvantage motivated the development of Akaike's B-Information Criterion (BIC) [35], Schwartz's criterion (SC) [36] and the ϕ criterion [37], which are strongly consistent. In addition, several criteria have been proposed to improve the performance of AIC, such as the AICc (for small data length) [38] and AICu [39] criteria, both aiming to correct the bias in the estimate for the expected Kullback-Leibler information. Another well-known criterion in this category is Rissanen's Minimum Description Length (MDL), which coincides with BIC and SC [40]. MDL aims to minimize the description length in a coding theoretic framework, to give the cheapest possible description of data (usually corrupted with noise) [26]. Beheshti and Dahleh [41] proposed a new MDL criterion, the objective of which is to obtain a minimum description length for the noise-free data (the true *signal*).

Most suggested model order selection criteria can be generalized as minimizing the product of the residual error (the output estimation error resulted from the model parameterization being considered) and some penalty factor related to model complexity or the logarithm of the product. This is a reflection of the parsimony principle which says that there should be a trade-off between model fit and model complexity [2]. Table 1-2 lists the formula of the above mentioned criteria for convenience (the formula of the new MDL, DEE and SEB necessitate detailed interpretation, therefore they are not included in this Table). It should be noted that there exists a vast variety of model selection criteria in the literature and those listed here only constitute a subset that is often employed in practice. Moreover, assumptions were usually made in the derivation of these criteria. Hence, a correct application of them may entail a thorough consultation of the original publications.

Pertinent to the nonlinear system identification problems, cross-validation approaches are still desirable especially when a fresh data set is affordable to be saved for validation purpose. On the other hand, the selection criteria presented above for linear system identification may be exploited or modified to solve nonlinear model selection problems when

reparameterization of the model involves linear components (see, e.g. [6, 42-44]). Lastly, estimation error metrics, such as residual variance, sum of squared errors (SSE), are also utilized to measure the goodness-of-fit in nonlinear modeling (e.g., for neural network models, see [42]).

Table 1-2 Examples of model order selection criteria

Cross-Validation Criteria		Information-Based Criteria	
FPE	$V_N(1+\frac{d}{N})/(1-\frac{d}{N})$	AIC	$\log(\frac{V_N}{N})+\frac{2d}{N}$
C_p	$\frac{V_N}{N\lambda}+2d-N$	AICc	$N\log V_N + N\frac{1+d/N}{1-(d+2)/N}$
GCV	$\frac{V_N}{(1-d/N)^2}$	AICu	$N\log\left(\frac{N}{N-d}V_N\right)+\frac{2N(d+1)}{N-d-2}$
SMS	$V_N(1+\frac{2d}{N})$	BIC/MDL /SC*	$V_N(1+\frac{d}{N}\cdot\log N)$
VM*	$V_N\left(1-\sqrt{\frac{d(1+\log(N/d))+\log N/2}{N}}\right)^{-1}$	ϕ*	$\log(\frac{V_N}{N})+d\frac{\log\log N}{N}$
SPE†	$V_N\cdot\frac{d}{N-d}$		

* denotes consistent model order selectors. † The consistency of SPE depends on the SNR level of the measured output data [32]. V_N is the mean squared residual error [2], d is the number of model parameters in the candidate model, N is the length of data available, λ is the known noise variance.

1.1.3 Model Validation

It is of great importance to validate the identified model once the preceding two steps are completed. General guideline for model validation is to assess how the model relates to observed data, to prior knowledge, and to its intended use. Specifically, often-employed methods include, but are not limited to: evaluating the estimated model parameters based on pos-

sible physical interpretation [2], model reduction attempts to detect redundancy in model structure [2], Chi-Square test and/or normality test of the residuals (if the noise is approximately Gaussian) [5], frequency domain analysis of the residuals (especially for white noise) [2, 5], run test of the randomness of the residuals [5], Durbin-Watson test of the residuals [5], correlation analysis between the input signal and the residuals [2, 5], *et al.*

If the model first obtained does not meet the validation requirements, the previous steps need to be repeated until a reasonable representation of the system is reached. Therefore, the system identification process can be an iterative task.

1.2 Cardiovascular System Identification

The cardiovascular system consists of the heart and the circulation. Its basic function is to transport oxygen and nutrients to the tissues of the body, to carry waste products away and to convey hormones from one part of the body to another. Hence, the cardiovascular system maintains an appropriate environment for the normal functioning of the cells. This mission is accomplished via a comprehensive regulatory system which includes the central nervous system, the autonomic nervous system, the renal system, local tissue control, and hormonal regulation *et al.* [45]. Because of its critical role, the cardiovascular system has been studied intensively over many years and monitoring and evaluation of cardiovascular function are conducted routinely in clinical practice.

To probe different aspects of the cardiovascular system, numerous techniques have been/are being developed ranging from most simple and reliable measures of blood pressure and heart rate to the more involved technologies, such as ultrasound imaging and implanted ventricular pressure transducers. The system identification approach may provide a solid technical basis for the study of the cardiovascular system partly because it has the following advantages. First, it enables an integrated characterization of the system with minimally disturbed physiologic state. This is because heart rate, blood pressure, respiratory signals, *et al.*, can be readily obtained with noninvasive techniques and the interactions between these

signals can reflect the underlying regulatory mechanisms of the cardiovascular system. The second advantage is that system identification technique facilitates a dynamic characterization of the cardiovascular system since it considers at least two-time statistics of the signals. A third advantage is that this technique can provide system characterization specific to each subject. Meanwhile, normalization of the signals enables a comparison among different subjects. For the cardiovascular system which is fairly complicated and contains many parameters whose values are unknown and subject-specific, the system identification approach is well suited for studying its dynamical behaviors and regulatory mechanisms. Both linear and nonlinear system identification techniques have been employed in investigating cardiovascular functioning. Next, we provide a brief review on some of the relevant studies in the literature.

1.2.1 Linear Cardiovascular System Identification

Non-parametric Modeling

The complex transfer function between two signals can be calculated nonparametrically by the ratio of the input-output cross-spectrum and the autospectral density function of the input. This method has been applied repeatedly in cardiovascular research. Some of the representative work is summarized here. Selman *et al.* investigated nonparametric linear transfer function relationships between respiration and heart rate (HR) [46]. This work demonstrated the adequacy of linear analysis in approximating the interaction underlying respiratory sinus arrhythmia (RSA). In this study, the subjects were required to perform fixed-rate breathing at distinct rates between 6 and 24 breaths per minute to enable a frequency sweep. Berger *et al.* [10] studied the transfer function relationships between direct parasympathetic or sympathetic nerve stimulation and the resulting HR variability in dogs. They concluded that the sino-atrial (SA) node operates as low-pass filters in response to parasympathetic or sympathetic stimulation, but the characteristics of the filters differ for different mean rates of neural stimulation. Therefore, the SA node may be modeled as a piece-wise linear device relative to autonomic control. Saul *et al.* demonstrated low-pass filter characteristics in the

relationship between instantaneous lung volume (ILV) and HR in humans [47]. They used a similar transfer function analysis technique as in [10]. The persistently exciting requirement of the input signal (ILV) for system identification is fulfilled by carrying out a random breathing protocol [48]. Berger *et al.* also applied a similar transfer function analysis technique to analyze the interaction between HR and arterial blood pressure (ABP) in dogs [49]. They showed that this relationship also exhibits low-pass filter characteristics with an initial delay of about 0.4s. Abundant other applications of nonparametric cardiovascular system identification exist in the literature, see, e.g. [50-52].

Despite the demonstrated effectiveness of the nonparametric system identification method, it poses some inherent limitations to the study of cardiovascular dynamics. For example, this method is unable to model closed-loop interactions present in cardiovascular regulation. It also encounters difficulty in coping with multi-input systems. In contrast, the parametric system identification methods provide convenient solutions to these problems.

Parametric Modeling

Saul *et al.* developed a linear parametric modeling approach based on their aforementioned nonparametric methods to study the closed-loop interactions between ABP, HR and ILV [53]. Their findings demonstrated the effectiveness of first-order analytic transfer functions in modeling the involved physiological dynamics. In a similar vein, Appel *et al.* also developed an LTI closed-loop model for the couplings between ABP, HR and ILV [54]. However, they adopted ARX models instead of pre-knowledge-based first order equations to enable a more flexible characterization. In a related framework, Perrott *et al.* developed an efficient candidate model construction and selection algorithm for multi-input ARX system identification with input delays [55]. Later, Mullen *et al.* [23] applied this algorithm to identify the closed-loop model formulated by Appel *et al.* They studied the impulse response functions representing the couplings between ABP, HR and ILV in healthy subjects before and after parasympathetic or sympathetic pharmaceutical blockade. Their findings indicated that the ABP→HR and ILV→HR interactions are mainly regulated by the autonomic nerv-

ous system, while the ILV→ABP coupling reflects the mechanical effects of respiration on ABP mediated in part by the effects of intrathoracic pressure on venous return. The above technique also proved successful in categorizing diabetic autonomic neuropathy patients [56]. Furthermore, Mukkamala *et al.* conducted a forward model-based validation of this closed-loop cardiovascular identification method [57]. The sensitivity of the method in detecting small changes in parameters characterizing autonomic function in the forward model is studied and their results consolidated the efficacy of the system identification method.

Also in the framework of studying the coupling mechanisms between HR and ABP, Virgilio *et al.* developed a multivariate autoregressive time-variant method to follow the transient changes in the signals [58]. Their method provides a means for physiologic characterization during nonstationary epochs. Yamada *et al.* also examined the effect of arterial baroreflex on HR with an ARX model [59]. The distinction of their study from the previous ones is that a random perturbation of blood pressure was enforced through cuff inflation. Kosaka *et al.* [60] proposed a system identification method using the delta operator to calculate a few hemodynamic parameters used in forward modeling. This work showed an example of the integration of system identification and forward modeling methods. As a further demonstration of the vast potential of system identification in cardiovascular research, Mukkamala *et al.* proposed a novel technique to noninvasively quantify the total peripheral resistance (TPR) baroreflex based on ABP and cardiac output measurements [61]. Their forward model-based analyses showed that this technique is able to track changes in the static gains of both the arterial and cardiopulmonary TPR baroreflex. An application of this method in studying TPR baroreflex after prolonged bed rest is presented in [62].

1.2.2 Nonlinear Cardiovascular System Identification

Considering the intrinsic complexity of the cardiovascular system, researchers have attempted to employ nonlinear system identification techniques to study its underlying physiological mechanisms. Ahmed *et al.* applied an algorithm of kernel identification of the Volterra series up to the second order to investigate the coupling between respiration and

HR [63]. They found that the response of the linear term (first-order kernel) exhibited a oscillatory-input and underdamped nature of the system, while the second-order kernel facilitated an indication of an escape-like phenomenon in the system. Similarly, Saul *et al.* also explored the possible mechanisms underlying the interaction between respiration and heart rate [64]. They postulated that the nonlinear component in this coupling may be the result of either classical nonlinear physiology or entrained nonlinear oscillators. More recently, Chon *et al.* performed a nonlinear analysis of the effect of fluctuations in ILV and ABP on HR variations utilizing a Laguerre expansion-based technique [7]. They found that the linear model accounted for approximately 67% of the variance in heart rate, while the nonlinear model accounted for approximately 80%. In a related body of work, Chon *et al.* applied the artificial neural network method to study the coupling between HR and ILV, the result of which is compared to traditional least squares estimation [6]. Only slight difference was detected in the identification results of these two methods.

To summarize the previous work on cardiovascular system identification, nonlinear identification methods may provide a more comprehensive characterization of the basic physiological mechanisms, especially when time-varying processes are involved. However, when the subjects are in a stable condition within the interested time frame, LTI modeling has proved to provide a very effective and efficient tool to probe the cardiovascular system.

1.3 Motivation

In LTI modeling of the cardiovascular system, an often-employed model structure is the ARX structure, the advantage of which has been discussed previously. A key question in the application of the ARX model is: which input and output delays are needed to represent the system? In principle, one could answer this question from the data and through an exhaustive search among all possible combinations of the input/output delays (candidate models). For example, if a maximum set of 10 input delays and 10 output delays is assumed to be involved, then an exhaustive search needs to be performed among $\sum_{i=1}^{20} C_{20}^{i}$ (=1048575) candidate models. This is not computationally practical. To make the problem tractable, the

delay terms in an ARX structure are usually added in, one at a time, in an order of increasing time shifts relative to the current output. This conventional approach is based on the assumption that the current output correlates more with the recent inputs/outputs than with the remote ones. It does not allow construction of data-specific candidate models. Furthermore, since it selects the model terms by their contribution in the time domain, this approach does not impose explicit frequency-related constraints. Such constraints may prove useful in physiological system identification since most signals involved in this problem are colored with their energy concentrated in certain frequency range.

To this end, we propose an LTI parametric system identification method based on weighted-principal component regression (WPCR). This method seeks solutions to achieve the desirable goal of letting the data determine the candidate models in an efficient manner. In addition, the candidate model terms considered by this method are components in the input (and output) signal with different asymptotic frequencies, which facilitates model selection with a consideration of frequency properties.

Based on the above WPCR approach, we intend to design practical methods to explicitly quantify parasympathetic responsiveness and sympathetic responsiveness in their control of cardiac function. This work is motivated by the lack of a readily available technique to distinctively quantify the strength of the two branches of autonomic control noninvasively. Previous studies on the interactions between ILV, HR and ABP signals have offered significant insights about the involvement of autonomic mediation in these coupling mechanisms. However, it still remains unclear how the parasympathetic and sympathetic control may be quantified based on certain features of the corresponding transfer relationships. We therefore explore the WPCR system identification-based solutions to this problem in the contexts of random breathing, spontaneous breathing and metronomic breathing of the subject under study.

Once the quantification techniques for cardiac autonomic control are made available, they may be applied in various practical scenarios in order to tackle some specific physiologic problems. We choose to study the effect of microgravity on cardiac autonomic control and orthostatic intolerance. The relevant significance of this problem to the medical considera-

tions about long-term and short-term space mission is well-recognized. Despite the extensive research effort devoted into this area, a universal consensus on the alterations of autonomic function (especially the sympathetic branch) after microgravity exposure has not been reached and the possible association of such alterations with orthostatic intolerance in astronauts after spaceflight is still to be resolved. We therefore apply our proposed autonomic quantification techniques to explore this problem, which also serves as a partial validation of the techniques.

1.4 Specific Aims

There are three specific aims associated with the research presented in this thesis. They are listed as follows:

1. To develop a system identification method based on the weighted-principal component regression approach for both open-loop and closed-loop physiologic systems.

2. To develop and evaluate methods for quantification of the functioning of cardiac autonomic nervous control based on the above system identification method.

3. To study the effects of prolonged bed rest (a simulation of microgravity) on cardiac autonomic control and possible association of those effects with orthostatic intolerance.

1.5 Thesis Organization

The current chapter provided an introduction of the general system identification method with an emphasis on the practical problems of model structure selection, parameter estimation and model order determination. We also conducted a brief review of the pertinent literature on cardiovascular system identification, in addition to a discussion of the motivation behind this thesis and the aims it pursued.

In the remainder of this thesis, we first lay out the theory of system identification based on the weighted-principal component regression (WPCR) method in Chapter 2, followed by a discussion of its frequency domain interpretation. The WPCR method is presented in the context of both an MA structure and an ARX structure. Subsequently, we discuss the application of the WPCR method in closed-loop system identification. Lastly, computer-simulated and experimental data were employed to demonstrate the applicability of the method.

Based on the WPCR method, in Chapter 3, we present the development of identification methods for quantitative characterization of the cardiac autonomic responsiveness which are suited for data obtained noninvasively during random interval breathing, spontaneous breathing or metronomic breathing. We then validate the proposed techniques with a thorough analysis of experimental data, followed by a discussion of the applicability of the methods.

In Chapter 4, we apply the techniques presented in Chapter 3 to study the effect of simulated microgravity on cardiac autonomic function and orthostatic intolerance. We start with a concise review of previous studies of autonomic function in association with microgravity exposure. Subsequently, we present the results of the application of our proposed techniques in analyzing data collected from 29 healthy male subjects in a 16-day head-down-tilt bed rest study. The physiological significance of our findings and the effectiveness of each technique are then discussed respectively.

Lastly, Chapter 5 concludes this document by summarizing the research presented in this thesis and proposing potential future studies.

Chapter 2

Weighted-Principal Component Regression Approach for System Identification

In Chapter 1, we reviewed conventional system identification techniques and their applications in studying cardiovascular dynamics. In this chapter, we propose a competitive approach for LTI system identification based on principal component regression (PCR) and evaluate its effectiveness in our intended application – system identification involving cardiovascular signals. We begin with a brief introduction of PCR and its related singular value decomposition (SVD) method. We then review the literature on the application of PCR and SVD in the fields of system identification and time series analysis. Next, we provide a detailed presentation of our proposed method and its interpretation in the frequency domain. Subsequently, we discuss the application of the proposed method in open-loop and closed-loop systems respectively. The performance of our method is compared with conventional approaches through both simulated and experimental data.

2.1 Introduction

The principal component regression (PCR) method belongs to the general principal component analysis (PCA) family. PCA was first introduced by Pearson *et al.* in 1901 [65] and developed independently by Hotelling in 1933 [66]. The central idea of PCA is to reduce the dimensionality of the data set in which there exists intercorrelation, while retaining as much as possible the variation present in the data [67]. This reduction is achieved by trans-

forming the data into principal components (PCs) and by discarding the PCs with small variances. To compute the PCs [67], the first step is to look for a linear function of the original variables in the data set which has maximum variance. The new variable resulting from this linear transformation is the first PC of the original data. Next, look for another linear function (PC) with maximum variance and uncorrelated with the previous one, and so on, so that the variance of each PC is maximized subject to being uncorrelated with the previous PCs. If there exists intercorrelation in the original variables, the first few PCs usually account for most of the variation present in the data. PCA is widely employed [67] to solve problems related to multivariate analysis, outlier detection, prediction modeling and process identification, *et al.* Regression analysis (or principal component regression – PCR) is one of the most actively researched areas related to PCA in recent years.

In traditional PCR analysis, the regressor variables are transformed into PCs and the PCs associated with relatively small variance are usually excluded from the regression. By retaining only a subset of PCs, the PCR method may reduce the complexity of a model structure and its associated computational load. Moreover, the problem of multicollinearity, a major difficulty in least squares estimation when there are near-constant linear functions between two or more of the regressors, is solved owing to the zero correlation between the PCs [68].

An efficient way to compute the PCs is through singular value decomposition (SVD) which is based on matrix theories. We will employ this algorithm in the weighted-PCR approach to be proposed in this chapter. Given an arbitrary matrix, X, of dimension $N \times p$, its SVD can be expressed as:

$$X = UDV^T \tag{2.1}$$

where the superscript T denotes matrix transposition. U and V are both orthonormal matrices. Their column vectors (we refer to those of U as PCs) are eigenvectors of the matrices XX^T and X^TX respectively. Note that the column vectors of U and V are sometimes referred to as *left singular vectors* and *right singular vectors* of X, respectively. D is a diagonal matrix with its diagonal elements (singular values) being the square root of the eigenvalues of

X^TX (or XX^T). The singular values correspond to the variance/energy of their respective PCs. The relationship between SVD and PCA is discussed in detail in [67].

2.2 Previous Applications of PCR and SVD

Although there are numerous applications of PCA in a variety of fields, in this section, we focus on the application of PCR and SVD in system identification and time series analysis since they are relevant to the intended scope of this thesis.

2.2.1 Time Series Analysis

In time series analysis, SVD and PCR are often employed in noise reduction [69, 70] and filtering [71], data compression [72], feature extraction [72, 73], linear prediction [74-76] and most importantly, spectral estimation. The application of SVD in parametric spectral estimation is analogous to that in system identification approaches in general. Therefore, we provide a detailed investigation on this topic.

Given a finite set of uniformly spaced samples of a signal, an autoregressive (AR) or autoregressive moving average (ARMA) model structure is often utilized to estimate the power spectrum of the signal parametrically. Those approaches based on an AR model can often be regarded as an extension of the Prony's method. Around two hundred years ago, Prony developed a simple procedure to approximate a signal by a weighted sum of exponentials [77]. Today "Prony's method" usually refers to the least squares extension of the method as presented, for example, by Hildebrand [78]. In this method [79], a short record of a data sequence $y(n)$, $n = 1,2, \quad , N$, is assumed to be composed of uniformly spaced samples of the summation of a signal $x(n)$ and white measurement noise $w(n)$. In turn, $x(n)$ is represented by a sum of weighted exponential signals. The number of exponential functions, their respective complex frequencies and weighting factors are unknown. Hildebrand demonstrated that $x(n)$ satisfies the following linear equation with constant coefficients:

$$\sum_{k=0}^{M} b(k)x(n-k) = 0, for \quad M < n < N \tag{2.2}$$

The roots of the prediction-error-filter polynomial $B(z)$ provide the values of the complex frequencies in $x(n)$. Hildebrand explicitly considered noisy data and solved for $B(z)$ through least squares estimate of the noisy version of Equation (2.2) (by substituting $x(n)$ with $y(n)$). Subsequently, the weighting factor of each exponential is estimated with a second least squares minimization.

It is well-known that the errors in signal parameters which are estimated by Prony's method can be large when the noise level is high [78, 79]. Tufts and Kumaresan [75] proposed an SVD-based method to improve the performance of the above Prony's spectral estimation in the presence of noise. They included an increased number of signal delays (greater than M – the true number of frequencies) in Equation (2.2). In solving the matrix form of Equation (2.2), the Hankel matrix of the signal $y(n)$ was represented by its SVD and only the first M PCs are retained to obtain a pseudoinverse of the Hankel matrix through which to compute the coefficients $b(k)$. This approximation is based on the well-known Eckart-Young theorem that the best rank-r approximation of a matrix A is given as the SVD of A with only r terms [67]. This method was shown to have improved performance at low SNRs. In a similar vein, Cadzow *et al.* [80, 81] proposed to generate the SVD of the extended-order autocorrelation matrix of $y(n)$ to achieve the same goal. Tufts and Kumaresan [82] also extended Prony's method in a forward-backward linear prediction setting and employed SVD to reduce the effect of noise in the autocorrelation matrix of the data. Note that other investigators presented closely related approaches as well [83, 84]. In the above methods, if M is not known *a priori*, an estimated value is usually established by inspecting the rate of decrease of the error in approximating the Hankel matrix or autocorrelation matrix corresponding to increasing values of M or by inspecting the contribution of singular values. M is determined as the value when the rate of decrease or the singular values are "satisfactorily" small.

Similarly, an ARMA model structure is also used to estimate the spectrum of time series [80, 81]. The MA terms are composed of unobservable white noise and the AR terms are composed of the time series to be analyzed. The AR coefficients of the ARMA model were

estimated from a set of normal equations analogous to the Yule-Walker equations for an AR process. The extended Yule-Walker equations were solved using a generalized inverse of an over-determined autocorrelation matrix. Given an estimate of the "true" ARMA model order, the over-determined autocorrelation matrix was replaced by a reduced-rank matrix obtained via SVD. Subsequently, the MA coefficients of the ARMA model were obtained after removing the effect of the autoregressive dynamics in the time series.

2.2.2 System Identification

In the field of system identification, PCR/SVD algorithm is also widely employed. For example, it is used in the frequency domain to replace the input and/or output variables by their PCs without much "loss of information" [85, 86]. SVD is also widely applied in neural network models [87, 88], subspace identification [89], total least squares algorithms [90], *et al.* In this section, we discuss the latter two applications in detail.

Subspace identification refers to the so called subspace-based state-space system identification (4SID). There are generally two classes of techniques in this category. One is called realization-based 4SID methods. The other one is called direct 4SID methods.

The realization-based 4SID method can be viewed as an extension of the state-space realization theory, a classic contribution of which is by Ho and Kalman [91], where a scheme for recovering the system matrices from impulse response measurements is outlined. Based on this theory, Kung introduced SVD as a tool to reduce the sensitivity to errors in the measured impulse response [92]. Kung's method uses a "large" dimension of the Hankel matrix H of the impulse response. In the presence of noise, the Hankel matrix will generically be of full rank. SVD can then be utilized to reduce the rank of H. The user must decide on the number of "significant" singular values, which in turn will determine the resulting system order. The observability and controllability matrices are then computed based on the reduced H and the system matrices can be obtained subsequently. This class of techniques is referred to as realization-based 4SID methods by Viberg [93]. The eigensystem

realization approach (ERA) [94], the Hankel-norm model reduction method [95], the Q-Markov COVER (covariance equivalent realization) method [96], *et al.*, are regarded as existing alternatives to Kung's approach. A problem inherent in this class of techniques is the difficulty of obtaining the impulse response, especially when the system is complex, e.g., multi-input multi-output (MIMO) systems or systems with large orders.

An alternative method of subspace identification is to extract the system matrices directly from the input/output data, without explicitly forming the impulse response. This class of algorithms is referred to as direct 4SID methods by Viberg [93]. Ljung [2] provides a detailed review on these methods. Using a state-space model, it is evident that the output vector can be expressed as a summation of three terms – the product of the observability matrix and the state vector, the product of an impulse response matrix (composed of system matrices) and the input vector, and the noise vector. A noisy estimate of the true observability matrix can then be obtained if the terms involving the input and the noise vectors can be cancelled by correlating the output vector with some variables called instruments. Such an instrument is often constructed using past input and past output provided that only future input and future output are utilized in the original summation and the system being studied operates in open-loop. SVD is employed next to reduce the effect of noise in the estimated observability matrix (this matrix is weighted sometimes to enhance its robustness to noise). The system order is estimated as the number of singular values that are significantly larger than 0 and the state vectors can be extracted from the singular vectors. The system matrices and the noise statistics may then be identified once the observability matrix is estimated. Different algorithms exist to implement the above procedures, such as the MOESP algorithm [97], the N4SID algorithm [20, 98], the IVM algorithm [93], and the CVA algorithm [99]. These algorithms differ by the weighting matrices applied to the estimated noisy observability matrix [2].

Total least squares (TLS) approach is a system identification technique that considers the scenario when measurements of system input and system output are both corrupted by

unknown noise[1]. A detailed discussion of the SVD-based TLS approach is provided in [100]. The solution of the system parameters is considered to be the vector that minimizes the weighted Frobenius norm of the total perturbation matrix which consists of the unknown error vectors embedded in both input and output signals. This minimization is subject to the constraint that the perturbed output vector is in the range of the perturbed data matrix. It has been proved [100] that such a solution is the right singular vector associated with the smallest singular value of the matrix composed of current output vector and current and past input vectors. The SVD algorithm is widely exploited to solve TLS problems partly due to its tolerance to quantization and low sensitivity to computational errors [101].

Cadzow and Solomon [102] employed an ARMA model in solving the TLS problem. To alleviate the bias in the solution of the Least Squares (LS) or Generalized Least Squares (GLS) methods when the input is corrupted by noise, they proposed to use an ARMA model whose order is believed to readily exceed that of the true model (assuming the noise-free input and output are related by an ARMA model). Then, SVD is performed on the matrix X containing all the input and output delayed vectors (including the current output). The vectors in X are prescaled by the input and output white noise variances that are assumed to be known *a priori* or through estimation. This procedure, aiming to alleviate the deleterious effects of noise in the singular values, ensures that the variance of the noise contaminating the rescaled input is equal to that in the output [102]. The solution of model parameters (AR and MA coefficients), which should be in the null space of matrix X in the noise-free case, is chosen to be a linear combination of the right singular vectors corresponding to the s smallest singular values, where s is the difference of the assumed ARMA model order and the true order. Note that the true order may be estimated by inspecting the singular values. The above method was demonstrated to behave in an unbiased manner on a standard example in which noise contaminates both the excitation and the response [102].

[1] The conventional LS problem does not consider input noise explicitly.

2.3 Preview and Motivation

In studying physiologic systems via system identification, the mathematical models employed merely serve as tools to describe the system behavior under certain approximations. The complexity of the systems often makes precise mathematical modeling an impossible task. Although the assumption of an appropriate model structure is important in system identification, in many scenarios, the ultimate goal is to obtain an accurate description of the system dynamics/behavior, as manifested through, for example, a precise estimate of the system impulse response or an accurate prediction of future outputs. The mathematical expression of the model itself only serves as a means to reach that goal.

To this end, we introduce a weighted-PCR (WPCR) method for LTI system identification. This method aims to obtain an accurate system impulse response and emphasizes less seeking for a "correct" model structure. We adopt the same basic concept as involved in the PCA applications discussed in Section 2.2, i.e. by using PCR, we aim to project the information in the time-dependent data onto a space of PCs and then choose a subset of PCs to reduce the effect of noise on parameter estimation. The proposed method has some similarity to the aforementioned parametric spectral estimation methods but it is applied in a system identification context where both the input and output signals are accessible. In contrast to the total least squares method, the WPCR method belongs to the traditional Prediction Error Method (PEM) family [2] because a subset of PCs is selected to obtain a minimum prediction error. To our knowledge, this PCR method together with the weighting scheme on the data matrix was not proposed previously in the field of system identification.

We employ the moving average (MA) or autoregressive exogenous input (ARX) structure to relate the system input and output signals in the WPCR method. These structures are widely applied in physiologic system identification because of their effectiveness and simplicity in practice. As discussed in Section 1.3, the conventional way of constructing candidate models is by adding to the structure one delayed input (or output) term at a time, in an order of increasing time shifts relative to the current output (see Figure 2-1 for an illustration of the conventional MA system identification). This conventional time-domain model selection approach incorporates the often-exploited *a priori* knowledge in system identification

that the current output correlates more with recent inputs/outputs than with remote ones. It does not allow construction of data-specific candidate models or impose explicit frequency-related constraints. Since most physiologic signals are colored, it may be beneficial to take into account the frequency information inherent in the signals in model selection.

The WPCR-based system identification method to be presented here seeks solutions to achieve the desirable goal of letting the data determine the candidate models in an efficient manner. In addition, the candidate model terms considered by this method are components in the input (and output) signal with different asymptotic frequencies (Figure 2-1), which facilitates model selection with a consideration of frequency properties. As will be demonstrated, the basis functions of the estimated impulse response with the WPCR method are sinusoids modulated by some weighting function (Figure 2-1).

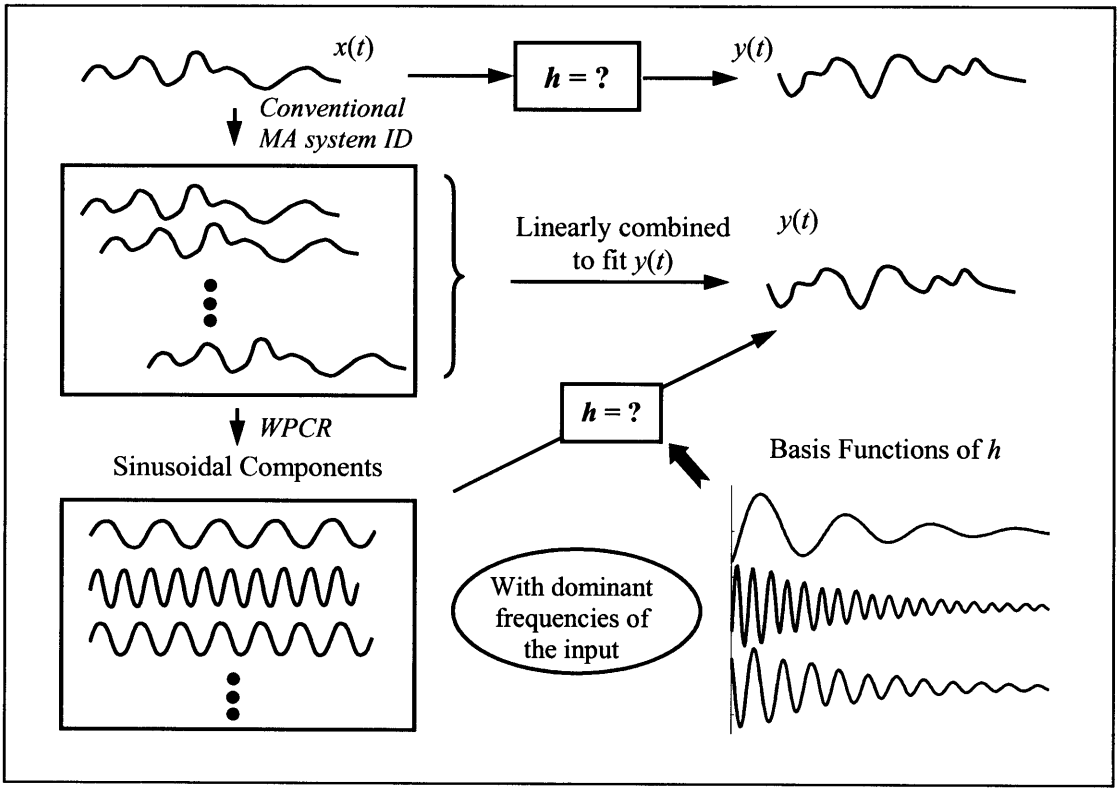

Figure 2-1 Graphical overview: the WPCR method and the conventional MA system identification

2.4 Basic PCR-Based System Identification Approach

In this section, we start with open-loop single-input single-output (SISO) systems with the input denoted as $x(t)$ and output as $y(t)$, where t is discrete time. The MA model (Equation (2.3)) without any weighting scheme is analyzed first for the sake of simplicity. Note that this model is appropriate provided that the system impulse response can be approximated by a finite number of samples without loss of accuracy.

$$Y = XA + E \tag{2.3}$$

where $Y = \begin{bmatrix} y(t) \\ y(t+1) \\ \vdots \\ y(t+N) \end{bmatrix}$, $X = \begin{bmatrix} x(t) & x(t-1) & \dots & x(t-p) \\ x(t+1) & x(t) & \dots & x(t-p+1) \\ \vdots & \vdots & \dots & \vdots \\ x(t+N) & x(t-1+N) & \dots & x(t-p+N) \end{bmatrix}$, $A = \begin{bmatrix} a_0 \\ a_1 \\ \vdots \\ a_p \end{bmatrix}$

and E is the error vector: $E = [e(t), e(t+1), \quad , e(t+N)]^{\mathrm{T}}$ that is often assumed to be uncorrelated with the input in open-loop systems.

The number of columns $(p+1)$ in X should be sufficiently large to cover the whole duration of the finite impulse response (FIR) function which can approximate the system relatively accurately. If $p+1$ is greater than the number of nonzero samples in the true impulse response, then the true value of the corresponding extraneous elements in A should be zero. We consider decomposing X into its principal components and solving the linear regression problem in the domain of PCs. The standard singular value decomposition (SVD) of X is (as presented in Equation (2.1) and rewritten below):

$$X = UDV^T \tag{2.4}$$

As aforementioned, the column vectors of U (principal components) are the eigenvectors of the matrix XX^T, the column vectors of V are the eigenvectors of the matrix X^TX, and D is a diagonal matrix with its diagonal elements (singular values) being the square root of the eigenvalues of X^TX (or XX^T).

Combining equations (2.3) and (2.4), we have:

$$Y = UDV^T A + E = UB + E \tag{2.5}$$

where $B \triangleq DV^T A$.

If some of the diagonal elements of D are small or nearly zero, it means that the corresponding PCs have small variances and consequently less information. We should, therefore, rank the PCs according to their singular values in evaluating their contributions to the output. Specifically, we rank the PCs in a descending order of singular values and form a series of matrices $\hat{U}$ each containing a subset of PCs by adding one PC at a time as a column vector. Hence, the matrices $\hat{U}$ differ by the number of columns involved and their associated regression equations ($Y = \hat{U}\hat{B} + \hat{E}$) represent the candidate models from which the "best" model should be selected. Note that these candidate models are data-specific. For model selection, we employ the widely used model order selection criteria (as discussed in Chapter 1), such as Akaike's Final Prediction Error (FPE) criterion [27] and Rissanen's minimum description length (MDL) criterion [40].

Assume q PCs are involved in the candidate model which minimizes the model selection criterion, we denote the corresponding diagonal singular value matrix as $\hat{D}$, and the corresponding matrix V which consists of only the eigenvectors in pair with those in $\hat{U}$ as $\hat{V}$ (the dimension of $\hat{U}$ is N x q, that of $\hat{D}$ is q x q, and that of $\hat{V}$ is p x q).

The least squares solution of B is:

$$\hat{B} = (\hat{U}^T\hat{U})^{-1}\hat{U}^T Y = \hat{U}^T Y \tag{2.6}$$

Therefore:

$$\hat{A} = \hat{V}\hat{D}^{-1}\hat{B} \tag{2.7}$$

In the above setting, the basis functions of $\hat{A}$ (the impulse response) are the column vectors in $\hat{V}$. Note that since the PCs are orthogonal, the linear least squares estimate of B via $\hat{U}$, the regressor matrix, has a succinct expression. Each entry in $\hat{B}$ is unbiasedly estimated. However, the estimate $\hat{A}$ is biased relative to the true A_0 in the MA structure in Equation (2.3) due to exclusion of some of the PCs in $\hat{U}$. In addition, it is evident that the

variance of each element in $\hat{B}$ is the same as the noise variance σ^2 (in case of white noise). Therefore, the variance for each element in $\hat{A}$ is:

$$\text{var}(\hat{a}_j) = (\sum_{k=1}^{q} \frac{\hat{V}_{kj}^2}{\hat{d}_k^2}), j = 1, \quad , p \tag{2.8}$$

where $\hat{d}_k$ is the k^{th} diagonal element of $\hat{D}$. $\hat{V}_{kj}$ denotes the j^{th} element of the k^{th} column vector of $\hat{V}$ ($\hat{V}_k$). It can be seen that by excluding the PCs associated with smaller $\hat{d}_k$'s, we are able to reduce the variances of the estimated model parameters. Hence, the PCR method provides an estimate of the system parameters based on a trade-off between bias and variance which may possibly reduce the mean-squared-error.

2.5 Frequency Domain Interpretation

In this section, we interpret the basic PCR approach in the frequency domain. It can be shown that the insights provided by a frequency domain analysis are very helpful in further understanding and improving the basic PCR method. First, we briefly summarize some well-known properties of Toeplitz matrices.

2.5.1 Property of Toeplitz Matrices

In the intended scope of this thesis, the physiological signals involved are usually obtained when the subjects/patients are in a stable, resting condition. Therefore, it is reasonable to assume that $x(t)$ and $y(t)$ are stationary signals. The covariance matrix of a stationary random signal is a symmetric Toeplitz matrix which means that its down-diagonal elements are the same. It has been proved in statistics that the eigenvectors of this matrix are asymptotically sinusoids with different frequencies if the covariance function of the signal is abso-

lutely summable[2] [85, 103]. Specifically, assume that u_t is stochastic with zero mean and is weakly stationary, that is, the s^{th} autocovariance $\gamma_s = E(u_t u_{t+s}), s = 0,\pm1,\pm2,...$ is independent of t. Therefore, the variance matrix Υ of T successive values of u_t is a symmetric Toeplitz matrix. It can be proved that the matrix Υ is asymptotically diagonalized by an orthogonal Fourier matrix F, whose first column F_1 has constant elements $1/\sqrt{T}$ [85]. If T is odd, assume $T = 2m+1$, then the $(2j)^{th}$ column F_{2j} of F is represented by:

$$\left[\sqrt{2/T}\cos(2\pi jt/T), t = 1,2,...,T\right], j = 1,2,...,m \tag{2.9}$$

the $(2j+1)^{th}$ column F_{2j+1} of F is represented by:

$$\left[\sqrt{2/T}\sin(2\pi jt/T), t = 1,2,...,T\right], j = 1,2,...,m \tag{2.10}$$

The eigenvalues associated with F_{2j} (j = 1, 2, , m) and also to F_{2j+1} (j = 0, 1, , m) are asymptotically:

$$\frac{1}{2\pi}\sum_{h=-\infty}^{\infty}\gamma(h)e^{-i2\pi hj/T} \tag{2.11}$$

If T is even, assume $T = 2m+2$, the first $2m+1$ eigenvectors are the same as above, there is an extra eigenvector $(1/\sqrt{T})[1,-1,1,...,-1]$ associated with $j = m+1$, and its corresponding eigenvalue is:

$$d_T = \frac{1}{2\pi}\sum_{h=-\infty}^{\infty}\gamma(h)\cos\pi h$$

(Appendix A provides a detailed proof of the above property based on the presentations in Refs. [85, 104].)

---

[2] Absolute summability of a sequence $\{x_j\}$ is defined as $\lim_{n\to\infty}\sum_{j=0}^{n}|x_j| < \infty$. Covariance functions of most stationary time series demonstrate this property.

2.5.2 Frequency Domain Interpretation of the PCR Method

For the matrix X defined in Equation (2.3), when $N \to \infty$, $p \to \infty$, $X^{\mathrm{T}}X$ and XX^{T} can be taken as approximations, within a scale factor, of the covariance matrix of $x(t)$. Therefore, based on the above property of the covariance matrix of a stationary time series, column vectors in the eigen-matrices U and V are sinusoids asymptotically. In addition, the singular values correspond to the "amplitudes" of these sinusoids. Therefore, the decomposition of matrix X in Equation (2.4) is asymptotically equivalent to representing the information inherent in X using sinusoids with different frequencies.

To illustrate the above property, we simulated a simple stationary time series $x(t)$ (Figure 2-2) sampled from a periodic, zero-mean square wave. The matrix X (dimension 1000 × 500) was constructed according to its definition in Equation (2.3). Due to the periodic nature of $x(t)$, the SVD of matrix X results in about 80 (the period of $x(t)$) nonzero singular values whose corresponding singular vectors are approximately sinusoidal. For illustration purpose, Figure 2-3 displays the first and third column vectors in U and V respectively (the second singular vector is not shown here since it has the same frequency (different phase) as the first one). It can be appreciated that the first column vectors of U and V have the same frequency as the dominant component in $x(t)$. Note that the singular vectors have been rearranged in descending order of their associated singular values. Therefore, the column indices are different from those in Equations (2.9) or (2.10). In addition, it needs to be pointed out that since the mean of $x(t)$ is zero, the eigen-matrix of the covariance matrix does not contain a column with constant elements.

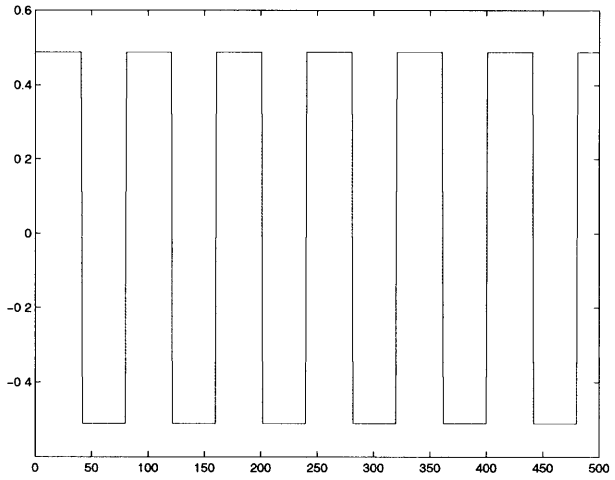

Figure 2-2 A simulated stationary time series (for illustration purpose, only 500 samples are shown here.)

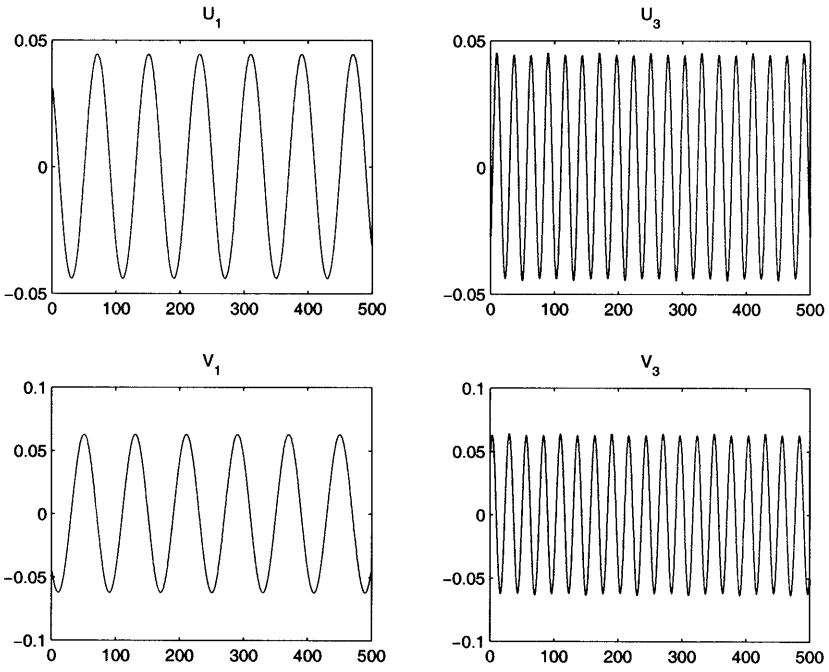

Figure 2-3 Singular value decomposition results of X (note that only the first 500 samples of U_1 and U_3 are shown here for illustration.)

Based on the above properties, the proposed PCR method can be interpreted as, asymptotically, selecting the dominant frequency components (PCs) of the input signal according

to their amplitudes and correlating them with the output signal. The computed coefficient vector $\hat{B}$ in Equation (2.6) corresponds to the "weight" by which each input frequency component is represented in the output. Asymptotically, the basis functions of the estimated impulse response (Equation (2.7)) are sinusoids (V_i) corresponding to the PCs involved in the regression. With the aid of a model order selection criterion, the PCR method chooses a subset of PCs, thereby regressing the output only upon the dominant frequency components of the input. Excluding the frequency components poorly represented in the input can improve the accuracy of the estimated model parameters, which may be appreciated by inspecting Equation (2.8) and also be demonstrated rigorously as follows.

Consider the least squares problem in Eqs. (2.5) and (2.6) in the frequency domain. We assume N→∞ such that:

$$\hat{B} = \arg\min_{B} E\varepsilon^2(t,B) = \arg\min_{B} \frac{1}{2\pi}\int_{-\pi}^{\pi} \Phi_{\varepsilon}(\omega,B)d\omega \tag{2.12}$$

where $\Phi_{\varepsilon}(\omega)$ represents the power spectrum of the residual error $\varepsilon(t)$. From Equation (2.5), we have:

$$Y = \sum_{i=1}^{p} U_i b_i + E \tag{2.13}$$

where U_i is the i^{th} column of matrix U and b_i is the i^{th} element in vector B. Therefore, at time t, $\varepsilon(t)$ can be expressed as:

$$\varepsilon(t) = y(t) - \sum_{i=1}^{p} u_i(t) b_i = \sum_{i=1}^{p} u_i(t)(b_{0i} - b_i) + v_0(t) \tag{2.14}$$

where b_{0i} represents the true coefficient corresponding to the i^{th} PC and $v_0(t)$ is the true noise term. Note that the true PCs and the ones in Equation (2.14) can be the same although the matrix X in Equation (2.3) may be unnecessarily large compared to the data matrix necessary to represent the true MA model of the system. This is because in the expression of the true system, the same matrix X as in Equation (2.3) can always be utilized while setting the coefficients in B_0 which correspond to the extraneous columns of X to be zero.

The variance of the residual error is:

$$\begin{aligned} E\varepsilon(t)\varepsilon(s) &= E\left[\sum_{i=1}^{p} u_i(t)u_i(s)(b_{0i}-b_i)^2\right] + Ev_0(t)v_0(s) \\ &+E\left[\sum_{i=1}^{p} u_i(t)(b_{0i}-b_i)v_0(s)\right] + E\left[\sum_{i=1}^{p} u_i(s)(b_{0i}-b_i)v_0(t)\right] \end{aligned} \tag{2.15}$$

Note that we have utilized the property that the PCs are orthogonal to each other. It is evident that the last two terms in Equation (2.15) reduce to zero because in open-loop systems, it is an acceptable assumption that the added noise is uncorrelated with the input $x(t)$. Using the equality in Equation (2.6), that is, $b_i = d_i V_i^T A$, where d_i is the i^{th} singular value, and V_i is the i^{th} column of matrix V, Equation (2.15) can be simplified into:

$$\begin{aligned} E\varepsilon(t)\varepsilon(s) &= E\left[\sum_{i=1}^{p} u_i(t)u_i(s)(d_i V_i^T(A_0 - A))^2\right] + Ev_0(t)v_0(s) \\ &= \sum_{i=1}^{p} d_i^2 E\left[u_i(t)u_i(s)\right]\left\|A_0 - A\right\|^2 + Ev_0(t)v_0(s) \end{aligned} \tag{2.16}$$

Therefore,

$$\hat{A} = \arg\min_{A} \frac{1}{2\pi}\int_{-\pi}^{\pi}\left[\sum_{i=1}^{p} d_i^2 \Phi_{u_i}(\omega)\left|A_0(e^{j\omega}) - A(e^{j\omega})\right|^2 + \Phi_{v_0}(\omega)\right]d\omega \tag{2.17}$$

Equation (2.17) indicates that, in the frequency domain, the least squares problem is weighted such that the fit between the actual and the estimated transfer functions is favored at frequencies associated with larger singular values. Since the PCR-based system identification technique chooses a subset of frequency components based on the singular values, the insignificant components that would be associated with larger estimation error in the model parameters are discarded, therefore reducing the error (variance) in system identification.

In practice, since only finite data are available, the asymptotic properties of the singular vectors may not be demonstrated precisely. In that case, they are not *pure* sinusoids, but often mixtures of several sinusoidal components. Those associated with large singular values consist of some dominant frequency components in the signal $x(t)$. This imperfect separation of difference frequency components is similar to the issue in Fourier analysis that the

resolution in the frequency domain is lower when fewer data are available. Nevertheless, the compromise of the asymptotic properties of singular vectors does not affect the above frequency domain interpretation of the PCR method.

Since a comparison of the PCR method and the traditional ARX method will be performed in later sections, we next briefly summarize the frequency domain interpretation of the ARX method in terms of the AR and MA transfer functions [2]. Specifically, assume the measured input-output signals are related according to the following system:

$$y(t) = G_0(q^{-1})x(t) + v_0(t) \tag{2.18}$$

and the estimated model is of a traditional ARX structure:

$$M(q^{-1})y(t) = N(q^{-1})x(t) + \varepsilon(t) \tag{2.19}$$

where q^{-1} is the delay operator, $M(q^{-1})$ and $N(q^{-1})$ contain the AR and MA transfer function operators respectively. It can be proved that the least squares problem in this case may be interpreted in the frequency domain as [2, 57]:

$$\hat{\theta} = \arg\min_{\theta} \frac{1}{2\pi} \int_{-\pi}^{\pi} \left|M(e^{j\omega})\right|^2 \left[\left| G_0(e^{j\omega}) - \frac{N(e^{j\omega})}{M(e^{j\omega})} \right|^2 \Phi_u(\omega) + \Phi_{v_0}(\omega) \right] d\omega \tag{2.20}$$

where θ denotes the vector including both AR and MA parameters. This equation also suggests that the least squares problem is weighted such that the fit between the actual and the estimated transfer functions is favored at frequencies where the quantity $\left|M(e^{j\omega})\right|^2 \Phi_u(\omega)$ is large [2, 57]. Since the traditional ARX model identification method does not impose a selection criterion in the frequency domain, the estimation accuracy may be compromised if the input spectrum has low amplitudes at some frequencies, i.e., when the signal is colored.

2.6 Weighted-PCR (WPCR)-Based System Identification Approach and Its Interpretation

As aforementioned, the *a priori* knowledge often utilized in solving system identification problems is that the current output is correlated more with recent inputs than with remote ones. In this section, we incorporate this pre-knowledge by imposing a weighting scheme on the input vectors to improve the PCR method. Specifically, we intend to define a weighting factor for each delayed input term, i.e. each column in the data matrix X, prior to solving the system identification problem. Therefore, a diagonal matrix W with its diagonal elements sorted in descending order needs to be constructed so that the matrix XW contains weighted delayed inputs vectors. The explicit values of the diagonal elements of W and the practical advantage of this weighting scheme will be discussed in Section 2.8.1.

Recall that the data matrix in Equation (2.3) is defined as:

$$X = \begin{bmatrix} x(t) & x(t-1) & \dots & x(t-p) \\ x(t+1) & x(t) & \dots & x(t-p+1) \\ \vdots & \vdots & \dots & \vdots \\ x(t+N) & x(t-1+N) & \dots & x(t-p+N) \end{bmatrix}$$

We denote the diagonal matrix W as: $W = \begin{bmatrix} w_0 & 0 & \cdots & 0 \\ 0 & w_1 & \ddots & 0 \\ \vdots & \ddots & \ddots & \vdots \\ 0 & \dots & 0 & w_p \end{bmatrix}$

The system identification problem now becomes:

$$Y = XWA_w + E \tag{2.21}$$

where W is pre-defined, A_w is the parameter vector to be identified and WA_w is equivalent to A in Equation (2.3). To solve for A_w, similar procedures as proposed in the basic PCR method can be carried out. Denote the SVD of XW as: $U_w D_w V_w^T$, then the regression equation (2.21) can be written as:

$$Y = U_w D_w V_w^T A_w + E \triangleq U_w B_w + E \tag{2.22}$$

Assume q PCs are selected to minimize the model order selection criterion and they correspond to the following matrices: $\hat{U}_w, \hat{V}_w, \hat{D}_w$, then we have:

$$\hat{B}_w = \hat{U}_w^T Y \tag{2.23}$$

and

$$\hat{A}_w = \hat{V}_w \hat{D}_w^{-1} \hat{B}_w \tag{2.24}$$

Therefore,

$$\hat{A} = W\hat{A}_w = W\hat{V}_w \hat{D}_w^{-1} \hat{B}_w \tag{2.25}$$

To explore the frequency domain interpretation of the weighted-PCR (WPCR) method, we consider the following matrix multiplication:

$$\begin{aligned}(XW)*(XW)^T = {} & w_0^2 \begin{bmatrix} x(t) \\ x(t+1) \\ \vdots \\ x(t+N) \end{bmatrix} \begin{bmatrix} x(t) & x(t+1) & \cdots & x(t+N) \end{bmatrix} + \cdots + \\ & w_p^2 \begin{bmatrix} x(t-p) \\ x(t-p+1) \\ \vdots \\ x(t-p+N) \end{bmatrix} \begin{bmatrix} x(t-p) & x(t-p+1) & \cdots & x(t-p+N) \end{bmatrix}\end{aligned} \tag{2.26}$$

It is evident that, asymptotically ($p \to \infty$), the above expression is approximately proportional to the covariance matrix of $x(t)$ (with the proportional factor $\sum_{i=0}^{p} w_i^2$). Therefore, according to the property of Toeplitz matrices presented previously, the eigenvectors of $(XW)(XW)^T$, i.e., the column vectors in U_w, are also sinusoids with different frequencies, asymptotically.

We next study the properties of D_w and V_w. Since the matrices U_w and V_w are orthonormal, according to the definition of SVD, we have:

$$\begin{aligned} WX^T U_{wi} &= d_{wi} V_{wi} \\ X^T U_i &= d_i V_i \end{aligned} \tag{2.27}$$

where the subscript i denotes the i^{th} column vector of the corresponding matrix and $i = 0, 1, \ldots, p$. Asymptotically, $U_{wi} = U_i$ because they both have unit norm and equivalent frequencies. (For simplicity, we assume the weighting procedure does not change the indices associated with the vectors in U.)[3] Therefore, the following equalities are valid asymptotically:

$$d_{wi}V_{wi} = WX^TU_{wi} = WX^TU_i = W(d_iV_i) = d_i(WV_i) \tag{2.28}$$

Thus,

$$V_{wi} = \frac{d_i}{d_{wi}}WV_i \tag{2.29}$$

Since it is known that V_{wi} has unit norm, we have:

$$\frac{d_i^2}{d_{wi}^2}V_i^TW^2V_i = 1 \tag{2.30}$$

That is:

$$d_{wi} = d_i\sqrt{\sum_{j=1}^{p} w_j^2V_{ij}^2} \tag{2.31}$$

where V_{ij} denotes the j^{th} element of the column vector V_i. Then, substitute Equation (2.31) into Equation (2.29), we have:

$$V_{wi} = \frac{WV_i}{\sqrt{\sum_{j=1}^{p} w_j^2V_{ij}^2}} \tag{2.32}$$

It can be seen that the columns in V_w are sinusoids of different frequencies proportionally modulated by the weighting function (weighted sinusoids). In addition, the singular values of the matrix XW are equivalent to the corresponding scaled singular values of the original matrix X.

---

[3] If the weighting matrix W changes the index of the column vectors in U, i.e., the order of the singular values is altered, the derivation of properties of V_w and D_w only differs by the notation of column indices. The conclusions to be presented later that column vectors in V_w are sinusoids with different frequencies modulated by the weighting matrix W and that diagonal elements in D_w are scaled version of those in D still hold.

The above asymptotic properties of the SVD of XW can be illustrated with the following example. The time series $x(t)$ is again the one demonstrated in Figure 2-2. We construct the matrix X with a dimension of 1000 × 500 and the diagonal elements of W are samples of the exponential function: $exp(-(i-1)/200)$, where i denotes the index of the diagonal elements. Figure 2-4 illustrates the first and third column vectors of U_w and V_w respectively. Note that the envelope of V_{w1} and V_{w3} proportionally fits the exponential weighting function (the red dash-dotted lines in Figure 2-4 are the V_{wi} computed based on Equation (2.32)).

In summary, with the weighting factors applied to the data matrix X, the left and right singular vectors are still sinusoids or weighted sinusoids asymptotically. The previous frequency domain interpretation about the proposed PCR approach is still applicable.

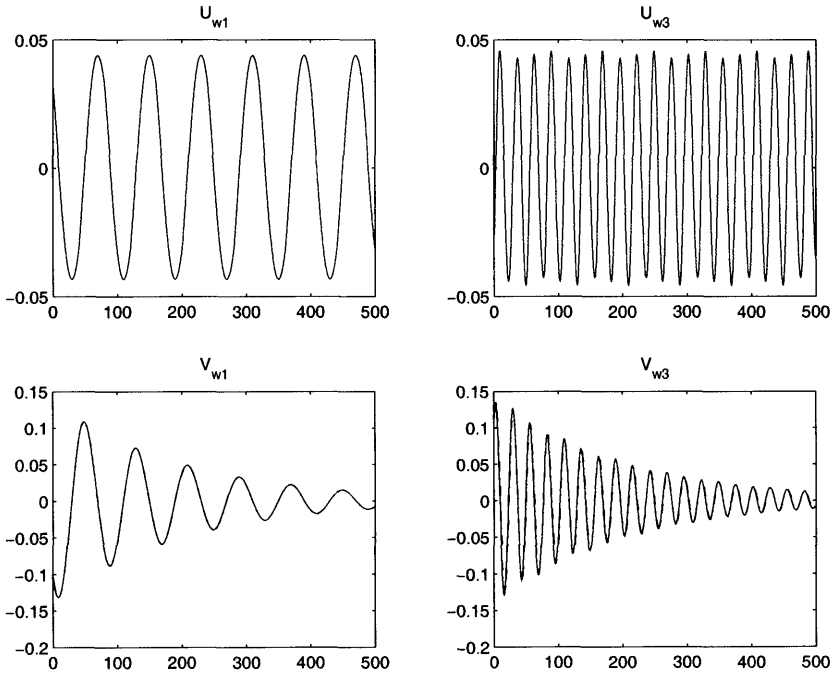

Figure 2-4 Singular value decomposition results of XW (note that only the first 500 samples of U_{w1} and U_{w3} are shown here for illustration; the dash-dotted lines in the lower two subplots represent V_{wi} computed based on Equation (2.32).)

Lastly, based on the above results, we can express the estimated parameter $\hat{A}$ as:

$$\begin{aligned}\hat{A} &= W\hat{A}_w = W\hat{V}_w\hat{D}_w^{-1}\hat{B}_w \\ &= W\sum_{i=1}^{q}\hat{V}_{wi}\frac{\hat{b}_{wi}}{\hat{d}_{wi}} \\ &= \sum_{i=1}^{q}\frac{1}{k^2}W^2\hat{V}_i\frac{\hat{b}_{wi}}{\hat{d}_i}, \quad \text{where } k=\sqrt{\sum_{j=1}^{p}w_j^2V_{ij}^2}\end{aligned} \tag{2.33}$$

where $\hat{V}_i$ is the i^{th} column vector of matrix $\hat{V}$. Note that Equations (2.31) and (2.32) have been incorporated into Equation (2.33). The above equality indicates that the basis functions of the estimated impulse response are $W^2\hat{V}_i$ ($i = 0, 1, \quad , q$), which are, asymptotically, sinusoids modulated by the weighting factors in W^2. When the noise is white, the variance of the m^{th} elements in $\hat{A}$ is:

$$\text{var}(\hat{a}_m) = \frac{w_m^4}{k^4}\cdot\left(\sum_{i=1}^{q}\frac{\hat{V}_{im}^2}{\hat{d}_i^2}\right)\sigma^2, \quad m = 1, 2, \quad , p \tag{2.34}$$

2.7 WPCR and ARX Structure

Since the output signal accessible in practice is usually a combination of the system output and some measurement noise, an ARX model structure, in which the output delays are included in the regression, may be advantageous because it provides room to model the noise and, thus, the possibility to reduce noise corruption in the estimated parameters. In this section, we discuss application of the WPCR approach in conjunction with ARX structures. To start, we include the delayed output vectors in the data matrix (as in Equation (2.3)) in addition to the input vectors. The system identification problem now becomes:

$$Y = \Phi A + E \tag{2.35}$$

where $\Phi = \begin{bmatrix} y(t-1) & \dots & y(t-m) & x(t) & \dots & x(t-p) \\ y(t) & \dots & y(t-m+1) & x(t+1) & \dots & x(t-p+1) \\ \vdots & \dots & \vdots & \vdots & \dots & \vdots \\ y(t-1+N) & \dots & y(t-m+N) & x(t+N) & \dots & x(t-p+N) \end{bmatrix}$, and $A = \begin{bmatrix} b_1 \\ \vdots \\ b_m \\ a_0 \\ \vdots \\ a_p \end{bmatrix}$

Simply substituting the matrix X in Equation (2.21) (the weighted MA equation) with the new matrix Φ, the same approach can be employed to estimate A as delineated for the MA structure previously. We should now investigate if there exists a similar frequency domain interpretation for the ARX structure.

For stationary data, it is obvious that the principal components of Φ (eigenvectors of $\Phi\Phi^T$), denoted as U_i, are still sinusoidal asymptotically (although contaminated by noise due to the inclusion of $y(t)$) using the same argument as for the MA structure. On the other hand, each of the eigenvectors of $\Phi^T\Phi$ (i.e., V_i) can be proved to be a concatenation of two sinusoids asymptotically.

To prove the above statement, consider the relationship between U_i and V_i:

$$\Phi^T U_i = d_i V_i \tag{2.36}$$

Denote Φ by two sub-matrices Φ_X and Φ_Y. Φ_X contains delays of the input vector and Φ_Y contains delays of the output vector. Equation (2.36) becomes:

$$\begin{bmatrix} \Phi_Y^T \\ \Phi_X^T \end{bmatrix} [U_i] = d_i \begin{bmatrix} V_i^U \\ V_i^L \end{bmatrix} \tag{2.37}$$

where V_i^U represents the upper part of V_i that has the same number of rows as Φ_X^T; V_i^L represents the lower part of V_i that has the same number of rows as Φ_Y^T. That is:

$$\Phi_Y^T U_i = d_i V_i^U \tag{2.38}$$

$$\Phi_X^T U_i = d_i V_i^L \tag{2.39}$$

It is evident that the left sides of the above two equations are convolutions. Since U_i is sinusoidal asymptotically, V_i^U and V_i^L are also sinusoids with the same frequency, but they may have different phase. Hence, V_i is a concatenation of two sinusoids asymptotically. Therefore, the asymptotic frequency domain interpretation of the PCR method is still valid using an ARX structure.

In addition, although the derivation of Equation (2.17) is based on an MA-structured model, it is also applicable to ARX models if the additive noise is white. Furthermore, the basis functions of the coefficient vector A are V_i's, i.e., a concatenation of two sinusoids. However, it is hard to derive the basis function for the system impulse response (denoted as h) due to the nonlinearity in the relationship between A and h.

When the matrix Φ is weighted by a pre-defined weighting matrix W (as in Equation (2.21)), assume $\Phi W = U_w D_w V_w^T$, then the PCs (U_{wi}) remain sinusoidal asymptotically and V_{wi} are related to V_i through Equation (2.29). The derivations are similar as presented in section 2.6.

Heuristically, the advantage of using an ARX structure may be due to the fact that delayed output vectors in matrix Φ contain frequency components from both the input and the noise. Because SVD is carried out on the matrix Φ as a whole, the frequency components from the input data were contributed by both Φ_X and Φ_Y, while the frequency components from the noise disturbance were only contributed by Φ_Y. Under certain circumstances, for example, when the input is colored and/or the noise is colored and out-of-band with the input spectrum, the WPCR-ARX method may result in a more accurate estimate of A.

2.8 Application of the WPCR Approach with MA Structures

In this section, we discuss the application of the WPCR approach with MA structures (WPCR-MA) in open-loop and closed-loop systems. Simulated impulse responses which resemble those involved in cardiovascular systems are employed to generate the input/output data. The performance of the WPCR approach is compared with that of the conventional

method in constructing candidate models for ARX system identification and Generalized Least Squares (GLS) system identification, i.e., adding to the structure one delayed input/output term at a time in an order of increasing shifts relative to the current output.

2.8.1 The Weighting Scheme

To apply the WPCR-MA method, we should first determine the functional form of the weighting factors in the diagonal matrix W. According to Equation (2.33), the weighting function imposes an envelope upon the basis function of the estimated impulse response. Since in the widely employed ARX model identification, basis functions of the estimated impulse response are real or complex exponentials, we consider using a similar exponential function as the weighting function for WPCR, i.e., the diagonal elements in W are defined as $e^{-n/\tau}$, $n = 0, 1, 2, \quad , p$. This weighting scheme assumes a larger weight for the recent delays in the data matrix than for the remote ones, which is consistent with the aforementioned *a priori* knowledge.

The next step is to determine the value of the time constant τ in the weighting function. Evidently, it should be affected at least partially by the duration of the true impulse response, which is, however, inaccessible. To solve this problem, one may search for the "best" value of τ according to the following procedure: 1) Use an MA model that has a sufficiently large order to fit the input-output data through ordinary least squares estimation; 2) Inspect the estimated impulse response, which may be heavily corrupted by noise, to determine the maximum number of columns (p) needed in the data matrix. Note that the above two steps are necessary for most system identification approaches. 3) Take $p/1.5$ as the upper bound of the range of possible values of τ; 4) The lower bound of this range can be taken as 1 in general or be determined also by inspecting the estimated impulse response in step 1) — If the minimum possible length is approximately l, then take the lower bound as $l/1.5$. 5) Perform WPCR-MA identification with τ varying in the range (with an increment being 1 or lower as needed) and select the value which leads to a minimum FPE or MDL. In steps 3) and 4), the factor 1.5 is chosen empirically by noting that at $n = 1.5\tau$ the exponential func-

tion $e^{-n/\tau}$ decays to 77.7% of the value corresponding to $n = 0$. Since our goal is to obtain an accurate estimate of the impulse response function, the effectiveness of the above procedure depends on the ability of FPE or MDL to minimize the impulse response error, which is equivalent to output prediction error.

To evaluate the performance of the above procedure in selecting a value of τ that leads to a small impulse response error, we simulated an LTI system $y(t) = h(t)*x(t) + e(t)$ using the transfer function, input spectra and noise spectra illustrated in Figure 2-5. This impulse response consists of two triangular shapes and it is not analytical. It is a typical representation of those often utilized in modeling cardiovascular autonomic control systems [57] which is a main application to be studied in this thesis. The simulated input is a colored process as are many physiologic signals. Two types of additive noise are implemented which are in-band or out-of-band relative to the input spectrum. The previously proposed procedure was carried out to determine the "best" value of τ and to compute its associated impulse response error. To obtain a "gold standard" for the value of τ, we explicitly computed the impulse response error in each simulation corresponding to every value of τ in the range being considered and take the optimal τ as the one leading to the minimum error. The impulse response error is defined as:

$$\text{Impulse response error} = 100 * \sqrt{(h_0 - \hat{h})^T (h_0 - \hat{h}) \Big/ h_0^T h_0} \tag{2.40}$$

where h_0 is the true impulse response function and $\hat{h}$ is the estimate.

100 realizations were simulated for each type of noise. In each simulation, 30 input delayed vectors of 1000 samples long were included in the data matrix; therefore the upper limit of the searching range of τ was 10. We specified the lower limit as 4 and used a unit increment. Figure 2-6 shows the impulse response errors resulted from the searching procedure and the "gold standard". The model order is selected by minimizing the MDL criterion (see Chapter 1).

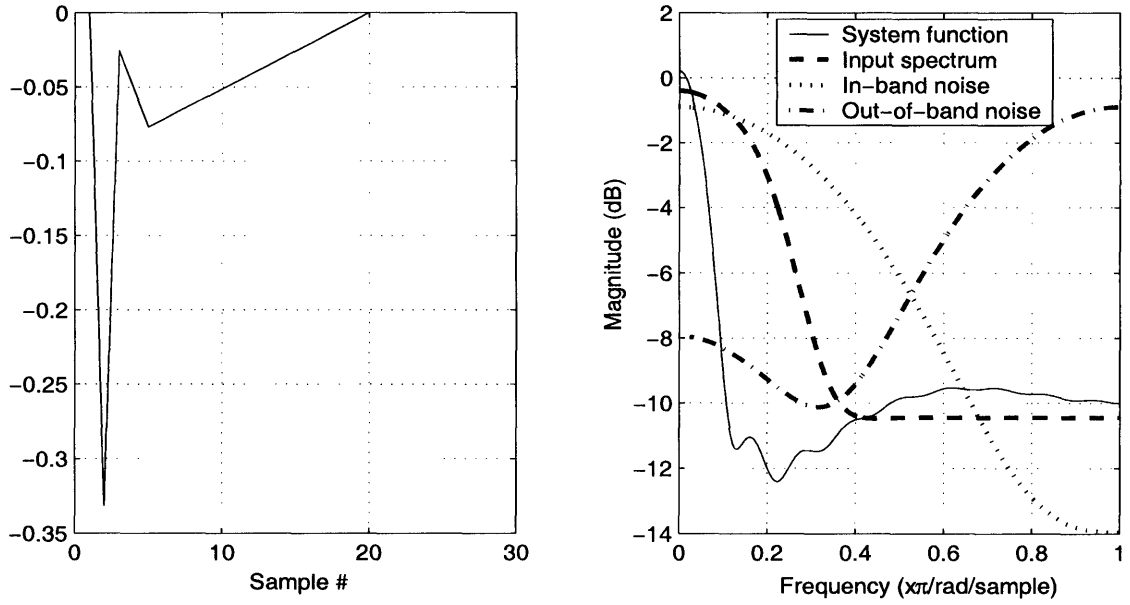

Figure 2-5 (a) Impulse response of the simulated system; (b) Frequency responses of the system transfer function (solid), the filter generating colored inputs (dashed), the in-band noise (dotted) and the out-of-band noise (dash-doted).

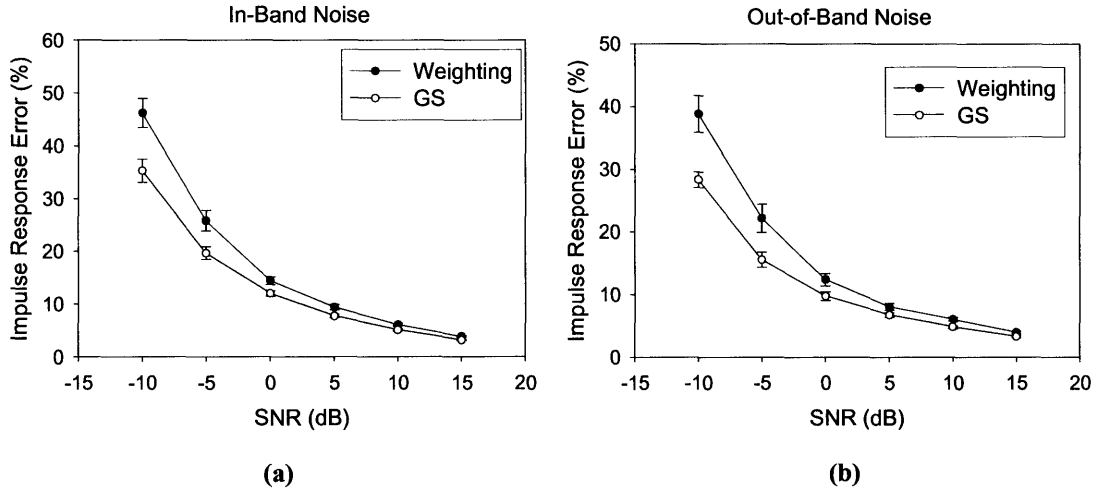

Figure 2-6 Comparison of impulse response errors estimated through the proposed searching procedure of the value of τ (Weighting) and through the "gold standard" estimation of τ (GS). The MDL criterion was employed. (a) simulation with in-band noise; (b) simulation with out-of-band noise. (Values are mean±1.96*SE of 100 noise realizations)

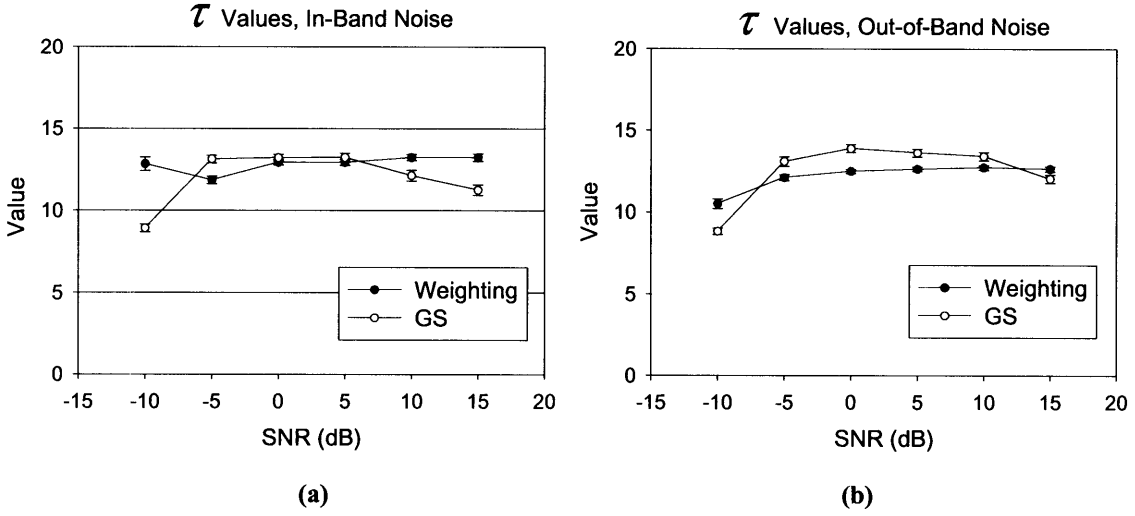

Figure 2-7 Value of τ obtained with the "gold standard" (GS) and the proposed searching procedure (Weighting). (a) simulation with in-band noise; (b) simulation with out-of-band noise. (Values are mean±1.96*SE of 100 noise realizations)

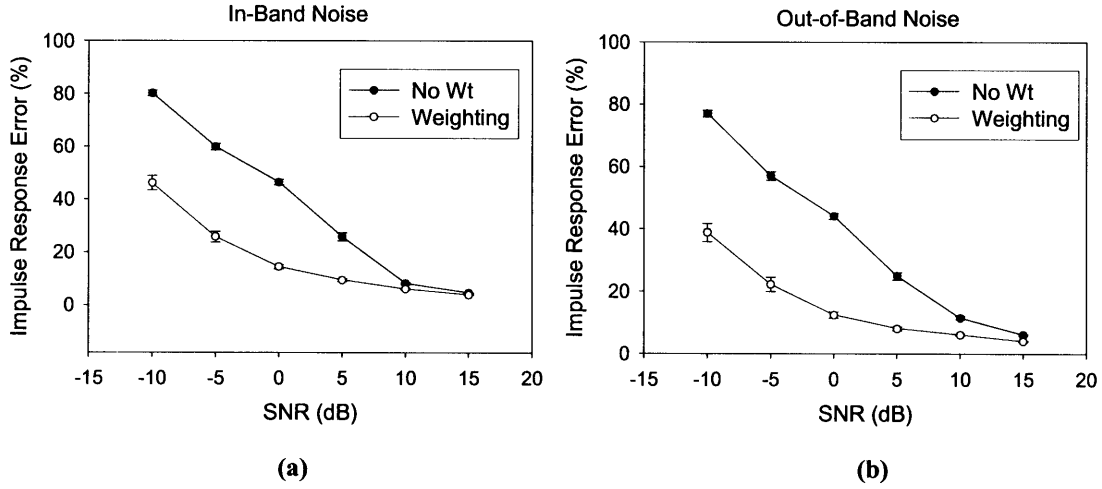

Figure 2-8 Comparison of impulse response errors estimated by the unweighted PCR method (No Wt) and the weighted PCR method (Weighting). (a) simulation with in-band noise; (b) simulation with out-of-band noise. (Values are mean±1.96*SE of 100 noise realizations)

Figure 2-7 shows the values of τ determined by the "gold standard" and the searching procedure respectively. Values resulted from the two methods are not statistically different (p = 0.32 for in-band noise, p = 0.57 for out-of-band noise using paired-t test). Both meth-

ods lead to values of τ around two thirds of the duration of the true impulse response (20/1.5).

For comparison purpose, we present results of the unweigthed-PCR-MA and WPCR-MA methods in Figure 2-8. It can be seen that the weighting scheme improved the identification accuracy significantly especially at low SNRs.

From a practical point of view when only finite data are available for system identification, the weighting scheme effectively enhances the performance of the PCR method due to the following reasons (in addition to the incorporation of *a priori* knowledge): 1) With the weighting scheme, the basis functions of the estimated impulse response (exponentially decaying sinusoids) are more appropriate for FIR systems than those in the unweighted case (sinusoids) since such systems always have their impulse responses decay to zero; 2) The distribution of weighted singular values is in a wider range and more regular (approximately an exponential function in case of white noise as illustrated in Figure 2-9) than the unweighted ones. Therefore, if the data matrix is disturbed by noise (e.g., in ARX structures) or if only finite data are available (which is the realistic case), the rank of the weighted singular values is more robust. This rank matters in the WPCR method because it determines the order according to which the PCs are added into the regression, thus affecting the value of MDL or FPE and how well they approximate the prediction error; 3) With finite data, the first few weighted singular values usually represent a larger portion of the total energy than the unweighted ones. Hence, the model order (number of PCs in regression) is often reduced by the weighting scheme which may enable a reduction in the variance of estimated model parameters. Similar weighting scheme may be proposed in studying noise-perturbed matrices in certain problems, such as in the total least squares (TLS) identification.

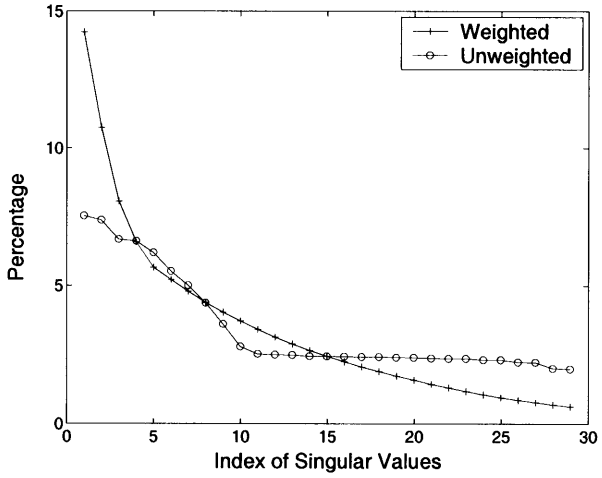

Figure 2-9 An example of normalized singular values ($d_i / \sum_{i=1}^{p+1} d_i$) of the unweighted data matrix and the corresponding values of the weighted data matrix

2.8.2 Open-loop Systems

In this section, we investigate the performance of the WPCR-MA method in identifying open-loop systems. The applications of this method in SISO and MISO system identification problems are very similar. For simplicity, only SISO systems are simulated here. The evaluation of the WPCR-MA method is enabled through comparisons with the conventional ARX model estimation approach. As aforementioned and discussed in Chapter 1, this ARX method is often used in physiologic system identification.

White Input

First, we simulate a SISO system with the transfer function demonstrated in Figure 2-5. Both the system input and the additive noise on the output are white random processes. 100 noise realizations were simulated and 1000 data samples were employed in system identification. For the WPCR method, 30 input delays were included in the data matrix and the weighting scheme proposed previously was incorporated. For the ARX method, the maximum model order evaluated contains 15 AR terms and 15 MA terms.

The impulse response errors based on the WPCR and the ARX methods are displayed in Figure 2-10. For illustration purpose, results of the basic PCR method without the weighting scheme are also included. It can be seen that the performance of the WPCR and ARX methods in this scenario is very similar and the weighting scheme of the WPCR method improves the estimation accuracy at low SNR levels. The improvement resulted from the weighting scheme can be explained by the same arguments presented in the last section. Compared to the conventional ARX method, as discussed in Section 2.5, an important property of the WPCR method is its ability to select dominant frequencies present in the data, and carry out a weighted-parameter estimation so that the coefficients associated with these frequencies are more accurately identified. However, in case of white input and white output noise, there is no room for this frequency selective property to play a role since all frequencies are equivalent in amplitudes and the PCs of the data matrix are ranked randomly and, therefore, weighted randomly by the weighting scheme. Hence, it is expected that the WPCR method does not possess any advantage over the ARX method in case of white signals.

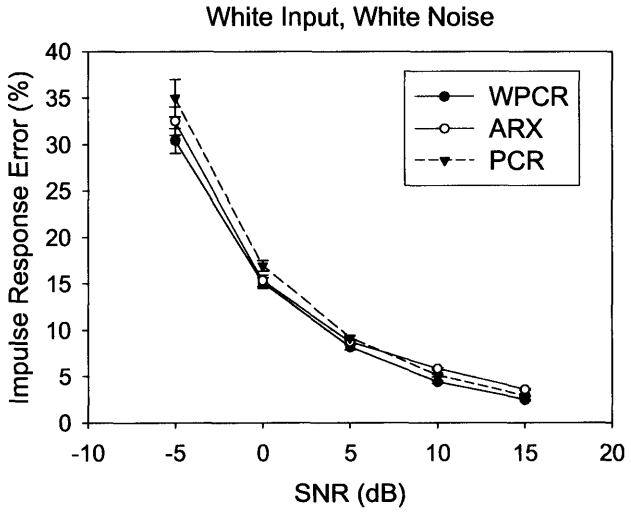

Figure 2-10 Comparison of impulse response errors estimated by the WPCR, PCR and the conventional ARX methods, MDL minimization was employed as the model selection criterion . The system input and the output additive noise are white processes. (Values are mean±1.96*SE of 100 noise realizations)

Colored Input

Using the same system function as in Figure 2-5, we generate the system output corresponding to colored input and colored output noise, the spectra of which are also illustrated in Figure 2-5. Since physiologic signals (e.g. blood pressure, heart rate) involved in system identification are often colored ones, our simulation resembles the realistic cardiovascular systems. We again compare the performance of the WPCR and the ARX methods. The same initial model orders and data length were used as employed for the white input simulations. Note that in theory, the ARX method is able to model both the system function and the noise spectrum. Figure 2-11 shows the impulse response errors induced by each method. It can be appreciated that the WPCR method outperforms the ARX method regardless of the type of output noise. In addition, note that the ARX method itself is more accurate in case of in-band noise than of out-of-band noise, while the performances of the WPCR method in the two cases are approximately equivalent.

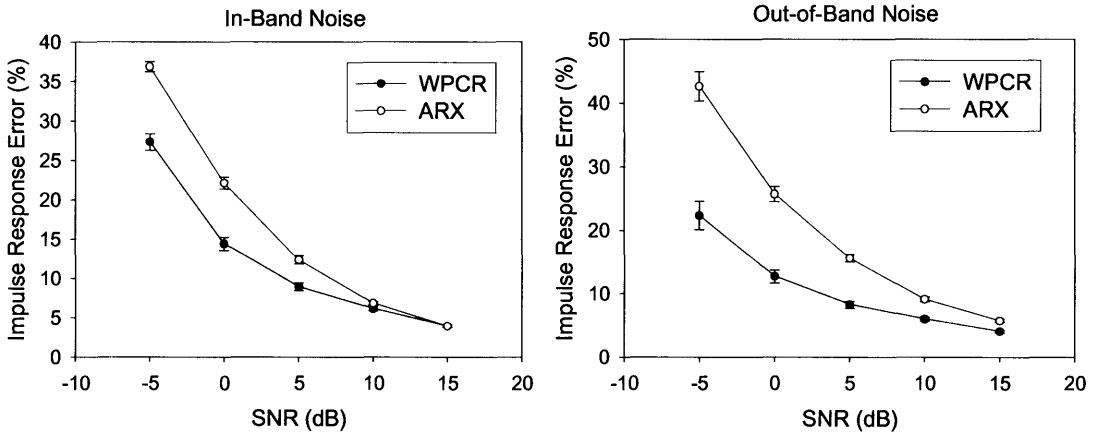

Figure 2-11 Comparison of impulse response errors estimated by the WPCR method and the conventional ARX method, MDL minimization was employed as the model selection criterion. The system input is a colored process. (a) simulation with in-band noise; (b) simulation with out-of-band noise. (Values are mean±1.96*SE of 100 noise realizations)

To further understand the above results, we illustrate the frequency responses of the system function identified by each method when the noise is in-band with the input (Figure 2-12) and when the noise is out-of-band (Figure 2-13).

Based on the estimated frequency responses, it is evident that the ARX method does not impose model selection constraints in the frequency domain while the WPCR method demonstrates this property. In case of in-band noise (low frequency-dominant), the ARX estimation error is relatively high at low frequencies due to the corruption of noise, while it is relatively low at high frequencies because of low noise level (Figure 2-12). In contrast, the WPCR estimation provides a good fit at low frequencies because the PCs with high frequencies (associated with small singular values) are excluded from the regression so that more weight is given to the low frequency coefficients to enhance their estimation accuracy (reduce variance). The spectrum of the WPCR estimate in the high frequency range reflects the summed effect of the dominant PCs at these frequencies which is small but not zero. This is because only finite data are used in system identification and the PCs are not strictly sinusoidal. In case of out-of-band noise (Figure 2-13), the ARX estimation error is relatively small in the low frequency range due to the low noise level (high SNR), while it is relatively high in the high frequency range because of increased noise corruption and decreased input energy (low SNR). Since the input spectrum has low amplitudes at high frequencies, the dominant PCs identified by the WPCR method are mainly associated with relatively low frequencies with little noise corruption. Therefore the WPCR estimate is accurate at these frequencies. Meanwhile, the frequency selective property of WPCR enables an exclusion of the high frequency PCs which have a low SNR. Hence, the overall estimation accuracy of the WPCR method outperforms that of the ARX method. Note that in case of out-of-band noise and low SNR, the WPCR method may still retain some extraneous PCs that represent the noise frequency to reduce the output prediction error. This trade-off explains why the WPCR estimation errors with out-of-band noise are not significantly smaller than those with in-band noise.

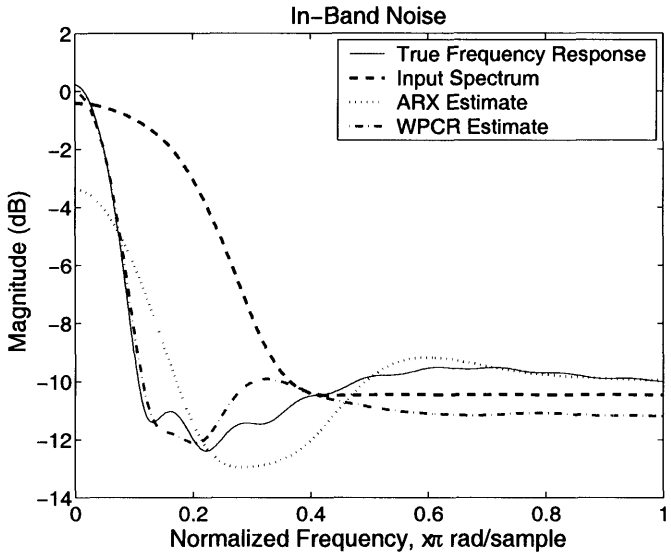

Figure 2-12 Comparison of frequency responses – true frequency response (solid line), ARX estimate (dotted line), WPCR estimate (dash-dotted line); The input spectrum is shown by the dashed line. Results are averaged over 100 simulations of in-band noise (SNR = -5 dB), whose spectrum is illustrated in Figure 2-5.

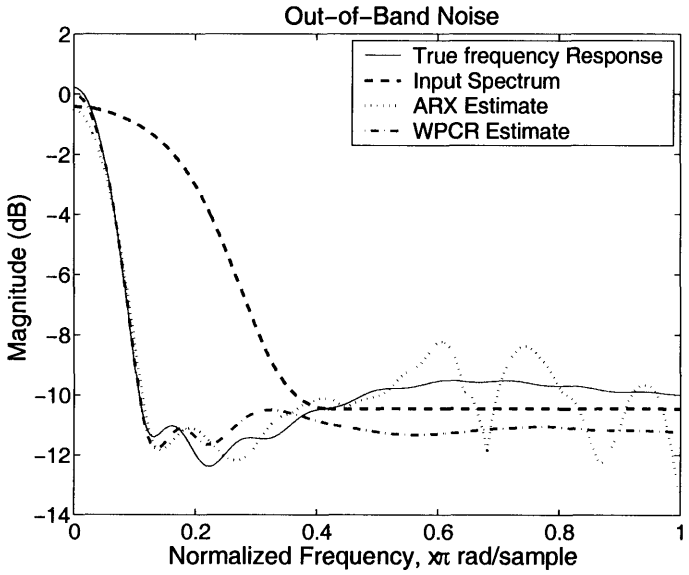

Figure 2-13 Comparison of frequency responses – true frequency response (solid line), ARX estimate (dotted line), WPCR estimate (dash-dotted line); The input spectrum is shown by the dashed line. Results are averaged over 100 simulations of out-of-band noise (SNR = -5 dB), whose spectrum is illustrated in Figure 2-5.

Narrow-Band Input

In system identification, it is generally required that the input signal be persistently exciting. From a frequency standpoint, the input should have enough frequency components to excite all the modes of the system, i.e., encompass the entire spectrum of the system function. However, under some circumstances, the signals involved are narrow-banded while it is still desirable to identify the system dynamics within the frequency range excited by the input as accurately as possible. For example, the breathing activity is an important factor inducing variability in heart rate (HR), blood pressure (BP) and other cardiovascular signals. This type of variability is mediated by autonomic reflexes, mechanical properties of the cardiovascular system, local vascular regulation, *et al.* Therefore, an identification of the system function relating instantaneous lung volume (ILV), HR, BP or other signals may help characterize these underlying mechanisms. Since during spontaneous breathing, the ILV signal is narrow-banded or even nearly sinusoidal, a complete identification of the involved system dynamics is not achievable. However, system identification limited to the frequency band of the ILV signal may still be informative under some circumstances (this specific topic will be discussed in detail in Chapter 3). In this section, we investigate the performance of the WPCR method in the general scenario of narrow-band input.

We simulate the input signal as consisting of two sinusoids plus very low-amplitude white noise ($x(t) = sin(0.02\pi t)/5+sin(0.06\pi t)/10+e(t)$), the spectrum of which is demonstrated in Figure 2-14. The output signal is then constructed utilizing the system function and low-frequency-dominant additive noise illustrated in Figure 2-5. The same initial model orders and data length were used as employed for the white input simulations for both WPCR and ARX identifications. Note that because of the limited frequency content in the input signal, the error in the estimated impulse responses is expected to be very significant. As an example, Figure 2-15 shows the averaged impulse responses estimated based on 100 noise realizations with an SNR of 0 dB using the WPCR method and the ARX method respectively. The impulse response error resulted from the WPCR method is 59.8 ± 0.68% and that from the ARX method is 320.3 ± 15.5%. These relatively large estimation errors are reflections of the fact that reliable estimate at frequencies outside of the input spectrum are not obtain-

able in linear systems. Therefore, we evaluate the performance of the system identification methods only at the two input frequencies. The percentage errors of the amplitude of the estimated frequency response resulted from the WPCR method and the ARX method are shown in Figure 2-16.

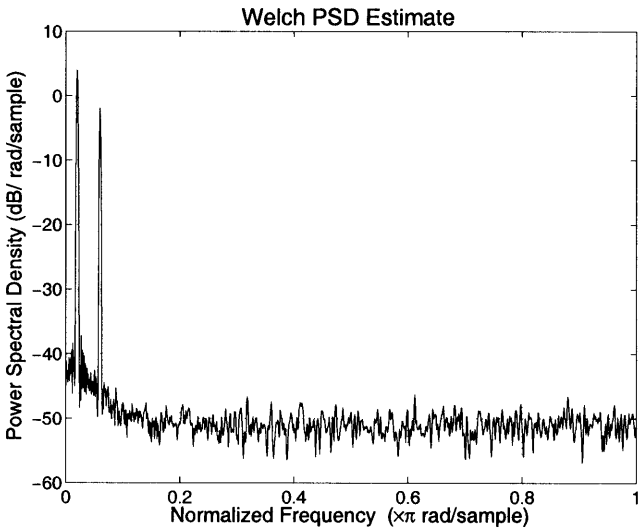

Figure 2-14 Input spectrum (consisting of two sinusoids and low-amplitude white noise); note that the amplitude of the lower frequency component is twice that of the higher frequency component.

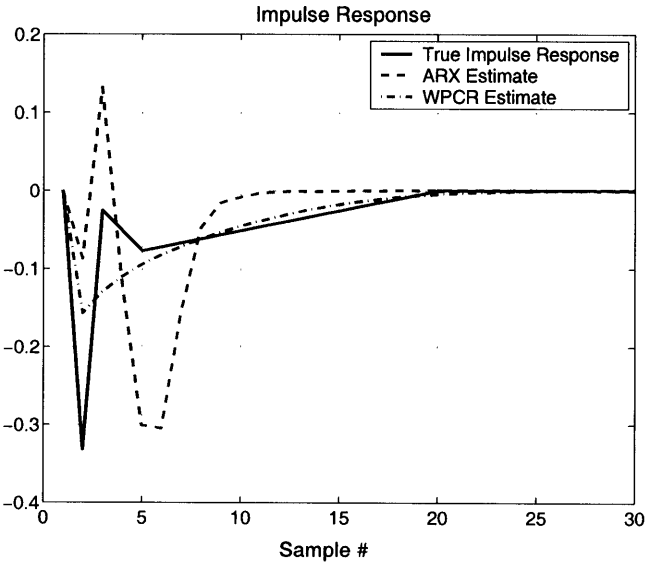

Figure 2-15 Impulse responses estimated by the WPCR method and the ARX method (average of 100 simulations, SNR = 0 dB)

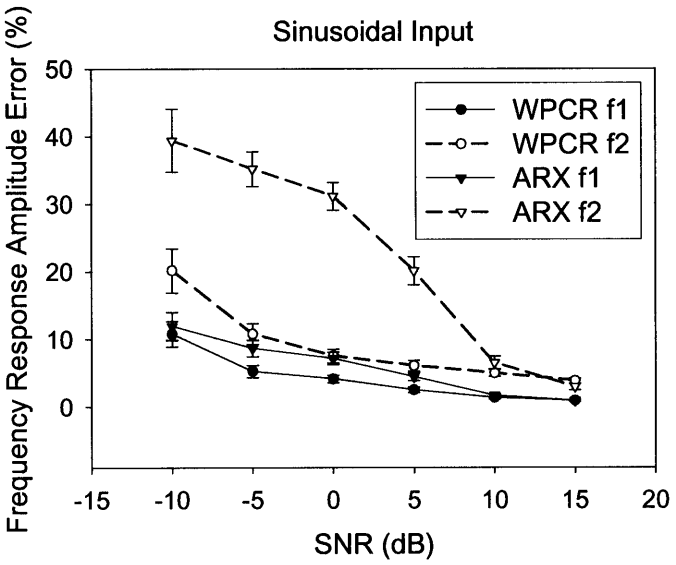

Figure 2-16 Error of frequency response amplitude at the two input frequencies, f1 = 0.02π, f2 = 0.06π

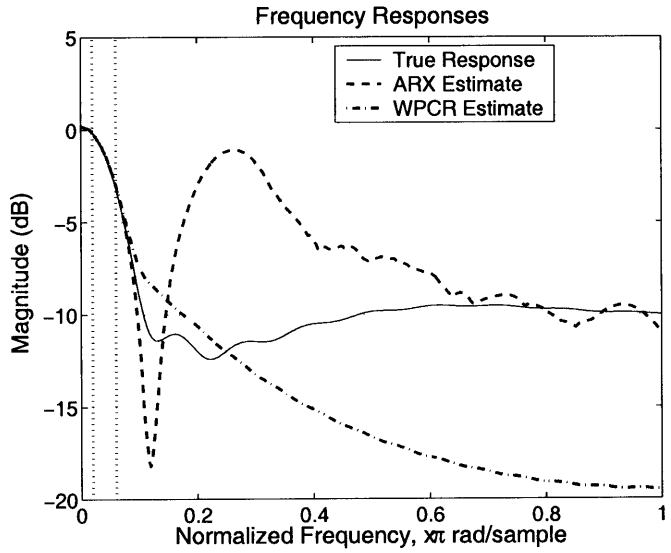

Figure 2-17 Comparison of system frequency responses estimated by the ARX method (dashed line) and the WPCR method (dotted line). This result is the average of 100 simulations at an SNR level of 10 dB. The true frequency response of the system is illustrated with the solid line. The two vertical dotted lines correspond to the two input frequencies.

As expected based on the discussion in previous sections, the frequency selective property of the WPCR method enables a more accurate estimate compared to the ARX method. Regardless of the method, the estimate at the first frequency (0.02π as in Figure 2-14) is more precise than that at the second frequency (0.06π as in Figure 2-14) due to the difference in the corresponding amplitudes of the two components (refer to Equation (2.17)). Note that this difference is rather significant in the result of the ARX method. In addition, simulations (not shown here) using the MA method demonstrated a result similar to that of the ARX method. Neither method imposes constraints in the frequency domain for model selection.

Figure 2-17 delineates the averaged frequency responses estimated using both methods with the SNR level being 10 dB. Although the amplitude errors at higher SNR shown in Figure 2-16 are equivalent for the two methods, the overall frequency response curves differ significantly. The ARX-estimated frequency response reflects its attempt to fit the output across the entire spectrum thus inducing large errors at frequencies where the input energy is low, while the WPCR method focuses on the estimation at the dominant input frequencies.

To summarize, in this section, we demonstrated, through simulated data, that the WPCR method outperforms the conventional ARX method when colored signals are involved in system identification. The major strength of the WPCR method lies in its frequency selective ability.

2.8.3 Closed-loop Systems

Brief Review on Closed-loop System Identification

Since many physiologic control mechanisms involve closed-loop interactions (e.g., the coupling mechanism between heart rate and arterial blood pressure), we consider the application of the WPCR approach in closed-loop systems. Figure 2-18 illustrates a typical closed-loop coupling between two signals x and y where H_1 and H_2 are the transfer functions in the feed-

forward and feed-backward pathways respectively and N_x and N_y are noise disturbances. In general, the noise terms are colored random processes. In addition, in contrast to the open-loop case, the noise processes (N_x, N_y) and the signal terms (x, y) are correlated with each other in closed-loop systems.

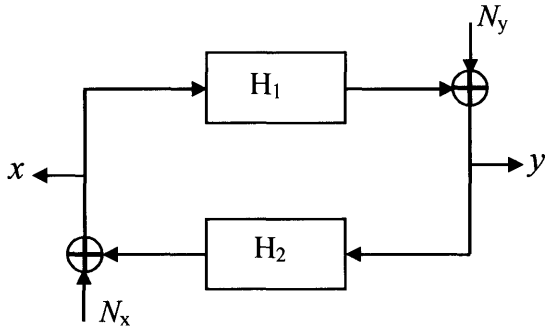

Figure 2-18 Block diagram of a closed-loop system with noise disturbances

Assume that the above system is stable and can be represented by the following equations:

$$\begin{aligned} y(t) &= \sum_{k=1}^{P} h_{1k} x(t-k) + N_y(t) \\ x(t) &= \sum_{k=1}^{Q} h_{2k} y(t-k) + N_x(t) \end{aligned} \tag{2.41}$$

We next discuss the identification of this closed-loop system using MA and ARX model structures. Equations (2.42) and (2.43) represent the two often-utilized LTI system models – the MA model and the ARX model respectively.

$$y(t) = \sum_{i=s}^{f} b_i x(t-i) + e(t) \tag{2.42}$$

$$y(t) = \sum_{i=s}^{f} b_i x(t-i) + \sum_{j=1}^{g} a_j y(t-j) + e(t) \tag{2.43}$$

These two models can be written into a unified form as follows:

$$y(t) = \phi^T(t)\theta + e(t) \tag{2.44}$$

where, for the MA model,

$$\phi^T(t) = [x(t-s),...,x(t-f)]$$
$$\theta^T = [b_s,...,b_f]$$

and, for the ARX model,

$$\phi^T(t) = [y(t-1),...,y(t-g),x(t-s),...,x(t-f)]$$
$$\theta^T = [a_1,...,a_g,b_s,...,b_f]$$

The least squares solution of Equation (2.44) is:

$$\hat{\theta} = \theta_0 + \left[\frac{1}{N}\sum_{t=1}^{N}\phi(t)\phi^T(t)\right]^{-1}\left[\frac{1}{N}\sum_{t=1}^{N}\phi(t)e(t)\right] \tag{2.45}$$

This estimate is consistent, i.e., $\hat{\theta} \to \theta_0$, when N$\to\infty$ if the following two conditions hold: 1) $E(\phi(t)\phi^T(t))$ is nonsingular; and 2) $E(\phi(t)e(t)) = 0$.

Although the true system has an MA structure in each pathway, identification using MA models gives inconsistent results because the colored noise processes are correlated with the signals x and y in a closed-loop system. That is, the second condition for consistency ($E(\phi(t)e(t)) = 0$) does not hold. On the other hand, the ARX model is able to identify the system function because 1) With the inclusion of the AR terms, $e(t)$ can be assumed to be a white noise process in Equation (2.43); 2) There is one delay (the value of k starts from 1 in Equation (2.41)) each in the feed-forward and the feed-backward pathways which makes this closed-loop system identifiable [105]. These two conditions ensure that the equality $E(\phi(t)e(t)) = 0$ is valid. Therefore, although the true system does not assume an ARX structure, the ARX system identification can provide a "best" approximation of the system within its limited set of candidate models. Equation (2.46) demonstrates the estimated system function and noise process of the true system using an ARX model (for the feedforward pathway).

$$Y(q^{-1}) = \underbrace{\frac{G_1(q^{-1})}{1+G_2(q^{-1})}}_{H_1(q^{-1})} X(q^{-1}) + \underbrace{\frac{1}{1+G_2(q^{-1})}}_{N_y(q^{-1})} E_y(q^{-1}) \tag{2.46}$$

where q^{-1} is the delay operator, $G_1(q^{-1}) = \sum_{i=1}^{f} b_i q^{-i}$ and $G_2(q^{-1}) = -\sum_{j=1}^{g} a_j q^{-j}$.

To solve for the parameters in Equation (2.46), the "direct approach" for closed-loop system identification can be employed. This approach applies the basic prediction error method in a straightforward manner – use the output y and the input x in the same way as for open loop operation, ignoring any possible feedback [2].

Application of the WPCR-MA Method in Closed-loop System Identification

Based on the above review, it is desirable to use the ARX structure associated with the WPCR method in closed-loop system identification. However, due to the nature of the WPCR method, an ARX structure may not render any advantage applied to a closed-loop system. The reason is as follows. 1) A consistent estimation is not the ultimate goal of the WPCR method because it decomposes the data matrix ϕ in Equation (2.44) into its principal components and only selects a *subset* of PCs to minimize the prediction error of $y(t)$. Therefore, even though the noise term $e(t)$ in the ARX model (Equation (2.43)) is white, the resulted parameter estimation is biased in nature and a consistent estimation is not reached. 2) Unlike in the open-loop systems where the past output terms in the data matrix ϕ reinforce the frequency components in the transfer function to be identified, in a closed-loop system, the past input/output vectors encompass frequency components intrinsic in both H_1 and H_2 (x and y vectors are related through both H_1 and H_2.) In this case, the dominant PCs reflect contributions by both system functions. Thus, the inclusion of the past output terms in the data matrix ϕ complicates the estimation of H_1 or H_2 in the closed-loop system.

In this section, we consider applying the WPCR-MA method in closed-loop systems. As previously discussed, using an MA structure, correlation between the data matrix and the

noise term causes a bias in the estimated model parameters. Although a consistent estimation is not the ultimate goal of the WPCR method, it is still important to reduce the bias resulted from undesired noise. In addition, there is one element in the WPCR estimation that requires unbiasedness – the estimated coefficients of the PCs ($\hat{B}$). To this end, we propose a procedure to pre-whiten the noise (equivalent to using a fixed noise model) so as to reduce its correlation with the input data.

The pre-whitening technique we employed can be described as follows. First, ordinary least-squares estimate ($\hat{A}_{LS}$) of the coefficient vector A in Equation (2.3) is computed with the same MA structure (same size) as used for WPCR identification. The residual error is expressed as:

$$\hat{E} = Y - X\hat{A}_{LS} \tag{2.47}$$

Subsequently, an autoregressive (AR) model of the residual is constructed, i.e.,

$$\hat{e}(t) = \sum_{i=1}^{n} a_i \hat{e}(t-i) + \varepsilon(t) \tag{2.48}$$

where $\varepsilon(t)$ is white. The model order n may be determined by employing one of the aforementioned model order selection criteria. In this way, a noise-whitening filter can be defined as:

$$h(z) = (1 - \sum_{i=1}^{n} a_i z^{-i}) \tag{2.49}$$

The input and output signals are then prefiltered by $h(z)$ before performing a WPCR estimation. Using this approach, we are approximating the real noise with the residual error in Equation (2.47). To improve the accuracy of this approximation, an iterative procedure can be carried out – once the model parameters are obtained through the WPCR method, the residual error can be computed again, and the pre-whitening and the WPCR procedures be repeated, until the estimated impulse response converges.

Based on the frequency domain properties of the WPCR method, the improvement in the impulse response estimation due to prewhitening can be explained as follows. 1) If the real

noise E_0 is in-band with X, then the error in the estimate of B_0, i.e. $\hat{B} - B_0 = U^T E_0$ can be large because U represents the frequency components in X which are correlated with and also dominant in E_0. Since prewhitening equalizes the strength of different frequencies in $\hat{E}$, it can reduce the error in the estimate of B_0. 2) If the real noise E_0 is out-of-band with X, the elements in $\hat{B}$ that correspond to the dominant frequencies in E_0 have a very low signal-to-noise ratio. If these values of $\hat{B}$ are large, their corresponding PCs may be selected in order to reach a smaller prediction error which results in an unnecessarily high model order and highly noisy estimate of the impulse response. Therefore, noise whitening could be beneficial in this case. In addition, the pre-whitening filter is in-band with the dominant PCs of X and out-of-band with the real noise. From this perspective, prewhitening may also enhance the dominant PCs of the data and reduce the error introduced by out-of-band noise.

The above pre-whitening strategy is similar to that in the Generalized Least Squares (GLS) method [15] first proposed by Clarke. The conventional GLS method also fits the residual error using an autoregressive structure iteratively to generate a noise model. Ordinary least squares estimation was employed to obtain the system parameters once the noise model is specified. In the following simulations, we compare the performance of the WPCR-MA method (with pre-whitening procedure) and the GLS method in closed-loop system identification.

Simulation Results

We simulated a stable closed-loop system using transfer functions illustrated in Figure 2-19. One of the systems is a low-pass filter mainly and the other is a high-pass filter. The noise spectra are delineated in Figure 2-20 and they ensure persistently exciting input to each system. Note that in each pathway of this closed-loop setting, the noise disturbance is out-of-band with its respective input signal. Thirty input delayed vectors were included in the MA model of the WPCR method and the maximum model evaluated by the GLS method contained 15 MA and 15 AR terms. The autoregressive structure utilized to model the residual error in both methods had a maximum order of 50. The MDL criterion was employed

in all model order selections. 1000 data samples were used in each simulation. Figure 2-21 displays the impulse response errors of the WPCR-MA method (with pre-whitening procedure) and the GLS method based on 100 noise realizations.

To study the performance of the two methods in the case when noise is in-band with the input, we simulated another closed-loop system. H_1 of this system remains the same as the one demonstrated in Figure 2-19. Figure 2-22 delineates the impulse response and frequency response of H_2 and the frequency characteristics of the noise terms. It is evident that the noises are in-band with their associated inputs in both pathways. Figure 2-23 displays the impulse response errors induced by the WPCR method and the GLS method respectively.

From the above results, it can be seen that the WPCR method outperforms the GLS method, especially when the noise is out-of-band with the input and/or the SNR level is low. The reasons behind these observations are essentially the same as discussed previously for the open-loop systems where the frequency selective ability of the WPCR method has proven to be a key factor. In addition, it should be noted that the GLS method is much more computationally intensive than the WPCR method.

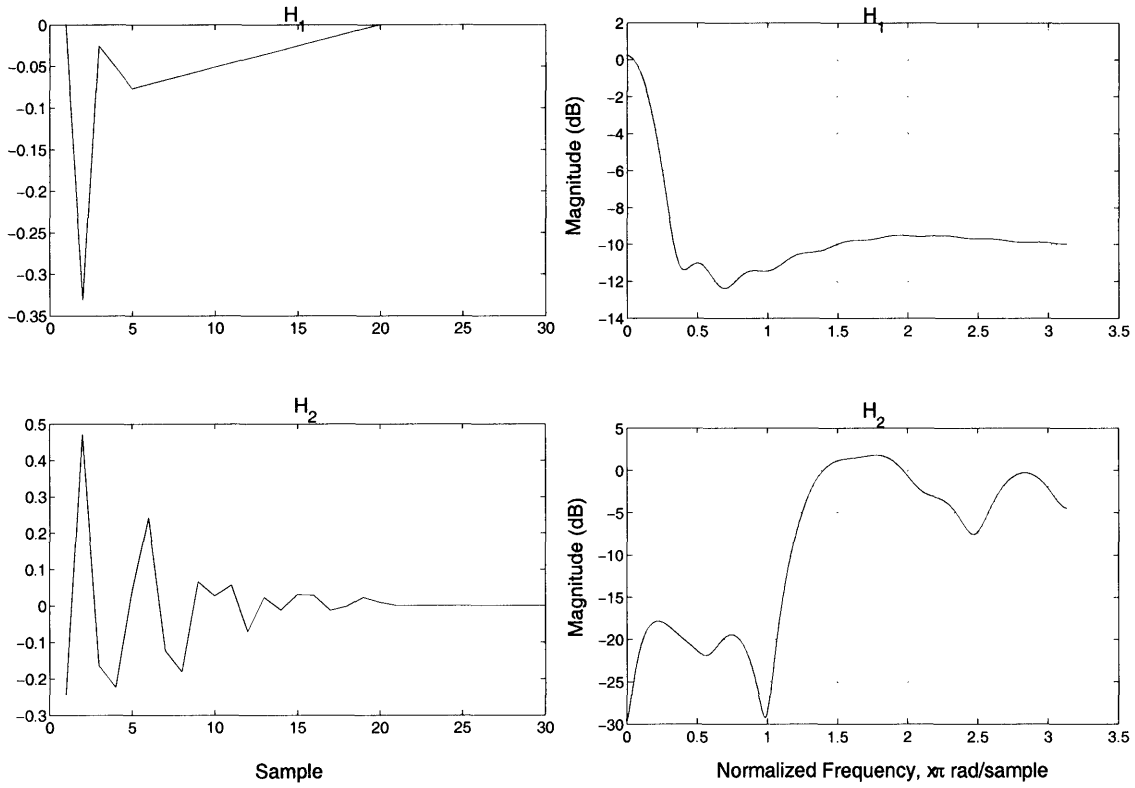

Figure 2-19 (a) impulse responses of the closed-loop system in Figure 2-18; (b) frequency responses of the corresponding transfer functions.

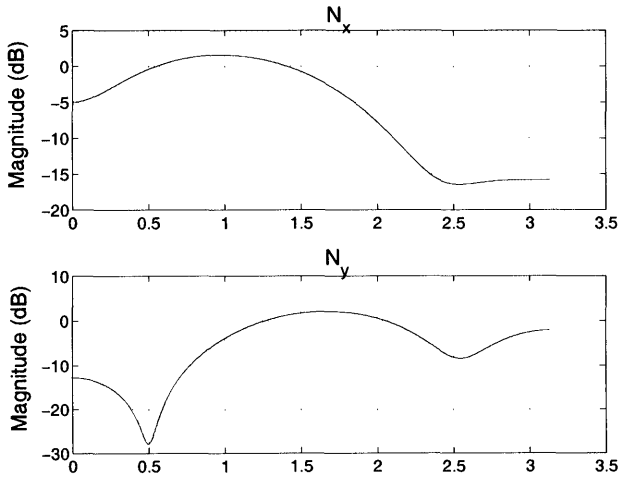

Figure 2-20 Noise spectra of the closed-loop system in Figure 2-18.

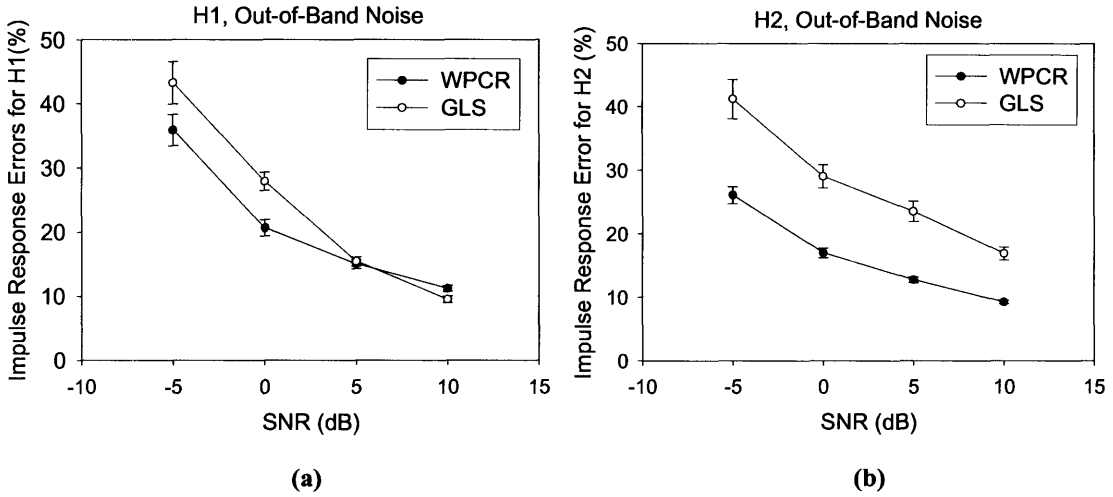

(a) (b)

Figure 2-21 Impulse response errors of the two systems involved in closed-loop (Figure 2-19). The noise is out-of-band with its respective input in each system. (a): H_1; (b) H_2 (MDL model selection criterion was employed, values are mean±1.96*SE of 100 noise realizations. Note that at SNR = -10 dB, the GLS method induces a very large error (~200%, not shown here), the WPCR method has an error of ~90%)

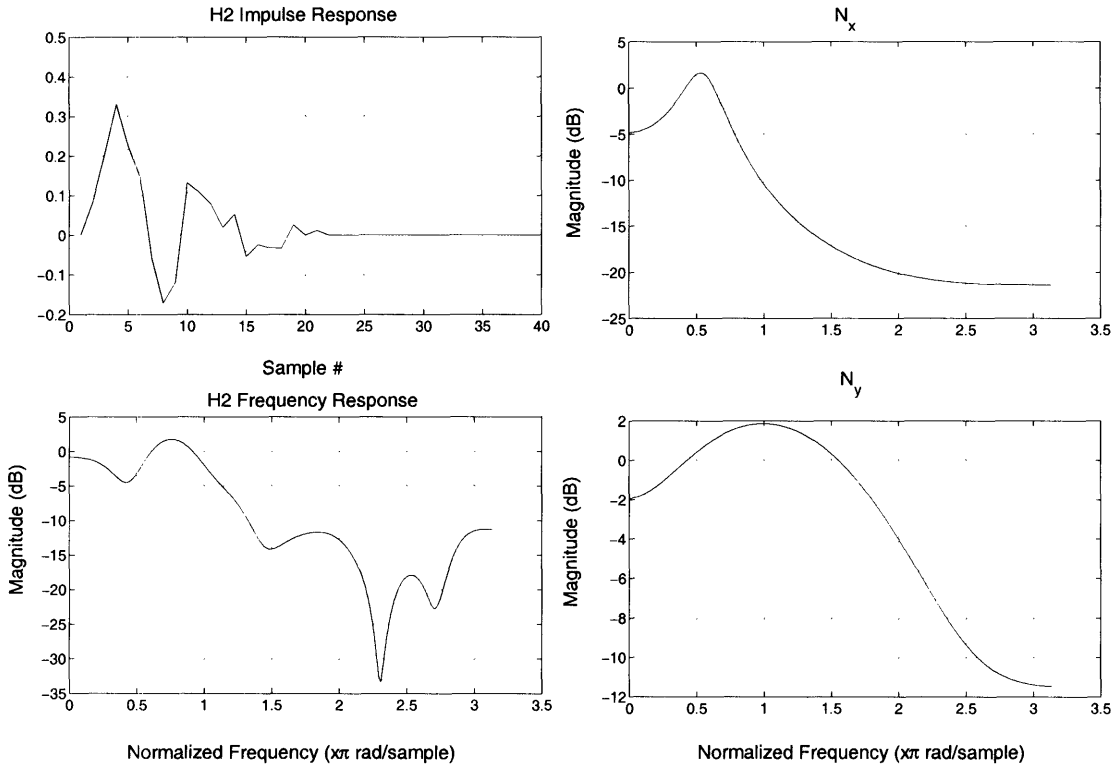

(a) (b)

Figure 2-22 Closed-loop system with in-band noises, H_1 is the same as demonstrated in Figure 2-19. (a): H_2 impulse response and frequency response; (b): Noise spectra.

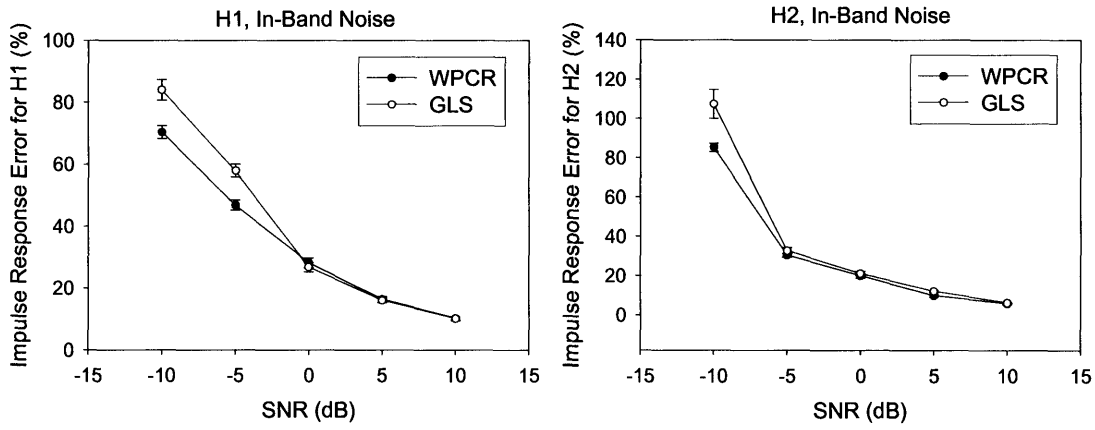

Figure 2-23 Impulse response error of the systems in Figure 2-22. The noise is in-band with its respective input in each system. (a): H_1; (b) H_2 (MDL model selection criterion was employed, values are mean±1.96*SE of 100 noise realizations.)

2.9 Application of the WPCR Approach with ARX Structures

In this section, we discuss the application of the WPCR method with an ARX structure (WPCR-ARX) in open-loop systems. As mentioned previously, due to the nonlinearity in the relationship between model parameters and system impulse response, it is not evident how pre-weighting on the data matrix affects basis functions of the estimated impulse response. Since one of the main advantages of pre-weighting in MA structures is that it practically modulates the basis functions of the estimated impulse response, it is not clear whether pre-weighting in the ARX structures renders significant advantage in theory. We now compare the weighted and non-weighted PCR-ARX methods through simulations.

To define the weighting factors involved in the WPCR-ARX method, we again incorporate the *a priori* knowledge that current output is correlated more closely with recent inputs/outputs than with remote ones. We first calculate the ordinary least squares estimate of the maximum ARX structure and denote the ratio of the computed coefficients of the first MA term and the first AR term as R. Then, the p+1 input vectors (as in Equation (2.35)) are weighted by $Re^{-n/\tau}$, n = 0, 1, , p and the m output vectors are weighted by $e^{-n/\tau}$, n = 1, 2, , m. This pre-weighting scheme ensures that appropriate relative weights are assigned to

the input and output vectors which is critical if multi-input signals are involved or if the input and output data have different units/physical meanings. The upper bound of the searching range of the time constant τ is assumed to be 2/3 of the number of input/output delays included in the data matrix.

The simulated data are the same as those employed in Section 2.8.2 for colored input. 100 noise realizations were simulated for each SNR value. In each simulation, 1000 data samples were employed. The ARX data matrix (as in Equation (2.35)) contains 15 input delayed vectors and 15 output delayed vectors. Figure 2-24 displays the impulse response error for the weighted PCR method and non-weighted PCR method. For comparison purpose, we include in this figure the results using the WPCR-MA method (demonstrated previously in Figure 2-11).

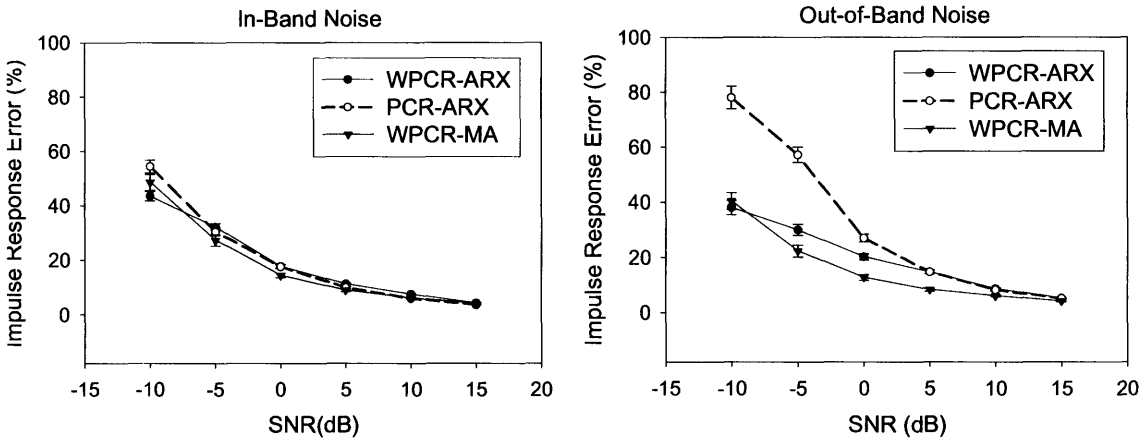

Figure 2-24 Comparison of impulse response errors estimated by the WPCR-ARX method, the unweighted PCR-ARX method and the WPCR-MA method, MDL minimization was employed as the model selection criterion. The system input is a colored process. (a) simulation with in-band noise; (b) simulation with out-of-band noise. (Values are mean±1.96*SE of 100 noise realizations)

The above results demonstrate that the WPCR-MA method slightly outperforms the WPCR-ARX method, both of which outperforms the conventional ARX method (refer to Figure 2-11). The weighting scheme improved the identification accuracy especially when the noise is out-of-band with the input. It should be pointed out that the WPCR-ARX

method has one significant advantage over the WPCR-MA method – it needs less input/output vectors in the model, i.e., a smaller data matrix. This advantage is evident when the length of the impulse response is large which necessitates a large data matrix using the WPCR-MA method and consequently, a high computational load in calculating the SVD of this matrix. Therefore, the WPCR-ARX method is appropriate when the anticipated system impulse response has a significant number of non-zero samples.

2.10 Application of the WPCR Method to Experimental Data[4]

To further evaluate the WPCR method, we study its performance in analyzing experimental data. The goal is to identify the short-term closed-loop cardiovascular regulation model (Figure 2-25) which was proposed in previous publications of our lab [23, 56].

[4] Some of the content in this section has been published in the Journal of Applied Physiology [106]

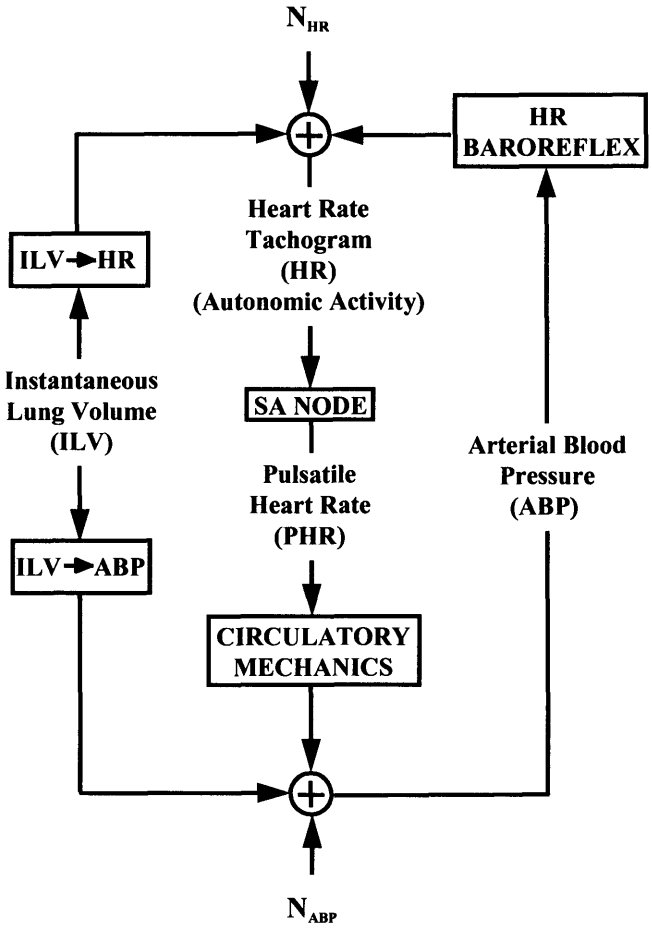

Figure 2-25 Closed-loop model of short-term cardiovascular regulation (Adapted from [23] with permission granted by the APS)

The accessible signals in this problem are second-to-second HR (heart rate tachogram), PHR (pulsatile heart rate), ILV (instantaneous lung volume) and ABP (arterial blood pressure). HR and PHR are derived from standard surface electrocardiograms (ECG). PHR is defined to be a train of impulses occurring at the times of contraction of the ventricles (Figure 2-26) [23]. HR is defined to be a stepwise continuous process (Figure 2-26, bottom trace) whose value corresponds to the reciprocal of the current inter-beat interval for the time period corresponding to the duration of that interval [23].

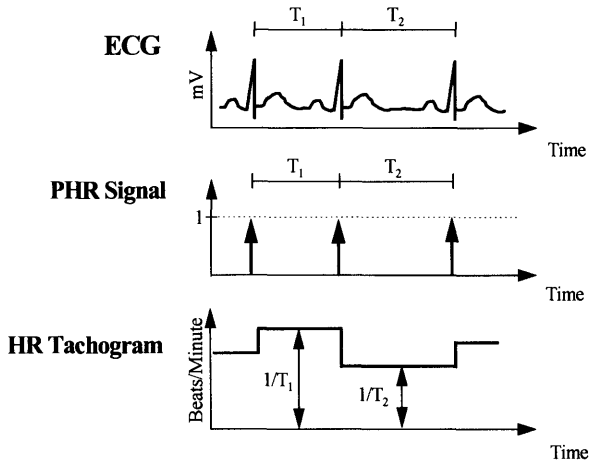

Figure 2-26 The relationship between HR, PHR, and ECG (adpated from [23] with permission granted by the APS).

The short-term closed-loop cardiovascular regulation model consists of four couplings – Circulatory Mechanics, HR Baroreflex, ILV→HR and ILV→ABP, whose transfer properties are represented below in terms of impulse response functions. We assume that the couplings of the small spontaneous fluctuations in these signals about their mean values may be represented by a linear, time invariant model. This model will generally change when there is a change in physiologic state. The linearity assumption has been tested and validated [6].

Circulatory Mechanics impulse response represents the ABP wavelet generated with each cardiac contraction. It primarily reflects the mechanical properties of the heart, great vessels and peripheral circulation. The amplitude of the Circulatory Mechanics impulse response is related to stroke volume, and the characteristic decay time of this impulse response is related to the product of peripheral resistance and arterial compliance. The HR Baroreflex represents the change in HR in response to an impulse in ABP mediated via the baroreceptor reflex pathway (see Chapter 3). The ILV→HR impulse response reflects the change in HR in response to a very rapid inspiration/expiration; this impulse response is centrally mediated via the autonomic nervous system. ILV→ABP represents the mechanical effects of respiration on ABP mediated in part by the effects of intrathoracic pressure on venous return.

In Figure 2-25, there is a fifth predefined coupling, sinoatrial (SA) node which relates HR and PHR. The SA node is an "integrate-and-fire" device and is not identified from the experimental data since its dynamics are predefined [23]. N_{HR} and N_{ABP} represent the fluctuations in HR and ABP respectively that are not attributable to the couplings discussed above. N_{HR} may reflect, for example, perturbations to HR resulting from cerebral inputs and N_{ABP} may represent perturbations to ABP resulting from autoregulation of local vascular resistance in different tissue beds [23].

Since this model contains a mixture of multi-input single-output, closed-loop, open-loop, causal and non-causal (ILV→HR) systems, the conventional ARX identification method is not suitable to handle its complexity efficiently. To solve this problem, our lab previously developed an efficient algorithm, namely, the Arma Parameter Reduction (APR) algorithm [55]. This method models the system in terms of ARX models and evaluates the candidate model terms based on their respective 'signal-to-noise ratio (SNR)'. Parameter estimates with high SNR are considered more important than those with low SNR. The APR method has been successfully applied in several studies [23, 56, 106].

In the remainder of this section, we discuss the application of the WPCR method in identifying the model in Figure 2-25 and compare its performance with that of the APR method.

The experimental data employed here was published previously in [106]. Briefly, 29 male subjects (age: 35.7±11.5 (SD) years, height: 70.3±2.5 (SD) inches, weight: 79.6±10.4 (SD) kilograms) were tested in the positions of supine, 30, 60 and 90 degree head-up tilt for baseline measurements. Approximately 6 minutes of standard surface ECG, ABP and ILV were recorded continuously and non-invasively after a stable state is achieved in each posture. Continuous blood pressure was recorded from the middle finger of the right or left hand using a fingertip cuff transducer (Portapres, TNO, or Finapres, Ohmeda). ILV was measured using a two-belt chest-abdomen inductance plethysmograph (Respitrace system, Ambulatory Monitoring Systems, Inc). Calibration of ILV was performed by having the subject alternately fill and empty an 800ml calibrated Spirobag. During data collection, the subjects were instructed to breathe in response to auditory cues spaced at random intervals ranging from 1 to 15 seconds with a mean of 5 seconds. This random breathing protocol

broadens the spectral content of ILV thereby satisfying the 'persistently exciting' requirement for signals involved in system identification while preserving normal ventilation [48]. The signals were sampled at 100 Hz during data collection.

The WPCR-MA method with prewhitening procedure was employed to identify the transfer relations involved in the closed-loop system consisting of ILV→HR and HR baroreflex utilizing 6-minute of data sampled at 1.25 Hz. Zero-mean ABP and HR were normalized with respect to their corresponding time-averaged values and zero-mean ILV with respect to its standard deviation. The open-loop system involving ILV→ABP and the circulatory mechanics were identified in two steps since the latter coupling requires a much wider bandwidth than the former one. Ninety-second segments of data sampled at 100 Hz were used in the first step to obtain an accurate identification of the circulatory mechanics transfer function. The WPCR-ARX method was employed here since the impulse responses have a very large number of nonzero samples (> 900) and thus the MA structure would be cumbersome. Note that in this step, the PHR, ILV and ABP signals should not be normalized. Next, to achieve an improved characterization of the ILV→ABP relation using a narrower bandwidth matched more closely to that of the true transfer function, the component of ABP due only to PHR was computed utilizing the circulatory mechanics relation identified in the first step and subtracted from the original ABP. The resulting ABP component and the ILV signal were then decimated to 1.25 Hz and a new ILV→ABP relation was obtained using the WPCR-MA method (SISO system). The signals were normalized in the same way as for the HR baroreflex and ILV→HR relations.

In accordance with previous studies [23, 56], the impulse response curves of the transfer relations were each characterized with two parameters: peak amplitude and characteristic time. These parameters are defined as:

$$\text{peak amplitude} = \begin{cases} |\min[h(t)]| & \textit{For HR Baroreflex response} \\ \max[h(t)] & \textit{For other impulse responses} \end{cases}$$

$$\text{characteristic time} = \frac{\int_{-\infty}^{+\infty} t|h(t)|dt}{\int_{-\infty}^{+\infty} |h(t)|dt}$$

where $h(t)$ is the impulse response function.

Mullen *et al.* [23] showed that the two impulse responses, HR baroreflex and ILV→HR, were nearly obliterated after total autonomic blockade. This indicates that these two couplings are mediated primarily by autonomic activity. Hence, we postulate that their peak amplitudes are determined mainly by parasympathetic responsiveness in HR regulation and the characteristic time reflects the sympathetic/parasympathetic balance because sympathetically mediated impulse response functions have much longer characteristic times than parasympathetically mediated ones. The peak of the circulatory mechanics response is related to stroke volume and its characteristic time is determined by the combined effect of vascular resistance, compliance and stroke volume. The ILV→ABP coupling is largely mechanically mediated.

It is well accepted that the postural change from supine to head-up tilt results in a relative shift from parasympathetic-dominant to sympathetic-dominant cardiovascular control [45]. We assess the validity of our techniques using this physiological observation. Table 2-1 and Table 2-2 present identification results using the WPCR and the previously employed APR methods [55] respectively. Consistent with physiological notions, it can be seen from Table 2-1 (WPCR method) that the peak amplitudes of the HR baroreflex (at 90° tilt) and ILV→HR impulse responses decreased significantly upon head-up-tilt, reflecting a reduction in the parasympathetic responsiveness. The corresponding characteristic times increased significantly reflecting a shift to sympathetic-dominant control upon head-up-tilt. The peak amplitude of the circulatory mechanics coupling decreased significantly upon head-up-tilt while its characteristic time increased significantly which can be explained by the reduction in stroke volume and increase in vascular resistance in the tilt positions. The ILV→ABP impulse response demonstrates an increase in peak amplitude and a decrease in characteristic time, which may be due to the change in intrathoracic pressure. Table 2-2 demonstrates the results reached by the APR method. The characteristic times of the ILV→HR impulse response identified by the APR method demonstrates more significant comparisons than those by the WPCR method. On the other hand, the APR method did not detect significant changes in the peak amplitude of the HR baroreflex impulse response at

any of the tilt postures and only showed an increase in the characteristic time at 90° tilt. The changes in the ILV→ABP parameters also seem to be more reliably identified by the WPCR method. In total, the APR method identified less significant comparisons (13) than the WPCR method (16). Note that the APR method leads to thirteen unstable estimates among all the cases computed, while results from the WPCR method are all stable. The unstable results have been excluded in the results shown in Table 2-2.

Table 2-1 Identification results of closed-loop cardiovascular regulation using the WPCR method (Data are from 29 subjects, Values are mean ± SE; Superscripts are *P* values of paried t-test relative to the supine posture, those that are statistically significant ($P < 0.05$) are shown in bold face.)

		Supine	*30°*	*60°*	*90°*
Peak (unitless, except Circ. Mech. – mmHg)	HR Baroreflex	0.40±0.04	0.41±0.07$^{0.96}$	0.34±0.05$^{0.26}$	0.32±0.03$^{\mathbf{0.035}}$
	ILV→HR (× 100)	1.87±0.17	1.43±0.15$^{\mathbf{0.0006}}$	1.08±0.14$^{\mathbf{2.3e\text{-}6}}$	0.97±0.13$^{\mathbf{4.7e\text{-}5}}$
	Circulatory Mechanics	62.1±2.08	51.8±2.68$^{\mathbf{0.0075}}$	43.4±3.07$^{\mathbf{9.8e\text{-}5}}$	45.8±2.53$^{\mathbf{1.5e\text{-}5}}$
	ILV→ABP (× 100)	0.60±0.06	0.68±0.11$^{0.42}$	1.02±0.20$^{\mathbf{0.031}}$	0.95±0.13$^{\mathbf{0.013}}$
Characteristic Time (sec)	HR Baroreflex	1.98±0.12	2.55±0.21$^{\mathbf{0.012}}$	2.63±0.23$^{\mathbf{0.045}}$	2.71±0.24$^{\mathbf{0.013}}$
	ILV→HR	1.74±0.13	1.95±0.19$^{0.65}$	2.17±0.19$^{0.12}$	2.01±0.13$^{\mathbf{0.03}}$
	Circulatory Mechanics	2.01±0.06	2.19±0.12$^{0.13}$	2.44±0.13$^{\mathbf{0.0052}}$	2.43±0.09$^{\mathbf{6.5e\text{-}5}}$
	ILV→ABP	7.37±0.61	6.29±0.65$^{0.38}$	7.07±0.61$^{0.62}$	5.32±0.37$^{\mathbf{0.012}}$

Table 2-2 Identification results of closed-loop cardiovascular regulation using the APR method (Data are from 29 subjects, Values are mean ± SE; Superscripts are *P* values of paried t-test relative to the supine posture, those that are statistically significant ($P < 0.05$) are shown in bold face.)

		Supine	*30°*	*60°*	*90°*
Peak (unitless, except Circ. Mech. – mmHg)	HR Baroreflex	0.43±0.04	0.55±0.19$^{0.56}$	0.54±0.18$^{0.58}$	0.34±0.04$^{0.10}$
	ILV→HR (× 100)	1.99±0.19	1.70±0.19$^{\mathbf{0.092}}$	1.14±0.13$^{\mathbf{9.5e\text{-}6}}$	0.96±0.14$^{\mathbf{7.2e\text{-}6}}$
	Circulatory Mechanics	61.4±2.07	50.9±2.68$^{\mathbf{0.005}}$	44.5±3.10$^{\mathbf{0.0002}}$	47.2±2.31$^{\mathbf{2.6e\text{-}5}}$
	ILV→ABP (× 100)	1.22±0.10	1.35±0.18$^{0.44}$	1.63±0.25$^{\mathbf{0.032}}$	2.74±0.12$^{0.22}$
Characteristic Time (sec)	HR Baroreflex	4.42±0.54	5.93±0.50$^{0.18}$	5.84±0.50$^{0.17}$	5.99±0.54$^{\mathbf{0.007}}$
	ILV→HR	3.24±0.36	5.72±0.81$^{\mathbf{0.0066}}$	6.15±0.69$^{\mathbf{0.0019}}$	5.65±0.67$^{\mathbf{0.0002}}$
	Circulatory Mechanics	1.70±0.07	2.08±0.13$^{\mathbf{0.0094}}$	2.07±0.17$^{\mathbf{0.0039}}$	1.98±0.08$^{\mathbf{0.0042}}$
	ILV→ABP	8.04±0.59	8.67±0.88$^{0.58}$	10.26±1.05$^{0.17}$	9.07±1.04$^{0.61}$

It should also be noted that the characteristic times of the HR baroreflex and the ILV→HR impulse responses computed by the APR method are seemingly larger than those computed by the WPCR method. A careful inspection indicates that in some cases, the APR method results in some additional dynamics in the latter part of the impulse responses (one example shown in Figure 2-27) which induces a large value of characteristic time. The mechanism of these dynamics is not clear. They may be caused by computational artifacts.

In summary, for the data presented above, the WPCR method may be more potentially robust in terms of computational stability. Compared to the APR method which has been applied successfully in studying cardiovascular regulatory mechanisms in previous publications [23, 56, 106], it demonstrated a better statistical significance in the results that are consistent with general physiological notions.

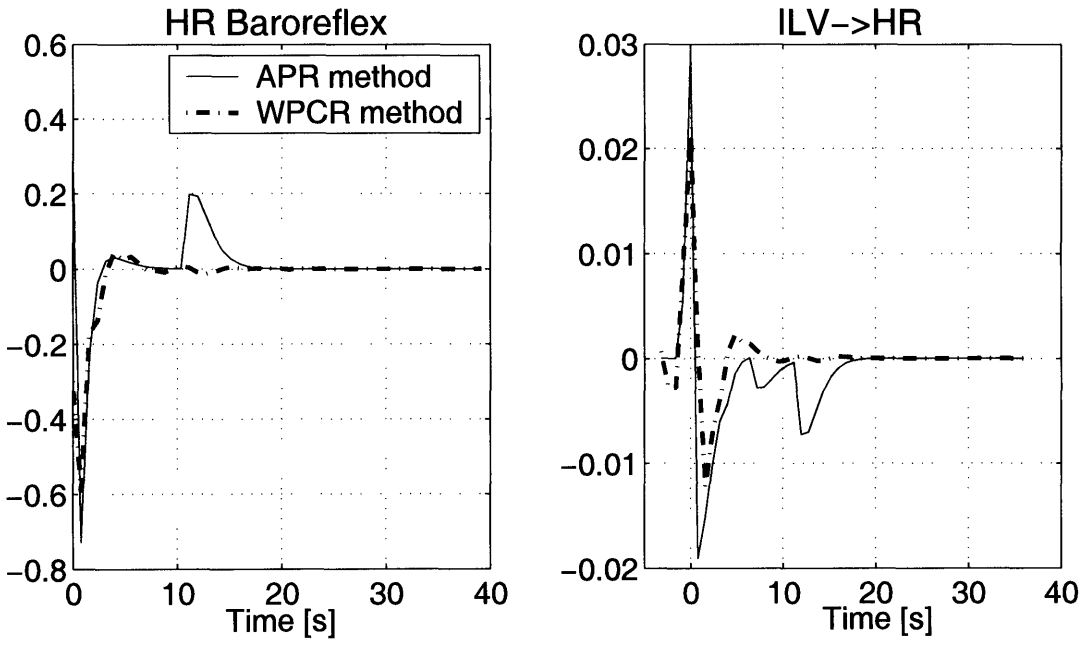

Figure 2-27 An example of the HR baroreflex and ILV→HR impulse responses of one subject at supine posture identified by the WPCR and the APR methods respectively

2.11 Conclusions

In this chapter, we presented a new system identification method named WPCR (Weighted-Principal Component Regression). This approach transforms the system identification problem from the time domain into the frequency domain asymptotically. The candidate models are the ones involving different subsets of PCs. Since the PCs reflect the dominant frequency components specific to the data matrix, the candidate models are also data specific. By excluding the frequency components poorly represented in the data, we improved the estimation accuracy of the model parameters when the signals involved in system identification are colored, as is the case for many physiologic signals. The weighting scheme in this method incorporates some often-employed *a priori* knowledge and realistically modulates the basis functions of the estimated impulse response (in case of MA structure). With finite data used in system identification, the weighting scheme may regularize the distribution of singular values and lower the estimated parameter variance via a reduction in model order.

Furthermore, the WPCR approach can circumvent some difficulties associated with conventional ARX model selection in the time domain, e.g., when the true system has input delays or multiple inputs [55]. As discussed in Chapter 1, in constructing candidate models, the delay terms in an ARX structure are usually added in, one at a time, in an order of increasing time shifts relative to the current output. This approach can not be applied to systems with input delays or multiple inputs. The WPCR approach circumvents these difficulties by transforming the model selection problem into the frequency domain, which is realized by lumping all input (and output) delays and decomposing them into PCs.

We applied the WPCR method in simulated systems whose impulse responses emulate those that are often present in physiologic systems (for examples, see [23]). We demonstrated that the WPCR method outperforms the traditional ARX and GLS methods in open-loop and closed-loop systems respectively when the input signals are colored. Moreover, the application of the WPCR method in experimental data showed more stable and statisti-

cally significant results that are consistent with physiological notions than the APR method which was successfully employed in previous studies.

Chapter 3

Noninvasive Quantification of Cardiac Autonomic Responsiveness

In Chapter 2, we proposed a new system identification method – the weighted principal component regression method and demonstrated that it is advantageous over the conventional ARX or GLS method for systems involving colored signals. As an application of this method, we now consider the practical problem of non-invasively evaluating cardiac autonomic responsiveness[5]. First, we provide a brief overview of the autonomic nervous system emphasizing its role in regulating cardiovascular physiology.

3.1 Autonomic Nervous System Overview

The autonomic system is the portion of the nervous system that controls the visceral functions of the body. It includes afferent nerves (from the Latin, ad = towards; ferro = carry), which convey sensory signals from the end-organs to the controlling centers in the brain (mainly the medulla, pons and hypothalamus) and efferent nerves (ex = from) which conducts information from these controlling centers to the muscles and all the organs of the body [45]. Efferent autonomic nerves have two major subdivisions called the sympathetic

[5] Since system identification models the relationship between the variation of the input and output signals, autonomic quantification based on system identification techniques reflects the relative fluctuation in autonomic tone, instead of the mean autonomic tone. We refer to this type of quantification as autonomic responsiveness in this thesis.

nervous system and the parasympathetic nervous system. Sympathetic nerves originate in the spinal cord between the segments T-1 and L-2 and pass into the sympathetic ganglia along the spine and then to their end-organs (Figure 3-1) [45]. Parasympathetic nerves reach the organs of the body through the cranial nerves III, VII, IX and X, and some sacral nerves (Figure 3-1) [45]. By means of these pathways, autonomic nervous control results in largely unconscious body adjustments such as changes in the size of the pupil, the digestive functions of the gastro-intestinal system, and dilatation or constriction of the bronchi.

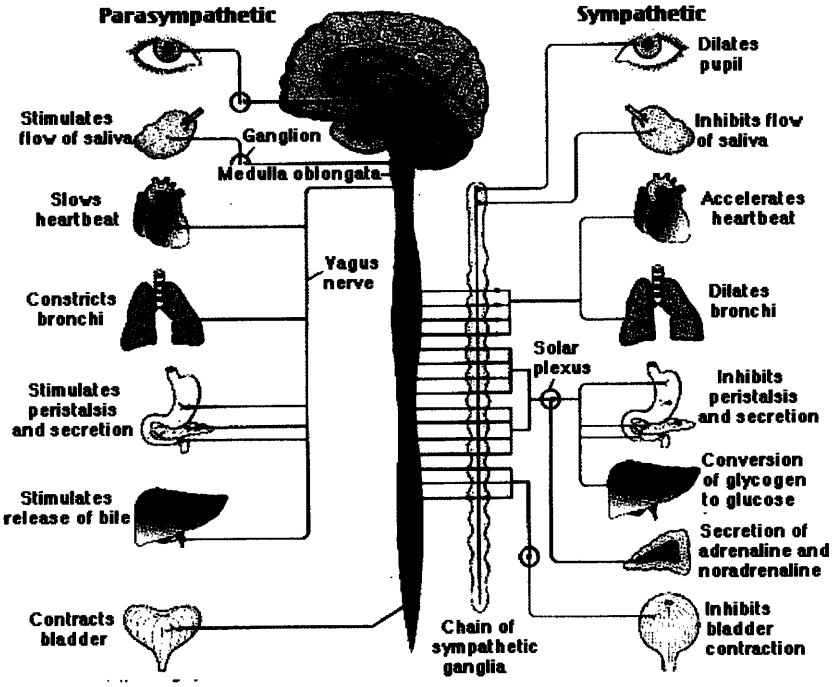

Figure 3-1 The sympathetic and parasympathetic nervous systems. Adapted from "Organization of the Nervous System" (http://users.rcn.com/jkimball. ma.ultranet/BiologyPages/P/PNS.html)

The autonomic system plays a major role in nervous regulation of the heart and the circulation. It controls the pumping activity of the heart and the constriction and dilatation of almost all arterioles and veins of the body. Specifically, stimulation of the parasympathetic system mainly decreases the heart rate by way of parasympathetic fibers carried to the heart in the vagus nerve. In contrast, stimulation of the sympathetic system increases the heart

rate and force of contraction. The α sympathetic system constricts the coronaries and the β_2 sympathetic system dilates them (α and β types are defined based on the types of adrenergic receptors). In addition, the sympathetic system most often causes constriction of blood vessels (with certain exceptions), enhances blood coagulation, increases glucose and lipids levels, while the parasympathetic system has little effect in these aspects [45].

As a result of the above properties, the autonomic nervous system facilitates rapid control of arterial blood pressure and enables redistribution of blood flow to different areas of the body. The control of blood flow redistribution is achieved partially by autonomic mediation of the contraction of blood vessels (vasomotor tone) as mentioned above (in addition to autoregulation). It is related to the autonomic control of blood pressure and the subsequent effect on cardiac output. The best known of autonomic nervous mechanisms for arterial pressure control is the baroreceptor reflex (i.e. baroreflex). Baroreceptors are spray-type nerve endings that are stimulated when stretched [45]. They are located mainly in the walls of the arteries, the most important of which are in the walls of each internal carotid artery (carotid sinus) and the aortic arch. The baroreceptor reflex is a feedback pathway that sends signals to the brain center in response to arterial pressure fluctuation and leads to autonomically mediated changes in heart rate, heart contraction and peripheral resistance, with the ultimate goal of maintaining arterial pressure within a normal range.

Due to the critical role played by the autonomic nervous system in normal physiological function and in the pathogenesis of many medical disorders, an accurate quantification of its functioning can help investigate certain diseases, symptoms or phenomena whose underlying mechanisms are still unclear, such as sudden cardiac death [107-109], microgravity exposure-induced syncope [106, 110, 111], circadian rhythms [112], *et al.* In addition, evaluation of the autonomic function is often necessary for patients with diabetes [113, 114], renal disease [115, 116], syncope [117, 118], ischemic heart disease [119, 120], chronic heart failure [121, 122], hypertension [123, 124], and other cardiovascular-related diseases to make diagnosis, design treatment plan and perform follow-up.

In the remainder of this chapter, we begin with a brief review on some of the previously employed approaches for the quantification of autonomic function. We then provide a detailed presentation of our proposed techniques which are based on the WPCR method. Depending on the breathing pattern of the subjects to be studied and the type of data available, different approaches should be utilized. We discuss the quantification of sympathetic and parasympathetic activity with respect to data collected during spontaneous breathing, random breathing and metronomic breathing respectively. Experimental data will be utilized to assess the performance of the methods.

3.2 Previous Approaches for Autonomic Function Quantification

The most intuitive way to evaluate autonomic function is by directly measuring the nerve firing activity using electrodes. For example, muscle sympathetic nerve activity (MSNA, e.g. from the peroneal nerve [125]) can be measured invasively to evaluate sympathetic function. Another intuitive method of autonomic quantification is the biochemical measurement of circulating transmitters in plasma secreted by the nerve fibers [45]. However, the correlation between the measured concentration of neurotransmitters and the autonomic tone is complicated by the duration of action, the diffusion ability of the neurotransmitters in the bloodstream, the width of the synaptic gap and the specific tissue associated with the nerve being studied, *et al.* [126]. Moreover, the above direct measurement techniques are invasive to different extents and relatively hard to operate.

Early non-invasive techniques for analysis of autonomic activity were based on evaluating heart rate or arterial blood pressure changes invoked by stimulation of cardiovascular reflexes. Heart rate response to provocative maneuvers such as deep respiration [127], postural change (tilt table testing or stand test) [128], and a Valsalva maneuver (the patient is usually asked to expire for 15 to 20 seconds against a resistance of, e.g., 40 mmHg, in an open loop system [129]) are often used to measure parasympathetic function. Sympathetic function is typically evaluated by measuring the blood pressure response to postural change [130], a cold pressor stimulus (the patient is usually asked to place his/her hand in cold wa-

ter for 60 seconds [131]), and isometric exercise (the patient is instructed to squeeze a hand-grip dynamometer for, e.g., 4 minutes [132]). These reflex tests suffer from similar problems. They are usually poorly standardized due to varying patient effort. Measurements of these responses are often made over a short period of time, and may produce atypical results solely due to natural variation [133].

Recent advances in signal processing have made it possible to non-invasively determine changes in autonomic activity with minimal active patient participation. The most widely used technique is the heart rate spectral analysis, which has been intensively studied since the early 80 s [134]. Three main spectral components were distinguished in a spectrum calculated from short-term recordings of heart rate: low-frequency peak (~0.04Hz), mid-frequency peak (~0.12Hz) and high-frequency peak (~respiration frequency). It was demonstrated that the mid- and high-frequency peaks are mediated by the parasympathetic system whereas both the sympathetic and parasympathetic system may mediate the low-frequency fluctuations [134]. In practice, power spectral component in the high frequency domain (0.15Hz ~ 0.40 Hz) is usually deemed as an indicator of parasympathetic activity, while spectral power in the low frequency domain (0.04 ~ 0.15Hz) is assumed to be an indicator of sympathetic activity [135]. Other similar quantifications have also been utilized. However, due to the overlapping of the effects of the two autonomic branches in the low frequency domain, an accurate estimation of the sympathetic function has not been provided through this method. In addition, a change in the high-frequency peak may be caused by changes of respiratory volume or rate [136]. Lack of correlation between vagal activity and the high-frequency peak has also been observed in conditions that involve a strong vagal stimulation [136].

In recent years, a series of advanced techniques have been developed for the purpose of autonomic function evaluation. Shin *et al.* [137] proposed the complex demodulation method to examine the time varying characteristics of the respiratory frequency peak and the low frequency (0 to 0.124 Hz) peak, supposedly related to parasympathetic and sympathetic activity respectively. Complex demodulation enables a description of amplitude and phase of particular frequency components of a time series as a function of time. Consequently,

this method can be used to study local changes of a signal over time. Note that it does not separate the effect of parasympathetic control from the sympathetic activity in the low frequency range. Other closely-related techniques have also been proposed in literature [138, 139].

Vetter *et al.* [140] analyzed the time-domain fluctuations in heart rate (HR) and arterial blood pressure (ABP) using the noncausal blind source separation (BSS) method. They assumed that HR and ABP are linear mixtures of the cardiac sympathetic and parasympathetic nerve activity related through the baroreflex pathway. BSS is a technique to separate the statistically independent source signals using only their convolutive mixtures. This method assumes mutual independence between the parasympathetic and sympathetic activity with respect to HR regulation. This assumption may not be valid in practice since it has been shown [141] that reciprocal relationships exist between the two autonomic branches. In addition, this method requires controlled breathing at 0.25 Hz to reduce the effect of respiration in the low frequency range (0 to 0.15 Hz) within which the BSS of the HR and ABP signals are performed. The authors also presented a similar method, but only requiring measurement of surface ECG [142]. They assumed that the RR and QT time series are linear mixtures of the cardiac sympathetic and parasympathetic nerve activity. A BSS algorithm for temporally correlated sources is applied to the RR and QT time series after noise reduction. This method is also based on the assumption of mutual independence of the sympathetic and parasympathetic nerve activity. It neglects the mechanical influence of respiration on ABP. The authors demonstrated that the sympathovagal balance (ratio between sympathetic and parasympathetic nerve activity) can be estimated relatively accurately compared to the conventional heart rate variability analysis. In a similar vein, Buckingham *et al.* [143] proposed to analyze beat-to-beat QT interval variability as a quantitative index of sympathetic activity provided that a reliable method of correcting for changes in heart rate can be developed.

The analysis of nonlinear dynamics [144] or chaos analysis [145] for evaluation of autonomic control processes has also been investigated in normal subjects and patients with cardiovascular diseases. Zhong *et al.* [4] proposed the application of a nonlinear analysis

method – principal dynamic modes (PDM) [146, 147] – to separately evaluate the contributions of autonomic nervous systems to heart rate variability. PDM analysis is a method for characterizing nonlinear physiological systems while reducing higher-order dimensions. The PDMs are computed from first- and second-order kernel estimates obtained from the data via a Laguerre expansion technique. The PDMs are orthogonal and no claim of uniqueness can be made [146]. The authors concluded that two dominant PDMs reflect parasympathetic and sympathetic activity respectively as manifested through data obtained during autonomic blockade.

The above methods employ advanced signal processing techniques. They may prove useful as noninvasive quantification of cardiac autonomic function. However, these methods can only separate sympathetic and parasympathetic function based on independence or orthogonality assumptions which are unrealistic and they have yet to be extensively validated or applied in clinical investigations. Nevertheless, the above studies are valuable in that they provide abundant insights for further development and improvement of related techniques and they demonstrate the effectiveness of signal processing and system analysis methodologies in tackling problems related to medicine and clinical practice.

3.3 Proposed Methods for Autonomic Function Quantification

In this section, we present three approaches to separately quantify cardiac sympathetic and parasympathetic control during random breathing, spontaneous breathing and metronomic breathing respectively. All methods are built upon the basis of system identification theory. They each require noninvasive measurements of one or more cardiovascular-related signals, such as, the surface ECG, ILV and ABP, depending on the specific clinical application.

3.3.1 Autonomic Function Quantification I – the Area Method[6]

This technique is developed based on the closed-loop cardiovascular control model presented in Chapter 2. In Section 2.10, we employed experimental data (random breathing ILV, ABP and HR) from 29 male subjects and discussed the closed-loop WPCR identification of these data. For illustration purpose, Figure 3-2 displays the impulse response functions identified for one subject, in addition to the noise spectra. The works of Triedman *et al.* [148] and Mullen *et al.* [23] demonstrated that both the positive wave and the negative wave in the ILV→HR impulse response and the negative waves in the HR baroreflex impulse response (see Figure 3-2) for humans were nearly obliterated after total cardiac autonomic blockade. Therefore, these two couplings are mainly regulated by the autonomic system. It is natural to postulate that certain characteristics of the impulse responses may contain information about autonomic tone. However, the key question is whether or not there is a way to distinctly identify the parasympathetic component and the sympathetic component.

Berger and coworkers [10] studied the dynamical behavior of the canine cardiac pacemaker – the sinoatrial (SA) node. The excitation of this system was achieved with a broad-band input signal whose frequency varied about some mean value in proportion to a band-limited Gaussian white-noise signal. The impulse responses of the sinoatrial node discharge rate under pure vagal stimulation and pure sympathetic stimulation at a mean rate of 4 Hz and 1 Hz, respectively, are shown in Figure 3-3, as adapted from [10]. The parasympathetic response reflects the lack of delay and the broad-band nature of the atrial response to vagal excitation, whereas the sympathetic response reveals a delay of roughly 2 s and a slow-changing feature [10]. Comparing Figure 3-3 to the ILV→HR impulse response in Figure 3-2, it can be appreciated that the parasympathetic and sympathetic impulse responses mimic, respectively, the initial upright wave and the delayed negative wave (with a reverse in polarity) in the ILV→HR impulse response.

[6] Much of the content in this section has been presented in the Journal of Applied Physiology [106].

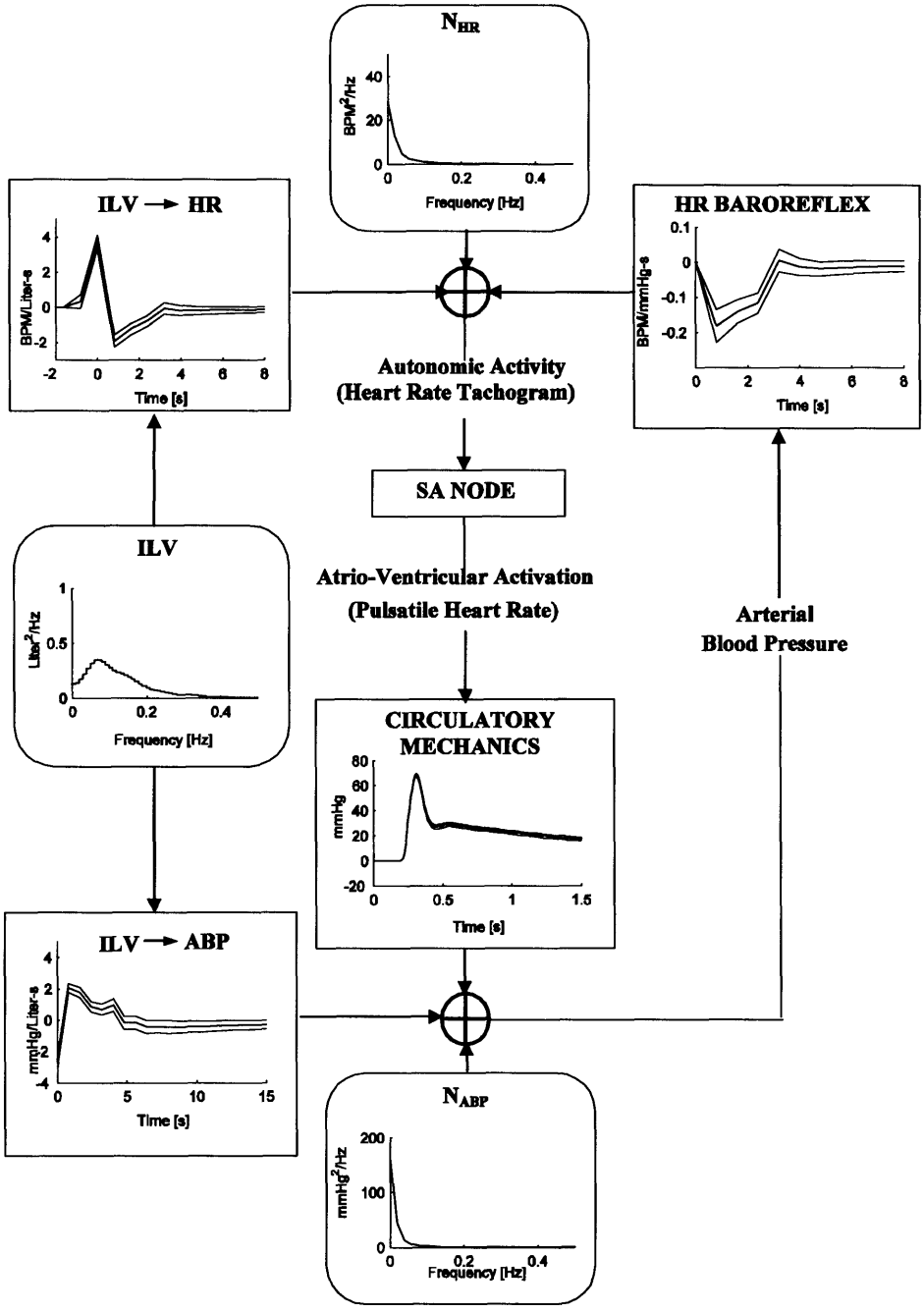

Figure 3-2 Closed-loop model of short-term cardiovascular regulation identified by means of cardiovascular system identification. Impulse response functions and noise sources are identified for a subject in the supine position pre-bed rest. Ninty-five percent confidence intervals are provided for impulse response functions. HR, heart rate tachogram; ILV, instantaneous lung volume; ABP, arterial blood pressure; SA, sinoatrial; N_{HR}, power spectrum of perturbations to HR not attributable to HR Baroreflex and ILV→HR; N_{ABP}, power spectrum of perturbations to ABP not attributable to Circulatory Mechanics and ILV→ABP (adapted from [106] with permission granted by the APS).

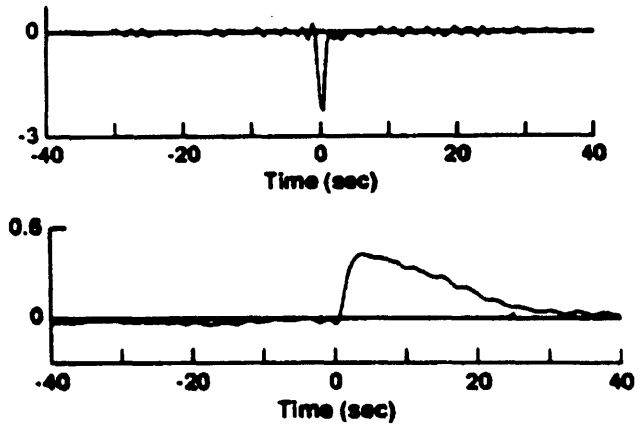

Figure 3-3 Impulse responses of the canine SA node discharge rate with vagal stimulation (upper) and sympathetic stimulation (lower) (adapted from [10] with permission granted by the APS)

The above experimental evidence indicates that the ILV→HR impulse response is mainly modulated by the autonomic system. Moreover, assuming linearity of the system, we can interpret and model it into two components as follows (Figure 3-4). The initial upright wave represents the brief increase in HR mediated by parasympathetic withdrawal as a result of an impulse ILV input (very rapid inspiration and expiration). The increase begins at time < 0, indicating that HR rises in anticipation of the corresponding inspiration which reflects the time delay between central initiation of cardio-respiratory activity and the physical onset of inspiration [10, 148]. The delayed negative deflection is the consequence of sympathetic withdrawal which is slower than the parasympathetic response. Therefore, the ILV→HR impulse response consists of two main separable components each reflecting the modulation of the sinoatrial node by autonomic efferent signals. If we divide the impulse response into two components at the point where it first crosses zero after reaching the peak (Figure 3-4), the areas covered by the two components quantify parasympathetic and β-sympathetic efferent activity responsiveness, respectively. Note that from Figure 3-3, there is no significant overlap in time between the parasympathetic response and the sympathetic response. Our separation approach assumes that this overlap can be neglected. We will refer to the above technique as the *Area method* in the subsequent sections.

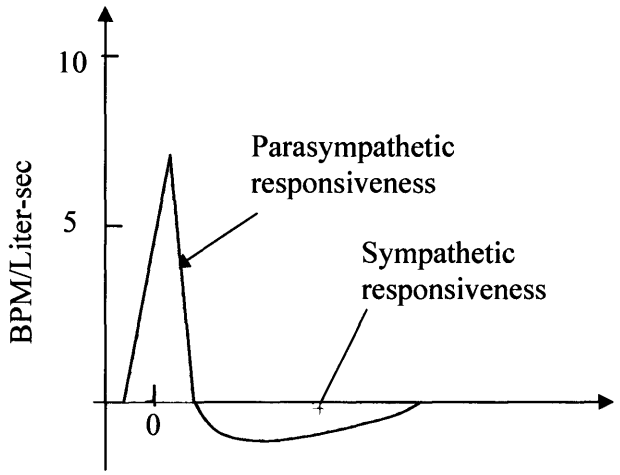

Figure 3-4 Model of a standard ILV→HR impulse response. The area of the initial upright wave represents parasympathetic responsiveness and that of the slower negative deflection represents sympathetic responsiveness. The axes are labeled only to provide an example of the scale (adapted from [106] with permission granted by the APS).

HR Baroreflex impulse response (see Figure 3-2 for example) can also be modeled as reflecting parasympathetic and sympathetic components. However, in response to an impulse change in ABP, stimulation of parasympathetic function and suppression of sympathetic function both lead to a decrease in HR. Due to their identical polarity, the responses in HR induced by the two autonomic mechanisms normally overlap each other in the HR Baroreflex impulse response and are hard to separate. Therefore, we only employ the ILV→HR impulse response to deduce autonomic responsiveness.

The Area technique has been applied to study autonomic function and its association with tilt intolerance in healthy human subjects before and after prolonged head-down-tilt bed rest (a ground-based simulation of microgravity) [106]. In [106], the APR method was employed to identify the impulse responses in the closed-loop model. As discussed in Chapter 2, our newly presented WPCR method can lead to statistically more significant results which

are also more computationally stable. In Section 3.4.2, we will validate the Area technique in association with the WPCR method via experimental data.

The above method for the quantification of autonomic responsiveness requires the subject to follow a random breathing protocol to obtain persistently exciting signals for system identification. Although this procedure could be easily performed in research labs, it may be cumbersome in clinical settings and an approach that works for spontaneous breathing measurements is more desirable and practical. Furthermore, the above technique needs three types of noninvasively measured signals – HR, ILV and ABP. However, in usual patient monitoring, the most conveniently measured signal is the surface ECG. Hence, a technique that requires only ECG measurements to quantify autonomic function is most practical and readily applicable. To this end, we propose, in the following section, a new quantification method for autonomic responsiveness which is also based on WPCR system identification.

3.3.2 Autonomic Function Quantification II – the SD Method

Before going into details about the proposed identification method, we need to note that instantaneous lung volume (ILV) signal can be extracted from surface ECG measurements. The most widely employed method is the EDR method (ECG-Derived Respiration) [149]. It is based on the phenomenon that physical influences of respiration lead to amplitude variations in the observed ECG and thus modulate the direction of the mean cardiac electrical axis. The authors [149] proposed a robust method to measure the fluctuations in the mean cardiac electrical axis (typically between 1° and 12° peak-to-peak) which was shown to be well-correlated with respiration through experimental data. Although the method works best when two ECG leads are available, it is possible to generate an EDR signal from only one lead [149]. Other techniques have also been investigated for respiration monitoring based on ECG signals, for example, the amplitude demodulation method [150], principal component analysis on the QRS parameters [151], *et al.* In addition, a type of commercially available electrodes may be utilized to measure respiratory impedance pneumography (RESP)

and ECG simultaneously. RESP measurement is accomplished by passing a very small high frequency electrical current across the ECG electrodes and measuring the change in impedance as the chest volume changes.

In this section, we propose a new method for the quantification of cardiac autonomic responsiveness utilizing ILV and HR data. Based on the above ILV-derivation techniques, our method only necessitates surface ECG measurement. One advantage of this method is its applicability to data collected during both spontaneous breathing and random breathing. Two problems need to be solved in the development of this method. First, the ILV signal during spontaneous breathing is generally narrow banded (0.15 ~ 0.25 Hz) and does not satisfy the 'persistently exciting' requirement imposed by conventional system identification techniques. The other difficulty is induced by the effect of arterial blood pressure on HR. Based on the discussion in the last section, the ILV→HR impulse response contains evident features which can be mapped to parasympathetic and sympathetic responsiveness. However, this impulse response can be obtained only when the ABP signal is also available such that the variations in HR due to ABP may be accounted for. With only ILV and HR, one may still attempt to identify the transfer relation between them (we denote it as ILV⇒HR to emphasize the hidden effect of ABP). However, since the HR baroreflex (or ABP→HR) pathway is also regulated by the autonomic nervous system, it is not apparent how parasympathetic and sympathetic regulation is reflected in the ILV⇒HR coupling. In the following section, we aim to explore the above questions and formulate the autonomic function identification method using ILV and HR only.

Parasympathetic Index

We first study the ILV⇒HR coupling to extract parasympathetic index from its impulse response function. For simplicity, the closed-loop cardiovascular regulation model (Figure 2-25) is redrawn in Figure 3-5 without explicitly showing the noise disturbances. In this model, the couplings presented in the rectangular boxes are assumed to be linear. The only nonlinear component is the SA node.

Based on Figure 3-5, the HR variations are induced through two main pathways as represented by the following equation (note that the noise terms are omitted):

$$\Delta HR = \Delta ILV * h_1 + \Delta ABP * h_2 \tag{2.50}$$

where h_1 and h_2 represent the transfer relations of ILV→HR and ABP→HR respectively.

Since the characteristics of the ILV→HR impulse response and their association with the autonomic function have been studied thoroughly in the last section, we intend to find some correlation between the features in the composite impulse response (ILV⇒HR, enclosed by the dotted box in Figure 3-5) and those in the ILV→HR coupling. Because our main interest here is to define a parasympathetic index based on the ILV⇒HR impulse response, we first consider the high frequency components in the HR data. If the contribution of the ABP signal to HR variation is relatively small in the high frequency range, then the ILV→HR coupling is the major contributor to HR variability in this range. In this case, the high frequency components in ILV⇒HR may have the same interpretation as those in the ILV→HR coupling. Therefore, it may be possible to define a parasympathetic index based solely on the ILV⇒HR impulse response.

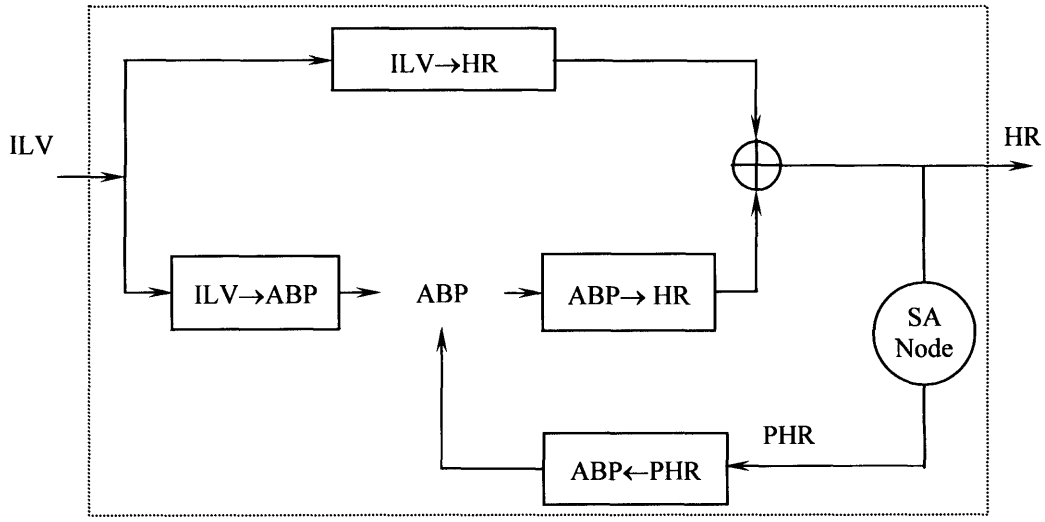

Figure 3-5 Short-term closed-loop cardiovascular regulation

To empirically demonstrate the above conjecture, we employ ILV, ABP and HR data from 10 healthy subjects (six males, four females, age: 23.9 ± 3.9 (SD) yr) obtained during both random breathing and spontaneous breathing. The data were collected in supine posture and 30° head-up-tilt posture respectively. The measurements were performed in the Clinical Research Center of the Massachusetts Institute of Technology and all subjects provided written, informed consent. We first consider the case of random breathing because the system identification method for this type of data is well established.

Approximately 6-minutes of ILV, ABP and HR signals were downsampled from 100 Hz to 1.25 Hz. The transfer functions ILV→HR and ABP→HR can be identified using the WPCR-MA method as presented in Chapter 2, Section 2.10 (same initial model orders, model selection criterion and closed loop pre-whitening and weighting schemes). Next, the HR components, which are due to ILV variation and ABP variation (denoted as HR_{ILV} and HR_{ABP}) respectively, are calculated. The averaged power density spectra of these components are shown in Figure 3-6. It can be appreciated that the HR_{ABP} signal is low-frequency dominant. Quantitatively, in the relatively high frequency range (0.15 Hz to 0.4 Hz), the power of HR is 42.4 (supine) (25.5 (tilt)) times that of HR_{ABP} and the power of HR_{ILV} is 26.1 (supine) (10.2 (tilt)) times that of HR_{ABP}. Hence, the contribution of ABP to HR in the high frequency range may be considered to be small and the ILV⇒HR transfer function within this range may possess similarity to the corresponding ILV→HR components. Figure 3-7 displays the averaged frequency responses of these two transfer functions to demonstrate this similarity.

Since only a parasympathetic index is being sought for in this section, we study the correlation of one specific high frequency-related component, the peak amplitude, of the ILV→HR and ILV⇒HR impulse responses. As discussed in Chapter 2 and [106], the former has been demonstrated to be a robust indicator of parasympathetic function. Figure 3-8 displays the averaged ILV→HR and ILV⇒HR impulse responses of the 10 subjects in both supine and 30° tilt postures identified by the WPCR method. Figure 3-9 shows the values of the peak amplitude of the two impulse responses of individual subjects and the corresponding correlation analysis. It is evident that the peak amplitude of the ILV⇒HR impulse re-

sponse is closely correlated with that of the ILV→HR impulse response. Therefore, the former may also serve as an indicator of parasympathetic responsiveness. In Sections 3.4.2 and 3.4.3, we will further validate this conclusion via experimental data.

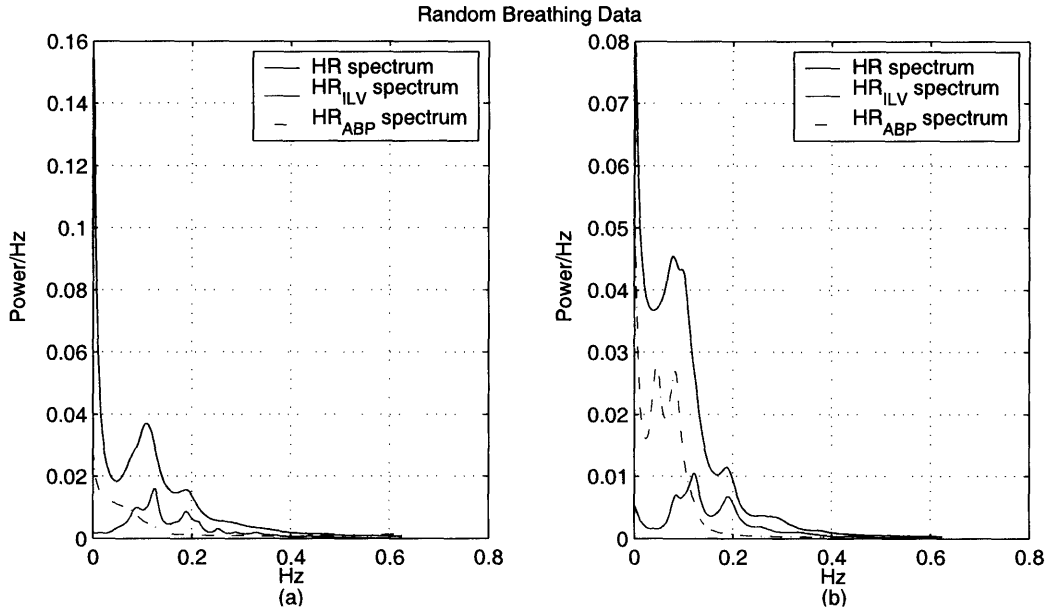

Figure 3-6 Power density spectra of the HR signal, the HR component due to ILV variations and the HR component due to ABP variations, random breathing data. (a) supine posture; (b) 30° tilt-up posture. Average of 10 subjects. Note that the HR signals have been normalized with respect to their respective mean value to reduce inter-subject variability

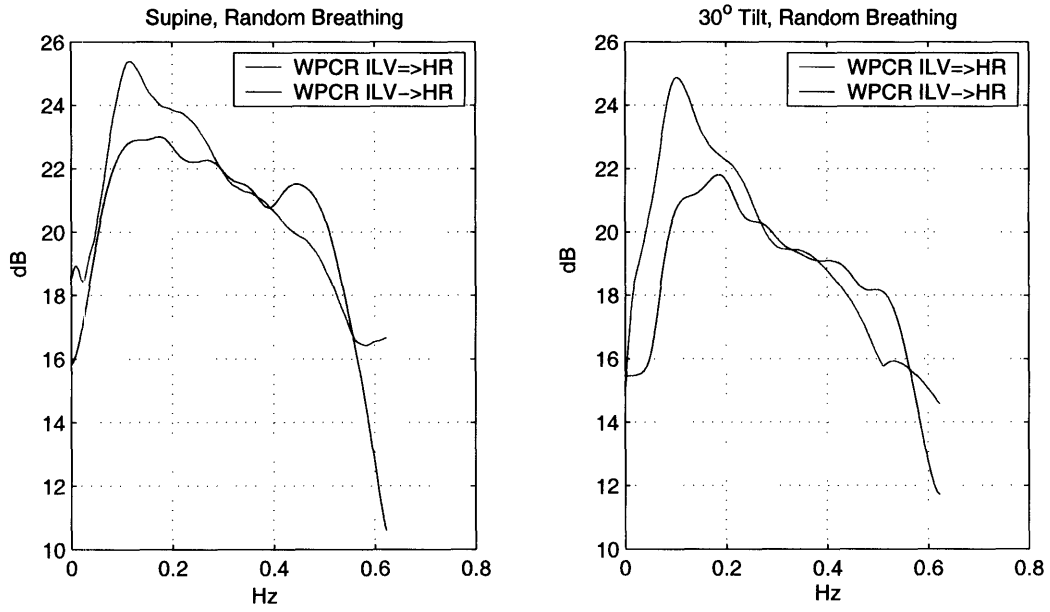

(a) (b)

Figure 3-7 Frequency responses of the ILV⇒HR and ILV→HR transfer functions identified by the WPCR method, random breathing data. (a) supine posture; (b) 30° tilt-up posture. Average of 10 subjects.

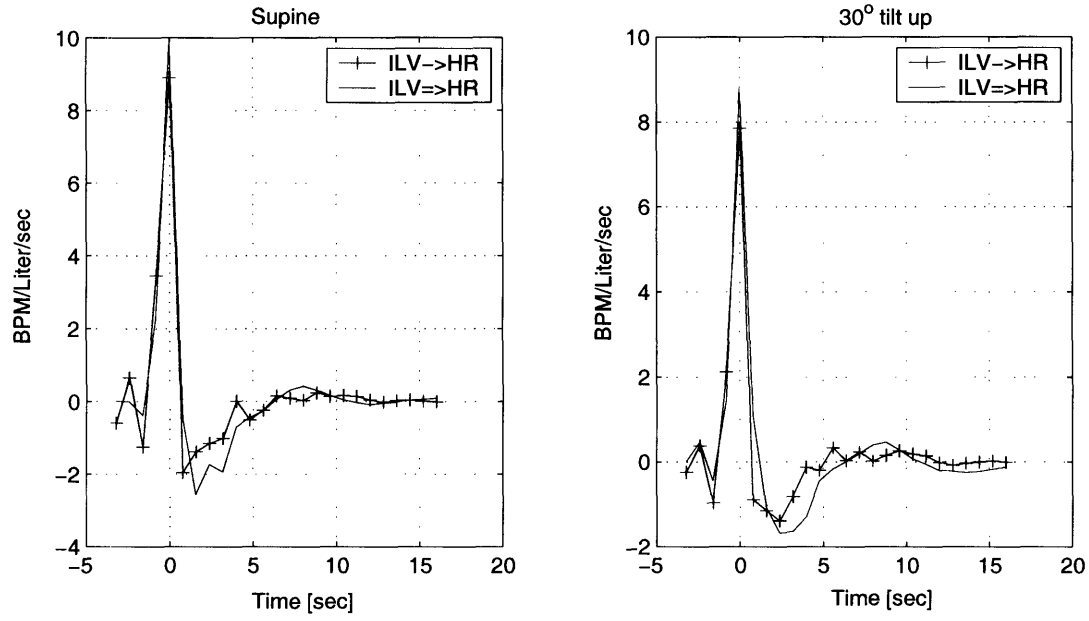

(a) (b)

Figure 3-8 Impulse responses of the ILV→HR and ILV⇒HR couplings, random breathing data. (a) supine posture; (b) 30° tilt-up posture. Average of 10 subjects.

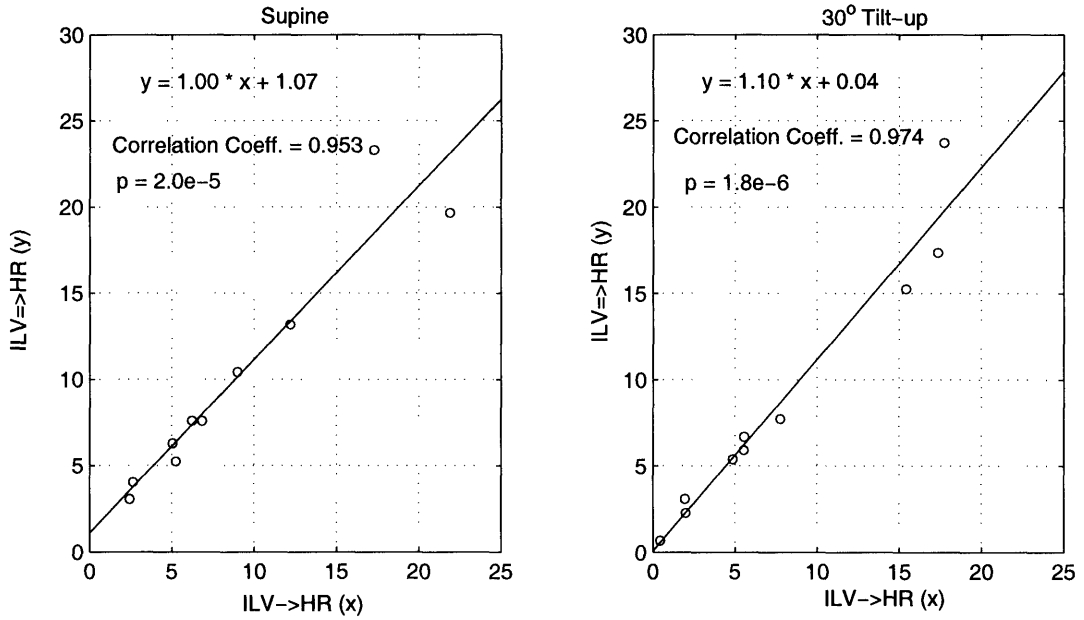

Figure 3-9 Correlation analysis of the peak amplitude (BPM/Liter/sec) of the ILV→HR and ILV⇒HR impulse responses, random breathing data. (a) supine posture; (b) 30° tilt-up posture

Next, we consider the case of spontaneous breathing. As aforementioned, the conventional system identification requirement of persistently exciting input signals is not satisfied by spontaneous breathing data. To illustrate this problem, an example of the ILV spectra of one subject during spontaneous breathing and random breathing is demonstrated in Figure 3-10. It is apparent that the ILV frequency content is concentrated in the relatively high frequency range in spontaneous breathing data, while significant low frequency components are present in random breathing ILV signals. Thus, the major low frequency components (< 0.15 Hz) present in the ILV⇒HR frequency response (see Figure 3-7) are underrepresented in the spontaneous ILV spectrum and the persistently exciting requirement of system identification is not satisfied.

The WPCR method is suitable to cope with spontaneous breathing data for the purpose of calculating a parasympathetic index. As demonstrated in Chapter 2 (Section 2.8.2) through computer simulations, this method is able to estimate the impulse response at frequencies

excited by the input signal relatively accurately owing to its frequency selective property, even when the input signal does not encompass the entire spectrum of the transfer function. Since in the current problem, spontaneous ILV signal has significant power in the high frequency range, we anticipate that the high frequency components in the impulse response, e.g., the peak of the ILV⇒HR impulse response, can be identified accurately with spontaneous breathing data. Further discussion in this aspect based on computer simulations is provided in Appendix B. Hereafter, the WPCR-ARX method will be employed to identify the ILV⇒HR impulse response. The same weighting scheme as presented in Chapter 2 (Section 2.8.1) will be incorporated. Note that because of the lack of information in the low frequency range of the ILV signal, it is not possible to estimate the low frequency components in the transfer function accurately via system identification.

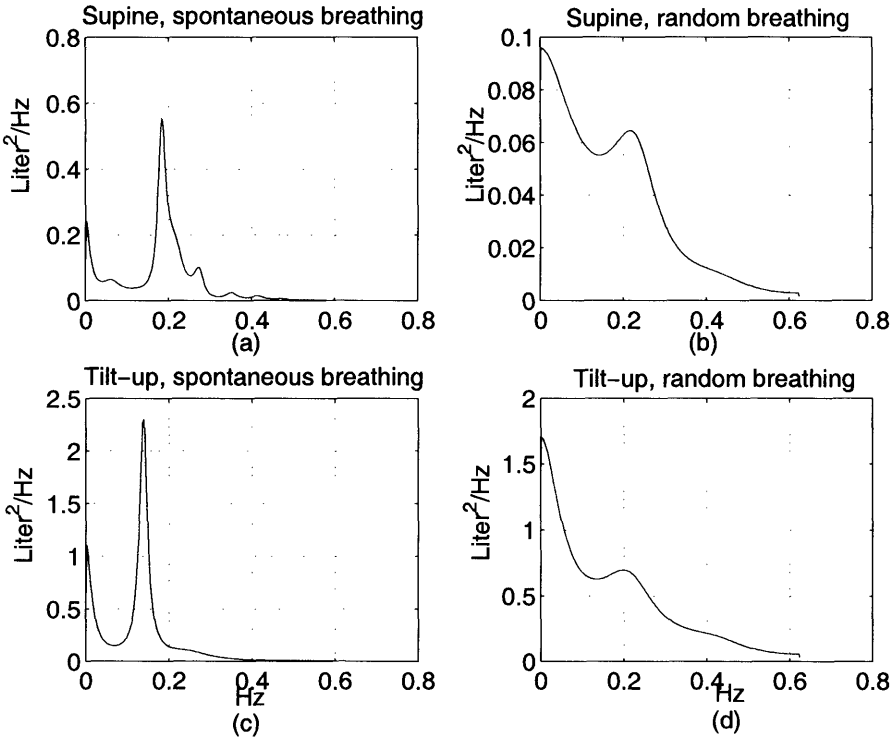

Figure 3-10 Power density spectrum of the ILV signal collected from one subject. (a) supine, spontaneous breathing; (b) supine, random breathing; (c) 30° tilt-up, spontaneous breathing; (d) 30° tilt-up, random breathing.

Figure 3-11 displays the averaged ILV⇒HR impulse responses identified using random breathing and spontaneous breathing data respectively in supine and tilt-up postures. Figure 3-12 compares the peak amplitude of the ILV⇒HR impulse response of each subject during random breathing and spontaneous breathing. The correlation analysis demonstrates that this value can be identified by the WPCR-ARX method with a good accuracy using spontaneous breathing data. In combination with the previous analyses on the random breathing case, we conclude that the peak of the ILV⇒HR impulse response during spontaneous breathing can also serve as a parasympathetic index. This conclusion will be further validated through experimental data in Section 3.4.3.

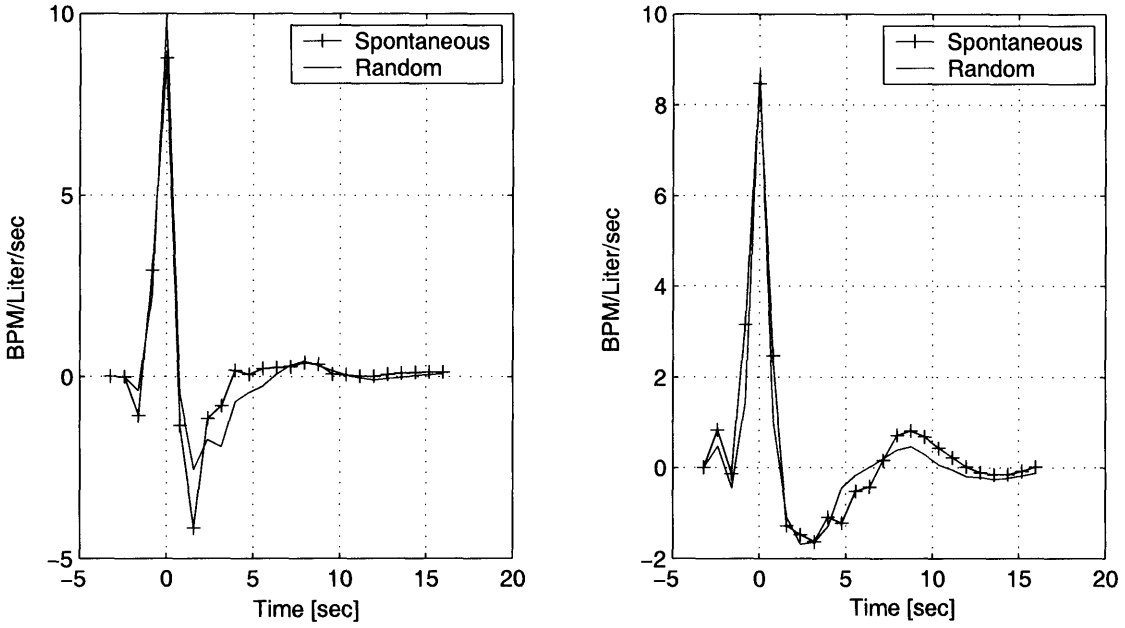

Figure 3-11 Comparison of ILV⇒HR impulse responses identified by the WPCR method using spontaneous and random breathing data. (a) supine posture; (b) 30° tilt-up. Average of 10 subjects.

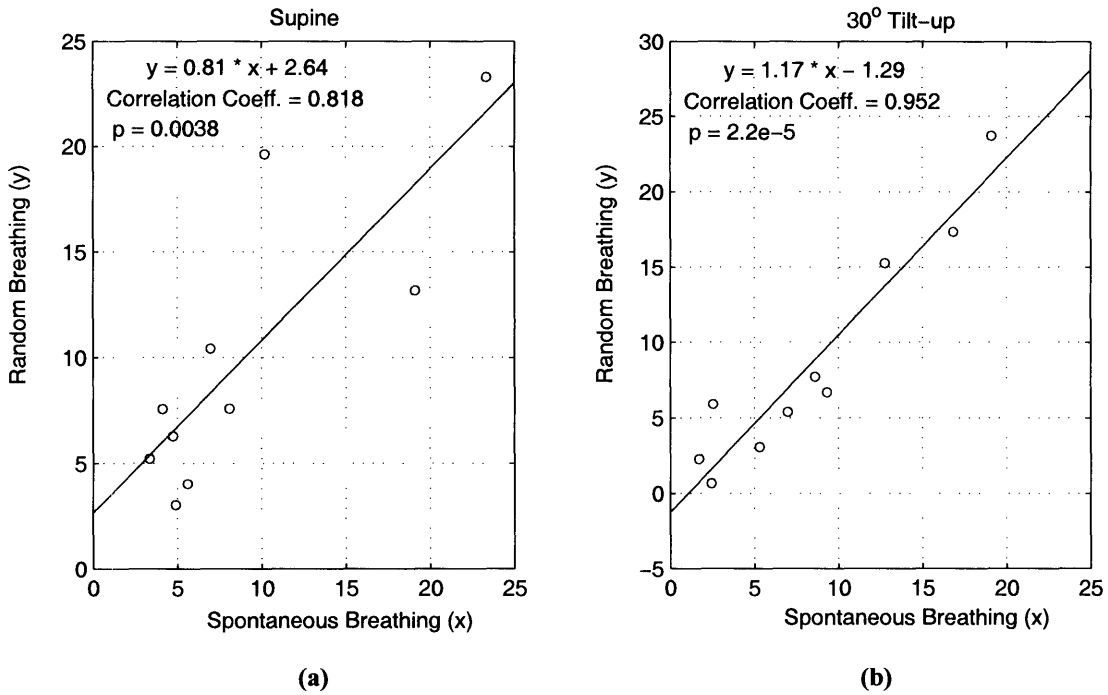

Figure 3-12 Correlation analysis of the peak amplitude (BPM/Liter/sec) of the ILV⇒HR impulse responses during spontaneous breathing and random breathing. (a) supine posture; (b) 30° tilt-up.

In summary, given the ILV and HR data (which can be derived from ECG) of one subject during either spontaneous breathing or random breathing, we can derive a parasympathetic index based on the WPCR system identification of the ILV⇒HR coupling.

Sympathetic Index

Since sympathetic control of the cardiovascular system is low-frequency related (0 ~ 0.15 Hz in general), the sympathetic responsiveness can not be easily quantified based on the ILV⇒HR impulse response due to the contribution of ABP to HR in the low frequency range. In this section, we present a simple, but robust method to extract sympathetic index.

In the forward modeling of autonomic control of heart rate variation, the integral pulse frequency modulation (IPFM) model [152] is often used to describe the response of the car-

diac pacemaker cells to neural stimulation. Specifically, the IPFM process integrates its input signal until reaching a predefined threshold, at which point a pulse is generated and the integrator is set to zero to start the integration anew. This process can be expressed as:

$$T = \int_{t_n}^{t_{n+1}} [m_0 + m(t)]dt \tag{2.51}$$

where m_0 is a constant contribution of the intrinsic cardiac pacemaker. $m(t)$ is the modulating signal. T is the predefined threshold that determines the intrinsic frequency of the generated pulses when $m(t)$ is equal to zero.

The modulating signal of the IPFM model reflects the parasympathetic and sympathetic regulation on the sinoatrial node. In the literature, this signal is often modeled as a linear function of the concentrations of the neurotransmitters combined by their corresponding receptors [153, 154], i.e.,

$$m(t) = k_1[NE](t) - k_2[Ach](t) \tag{2.52}$$

where $[Ach]$ denotes the concentration of the parasympathetic neurotransmitter (acetylcoline) and $[NE]$ denotes that of the sympathetic one (norepinephrine). The parameters k_1 and k_2 are some fixed proportional coefficients indicating the input to the pacemaker cell generated by unit concentration neurotransmitter.

Based on the IPFM model, if representing the averaged $[NE](t)$ in the time interval $[t_n, t_{n+1}]$ as $\overline{[NE]}[n]$, and that of $[Ach](t)$ as $\overline{[Ach]}[n]$, we have:

$$HR[n] = \frac{1}{T}\left(m_0 + k_1\overline{[NE]}[n] - k_2\overline{[Ach]}[n]\right) \tag{2.53}$$

where $HR[n] = 1/(t_{n+1} - t_n)$ is a measure of instantaneous heart rate. Therefore, HR is linearly related to the beat-averaged concentrations of the effective neurotransmitters (those that are bound with receptors) which are in turn determined by the variation in the firing frequency of the autonomic nerves and the chemical kinetics involved. This linear model has been incorporated in the forward modeling of autonomic control of heart rate and simulation

results that are consistent with experimental findings have been demonstrated in the literature [153, 154].

Based on Equation (2.53), it is apparent that variation in HR is contributed by two components: one is due to parasympathetic regulation, the other is due to sympathetic regulation. Importantly, a linear model may be assumed in relating these two components to the change in HR. Inspired by this model, we utilize a similar linearity assumption in the following representation of HR variation:

$$\Delta(HR_{\omega}) = \alpha S_I + \beta P_I + \Delta HR^0 \tag{2.54}$$

where $\Delta(HR_{\omega})$ denotes the "change" of HR in a low frequency range to be defined. The parameters α and β are two coefficients whose values are to be determined below. S_I is the sympathetic index to be computed which should be related to the change in HR resulted from sympathetic regulation, while P_I denotes the parasympathetic index to be defined which reflects the change in HR owing to parasympathetic regulation. ΔHR^0 is the residual HR variability when both the parasympathetic and sympathetic control on HR are completely obliterated (i.e., $S_I = 0$, $P_I = 0$, complete autonomic blockade). It may be due to measurement noise or some mechanical mechanisms affecting HR [148]. Qualitatively, Equation (2.54) is a mathematical expression of the *a priori* knowledge that HR variability in the low frequency range reflects a combined effect of sympathetic and parasympathetic modulation on HR.

Next, we define the specific computation of $\Delta(HR_{\omega})$. A natural choice for a scalar representation of variation in a time series may be the standard deviation (or variance). However, this measure is merely a quantification of variability in consideration of the entire frequency spectrum. To have a more specific characterization, we limit the computation of HR change in a particular frequency range, denoted by the subscript ω in $\Delta(HR_{\omega})$. Since our goal is to quantify the sympathetic function which is low frequency dominant, we define this frequency range to be between 0.05 Hz and 0.15 Hz. Note that a similar range is often utilized to derive directly a sympathetic index based on HR spectral analysis [135], which is not accurate due to the additional effect of parasympathetic control. The frequency components

below 0.05 Hz may be closely related to the $1/f$ disturbance [57] or baseline drift. Thus, we exclude those components in our current analysis.

For the parasympathetic index P_I, we propose to use the normalized (to be discussed) peak amplitude ($P_{\max}$) of the ILV⇒HR impulse response (computed with ILV being divided by its standard deviation). As discussed previously, $P_{\max}$ reflects parasympathetically mediated HR alteration excited by an impulse change in ILV. Note that although $\Delta(HR_\omega)$ and P_I defined above both quantify HR change (with the same unit, e.g. beat/min), they differ in their physical meanings. Thus, a proportional coefficient α is needed to represent the amount of $\Delta(HR_\omega)$ that is equivalent to a unit P_I.

In order to compute S_I based on Equation (2.54), we need to calculate the unknown coefficients α, β and ΔHR^0. When the alterations in the autonomic function are not very drastic so as to challenge the extremities of the operating range, the values of these coefficients can be assumed to remain constant among subjects. This assumption is corroborated by the findings presented in [155]. We therefore propose to compute the unknown coefficients empirically through experimental data. A data set containing 14 subjects under various autonomic blockade conditions in supine and standing postures is employed (we name this data set the CRC data). The data were published in a previous study [23]. The subjects are healthy male nonsmoking volunteers (ages 19-38 yr, median 21 yr). ILV, ABP and ECG signals were obtained with the subjects following a random breathing protocol [23]. After collection of control data in the supine or standing posture, seven subjects received atropine (0.03 mg/kg iv, a competitive antagonist of the muscarinic cholinergic receptors/parasympathetic receptors), and data in each posture were again recorded [23]. These subjects then received propranolol (0.2 mg/kg iv, a non-selective beta-adrenergic receptor blocking agent), and a final set of recordings in each posture was obtained. The remaining seven subjects received the same dosages of drugs but in the reverse order [23]. We employ approximately 6 minutes of data in the analyses hereafter which were downsampled to 1.5 Hz from 360 Hz.

Before proceeding with the computation of the unknown coefficients, we first evaluate the linearity assumption between $\Delta(HR_\omega)$ and P_I in Equation (2.54) utilizing the CRC database.

Figure 3-13 is the scatter plot of $\Delta(HR_{\omega})$, as defined above, versus the values of the peak amplitude (P_{max}) of the ILV⇒HR impulse response. Each sample point in the plot denotes one subject in one of the following conditions: supine with propranolol injection and standing with propranolol injection. The line indicates the linear regression of the scattered samples whose correlation coefficient is 0.80. Since propranolol administration is expected to block the sympathetic pathway, this result supports the assumption of a linear relationship between P_I and $\Delta(HR_{\omega})$, at least in the range encompassed by the samples in Figure 3-13. In reality, the dosage of propranolol may not be adequate for a complete sympathetic blockade which may induce the deviation of the samples from a linear relation in Figure 3-13. Since the sympathetic pathway is a counterpart of the parasympathetic control, it is acceptable to also assume linearity in the relationship of a sympathetic index and $\Delta(HR_{\omega})$, at least as a first attempt.

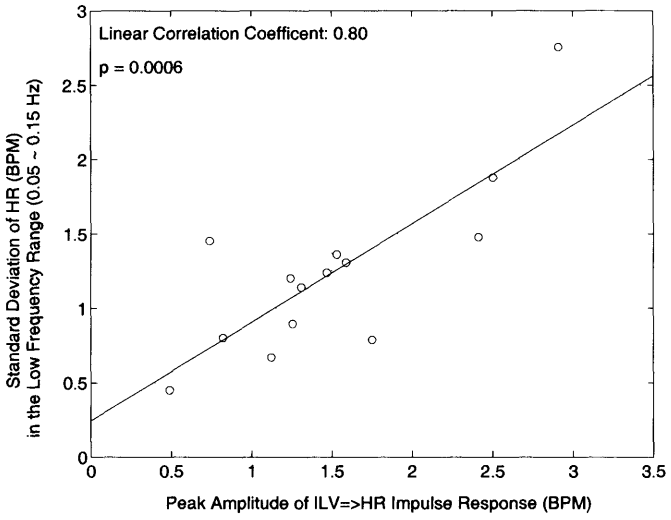

Figure 3-13 Scatter plot of the standard deviation of HR versus the peak amplitude of the ILV⇒HR impulse response, seven subjects in the CRC database in SUP and STP conditions.

Next, we define P_I as a normalized version of the peak amplitude (P_{max}) of the ILV⇒HR impulse response.

$$P_I = k_p \cdot P_{\max} + k_0 \qquad \begin{cases} P_I = 0, & at \quad SUB \\ P_I = 1, & at \quad SUC \end{cases} \tag{2.55}$$

where SUB denotes the SUpine, autonomic double Blockade condition, and SUC denotes the SUpine, Control condition. Data of the 14 subjects under these two conditions can be used to compute the coefficients k_p and k_0. Note that k_0 is not zero in general since $P_{\max}$ is not usually zero at SUB due to residual mechanical effects or measurement noise.

Subsequently, we defined the normalized range of S_I,

$$S_I = \begin{cases} 0, & at \quad SUB \\ 1, & at \quad STC \end{cases} \tag{2.56}$$

where STC denotes the STanding, Control condition. Therefore, ΔHR^0 can be computed as the averaged standard deviation of HR in the low frequency range (0.05-0.15 Hz) of the 14 subjects at SUB. Subsequently, α and β can be calculated using the data at STC with S_I being 1 and P_I being computed through Equation (2.55).

In the identification of the ILV⇒HR coupling, we normalize the ILV signal by its standard deviation to account for the baseline difference in respiration need among subjects due to, for example, different height, weight or metabolic rate, *et al.* Although the unknown constants in Equation (2.54) are calculated using random breathing data, they are also applicable to spontaneous breathing data after ILV normalization because random breathing does not affect the normal operation of the autonomic system [48]. However, the values of the autonomic indices of the same subject during random and spontaneous breathing are not identical, which will be discussed in more detail in Section 3.5.

To summarize, the parasympathetic and sympathetic indices of any subject can be obtained given the HR and ILV signals (both of which may be derived from surface ECG) during either random or spontaneous breathing. Henceforth, we will refer to the above method as the *SD method* for autonomic function quantification.

3.3.3 Autonomic Function Quantification III – the SD_m Method

The Area and the SD methods require that the ILV signal contains significant power either in the whole frequency range being studied or in the high frequency range. However, there are cases when only data during metronomic breathing are available, e.g., when the patient is on a ventilator. In such situations, the above system identification involving the ILV signal is not practically realizable. To this end, we propose a slightly modified SD method (the *SD_m method*) for autonomic function quantification using metronomic ILV and HR signals.

Since the metronomic ILV signal has significant power at only one frequency, its effect on HR is also concentrated at the same frequency based on the linearity assumption. In addition, this frequency, i.e., the rate of controlled breathing, is usually higher than 0.15 Hz (higher than the upper limit of the effective range of sympathetic frequency response). Therefore, HR variability at this frequency is mainly regulated by the parasympathetic system. Moreover, as demonstrated previously (Figure 3-6), HR power around the usual respiration frequency is mainly accounted for by ILV variation through the coupling of ILV→HR with the contribution of the ABP signal being negligible. Therefore, the coupling of the respiration frequency components in ILV and HR can serve as a basis for the derivation of a parasympathetic index. In practice, the amplitude of the ILV→HR frequency response at the metronomic breathing frequency computed as the ratio between the amplitudes of HR and ILV Fourier Transforms at this frequency may be employed to derive the parasympathetic index (this method belongs to the nonparametric system identification family).

Since significant amounts of energy in the metronomic ILV and HR signals are concentrated at the respiration frequency, the signal-to-noise ratio at this frequency is usually high. Therefore, the above defined parasympathetic index is expected to be relatively accurately computed. For random breathing or spontaneous breathing data, similar methods should not be applied because the respiration-related spectrum is fairly broad-band and a high signal-to-noise ratio at any particular frequency is not ensured.

For the sympathetic index, the model in Equation (2.54) of the SD method can still be utilized due to a similar argument as in section 3.3.2. Ideally, a database with autonomic

blockade during metronomic breathing should be employed to normalize the parasympathetic index and compute the coefficients in Equation (2.54). With the lack of such a database, the values calculated based on the CRC data may also be exploited, at least for the purpose of validating the method. This approximation is based on the fact that the parasympathetic impulse response (h_p) usually has a brief duration (about 2 s, see Figure 3-3). With a sample frequency of 1.25 Hz normally employed in data analysis, h_p usually encompasses two or three time intervals. It is expected that the value at the peak is significantly larger than at the other samples due to the abrupt feature of this impulse response. From these arguments and the definition of a frequency response:

$$H_p(\omega) = \sum_n h_p[n] \cdot e^{-j\omega n}, \tag{2.57}$$

the amplitude of $H_p(\omega)$ may be approximated by the peak of $h_p[n]$ without much compromise of accuracy.

In summary, in cases of metronomic breathing, a parasympathetic index can be derived from the amplitude of the ILV→HR frequency response at the metronomic breathing frequency and a sympathetic index can be computed based on Equation (2.54) and the CRC database.

3.4 Validation Results

In this section, we apply the above proposed methods (Area, SD and SDm) to analyze experimental data obtained during random breathing, spontaneous breathing and metronomic breathing respectively. These applications allow a validation and a further exploration of the properties of each method.

3.4.1 System Identification Using EDR Signals

Before engaging in the validation of the techniques for autonomic function identification, we first demonstrate through a few examples that the ECG-Derived Respiration (EDR) signals can be utilized as a substitute of ILV in the identification of the ILV⇒HR impulse response. As discussed in Section 3.3.2, the EDR technique derives a respiration signal from the ECG data based on the phenomenon that respiration modulates the mean cardiac electrical axis [149]. This technique provides one sample of the EDR signal per cardiac cycle by computing the area of each QRS complex. Given that heart rate is almost always greater than twice the respiration rate, it suffices to interpolate the samples using cubic splines to produce a continuous EDR signal [149]. In theory, two ECG signals measured simultaneously are needed to compute the changes in the mean cardiac electrical axis. If only one ECG lead is available, QRS area measurements from that lead can still be used as an approximation to the respiration signal. In this case, it is desirable to have the lead axis significantly different from the mean electrical axis to obtain a relatively large signal [149].

To demonstrate the applicability of the EDR technique in identifying the ILV⇒HR impulse response, we take one set of data from the MIMIC database [156] published in PhysioNet [157]. This specific example is obtained from a male, 52 year old ICU patient with congestive heart failure lying in the supine position during spontaneous breathing. EDR is derived based on two ECG signals (with a sample frequency of 500 Hz) from leads V and II. Figure 3-14(a) displays one segment of the EDR signal (at a sample frequency of 125 Hz) and the corresponding ILV signal measured directly via impedance pneumograph. Note that the two signals are zero-meaned and normalized by their respective standard deviation in the frequency range of 0.15 to 0.4 Hz where the major respiratory energy resides. The impulse responses identified with these two signals (~ 6 min long) after being downsampled to 1.25 Hz are shown in Figure 3-14(b). It can be seen that the EDR signal agrees with the ILV signals fairly well and enables an EDR⇒HR impulse response that is analogous to the ILV⇒HR impulse response. In Figure 3-14(a), the EDR signal seems to be shifted left relative to the ILV signal which may be due to the low sampling rate (one per beat) in the computation of the EDR samples. This shift does not present a problem for the

current system identification as long as enough causal and non-causal input delays are included in the WPCR method (the ILV⇒HR coupling is non-causal) and only the value of the peak amplitude of the identified impulse response is sought. Note that the shape of the impulse responses in Figure 3-14(b) appears to be different from those presented previously; this may be due to some alterations in the patient's autonomic control as a result of treatment or long-term heart disease.

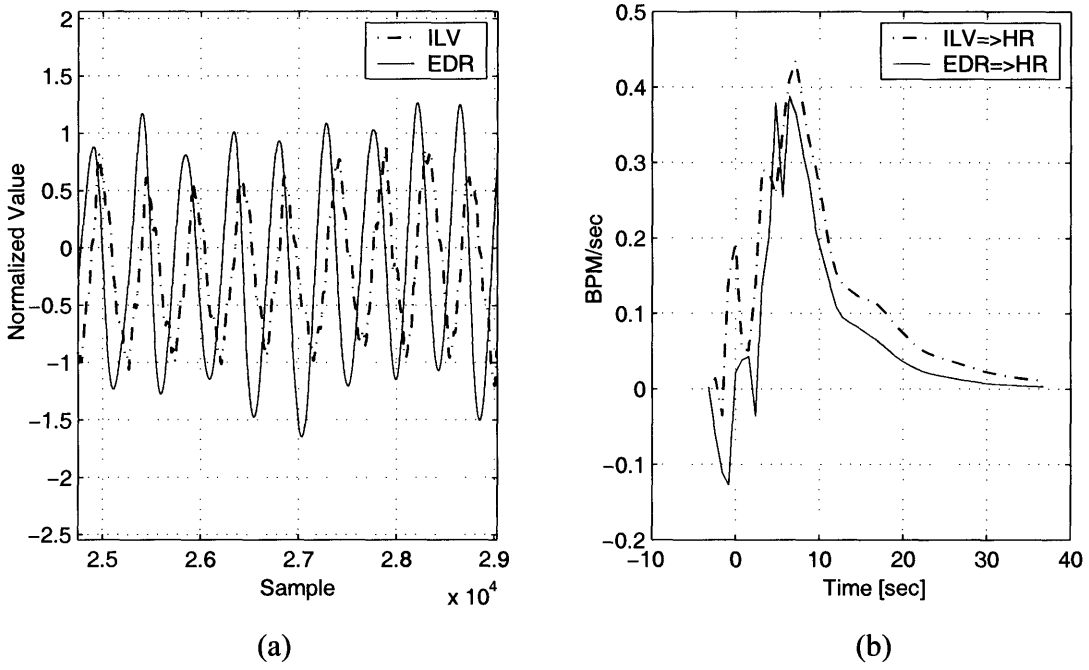

Figure 3-14 (a) two-lead ECG-based EDR signal and the ILV signal from direct meaurement on a ICU patient during spontaneous breathing; (b) the impulse responses identified using the EDR and the ILV signals respectively

In the databases to be used for validation in the next section, only one ECG signal is available. In this scenario, it is still possible to derive a reliable EDR signal if the ECG lead is significantly different from the mean cardiac electrical axis. As an example, Figure 3-15(a) and (b) demonstrate, respectively, the EDR signal and the respective impulse responses based on the EDR and ILV data of a healthy subject in standing posture during spontaneous breathing (the data are from the AGE database, see Section 3.4.3). Figure 3-16

demonstrates the EDR and ILV signals and their power density spectra for a healthy subject in the supine position during metronomic breathing (the data are from the AM database, see Section 3.4.4). In the above analysis, approximately 6 minutes of signals at a frequency of 1.5 Hz were employed. It can be appreciated that for the purpose of deriving a parasympathetic index as described in the last section, the EDR signal can be used as a substitute for the direct measurement of ILV.

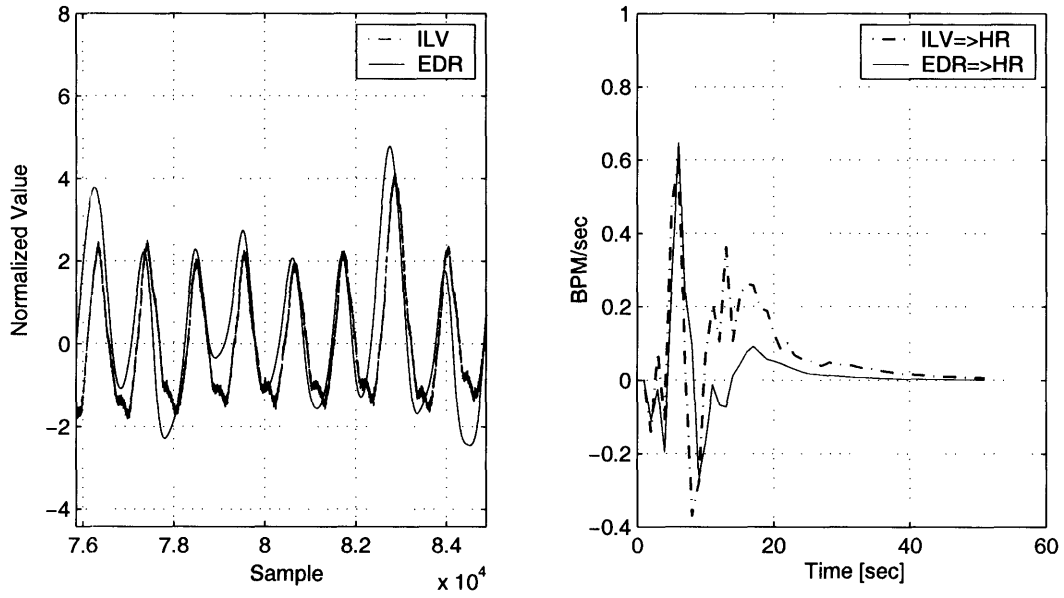

(a) (b)

Figure 3-15 (a) the one-lead ECG-based EDR signal and the ILV signal from direct meaurement on a healthy subject during spontaneous breathing; (b) the impulse responses identified using the EDR and the ILV signals respectively

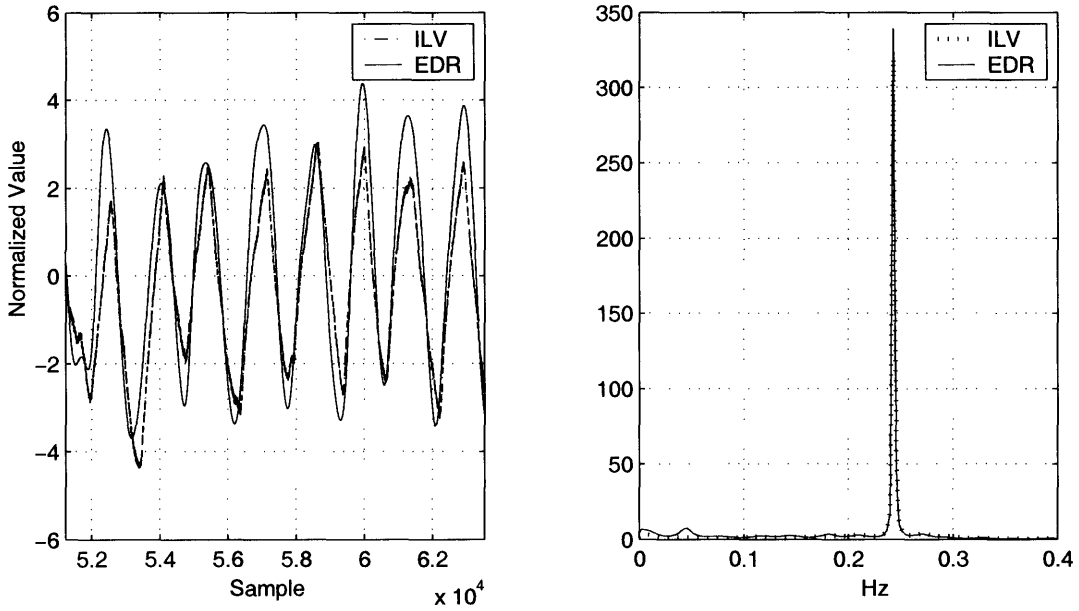

Figure 3-16 (a) the one-lead ECG-based EDR signal and the ILV signal from direct meaurement on a healthy subject during metronomic breathing; (b) the power spectra of the EDR and ILV signals

In the remainder of this chapter, we present the identification results of the previously proposed methods for autonomic function quantification utilizing experimental data. The effectiveness of each method will be evaluated based on well-known physiologic knowledge relevant to specific experimental interventions. Since only one-lead ECG signals are available in the databases to be employed and the placement of the ECG leads was not optimized specifically to derive an accurate EDR signal, we will use directly measured ILV signals in system identification.

3.4.2 Random Breathing Data

We analyzed two databases to validate the two methods applicable to random breathing data – the Area method (Section 3.3.1) and the SD method (Section 3.3.2). The first data set is the one containing the training data of the SD method, i.e., the CRC data. Since only data at

SUC, STC and SUB conditions were employed to generate the model, the identification results for the other conditions still provide insights in evaluating the performance of the SD method.

Although all fourteen subjects were tested in the SUC, STC, SUB and STB conditions, only seven subjects are involved in the SUP and STP conditions and another seven are involved in the SUA and STA conditions. Figure 3-17 illustrates the parasympathetic and sympathetic indices identified by the Area method. Table 3-1 shows the corresponding *P* values of the paired-T tests (for 14-subject comparisons) or Wilcoxon's signrank tests (for 7-subject comparisons) between the supine and the standing conditions and between the control and blockade conditions. Statistical comparisons among the parasympathetic indices demonstrate precisely the expected results consistent with general physiologic notion. For example, it decreases significantly upon standing when the parasympathetic control is not blocked. For each case of parasympathetic blockade, it decreases significantly compared with the corresponding control condition. On the other hand, the sympathetic index is not able to track changes due to postural shift in this data set. There is a significant drop in the sympathetic index during STB and STP compared to the control condition (STC). The *P* values are also nearly significant for SUB condition compared with their respective control cases. Note that the sympathetic tone may withdraw to some extent when the parasympathetic pathway is blocked (e.g. STC *vs.* STA in Table 3-1) and *vice versa*. This is due to the compensation mechanisms in autonomic control – a withdrawal of the unblocked branch is to compensate for the change in HR due to the blockade of the other branch.

Figure 3-18 and Table 3-2 demonstrates the results of the SD method on the CRC data. Similar to the results of the Area method, the parasympathetic index accurately demonstrates the expected alteration with each intervention consistent with physiologic notions. In addition, the sympathetic index also demonstrates statistically significant changes upon postural shift (SUC *vs.* STC; the significantly higher value at STB than at SUB may be due to incomplete blockade). In cases of sympathetic blockade (except SUP), statistically significant reductions in the sympathetic index are detected (SUC *vs.* SUB, STC *vs.* STB, STC *vs.* STP). The insignificant comparison between SUC and SUP may be reasonable because it is

known that the baseline sympathetic activity in the supine posture is fairly weak [45]. The sympathetic index decreased significantly at STA which may be a consequence of the compensation mechanism aforementioned.

The second database employed here is named the TDR database. Ten healthy volunteers (five males and five females) were studied (age: 25.2 ± 3.7 (SD) yr; height: 170.3 ± 8.6 cm; weight: 68.2 ± 8.4 kg). The experimental protocol has been described in [158]. Approximately 5 minutes of ILV, ABP and ECG recordings at a sample frequency of 100 Hz were collected on two different days. On one day, the subjects were tested in the supine position before and after administration of first propranolol (14.6 mg iv) and then atropine (0.04 mg/kg iv). On the other day, the medications were given in a reverse order while the subjects were tested in a 30° head-up tilt position [158]. Four subjects were tested in the supine position and six in the tilted position on the first day in a randomized order. The TDR data analyzed in this section were obtained with the subjects following a random breathing protocol. Spontaneous breathing data were also collected (TDS data) and will be analyzed in the next section.

Figure 3-19 and Table 3-3 demonstrate the results of the Area method on the TDR data. It can be seen that the changes in parasympathetic control due to autonomic blockade have been identified accurately, while a nearly statistically significant drop is detected upon merely a 30° tilt. The sympathetic index also tracks the changes due to autonomic blockade significantly and consistent with physiologic knowledge, except that the comparison between SUC and SUP is not significant. The change in the sympathetic function due to 30° tilt is not identified statistically.

Figure 3-20 and Table 3-4 demonstrates the results of the SD method on the TDR data. Similar to the Area method, the SD method identifies all the changes significantly in parasympathetic control due to autonomic blockade, while the change due to a 30° tilt is not detected statistically. The sympathetic index also tracks the changes due to autonomic blockade significantly, except that the comparison between SUC and SUP is not significant. The change in the sympathetic index due to 30° tilt is nearly significant.

To further study the performance of the SD and the Area methods, we performed correlation analysis between the averaged autonomic indices identified by the two methods for the above two databases respectively (Figure 3-21 and Figure 3-22). The parasympathetic index resulted from the two methods reached a high correlation coefficient, while the sympathetic indices correlate less closely. We will discuss these results in detail in Section 3.5.

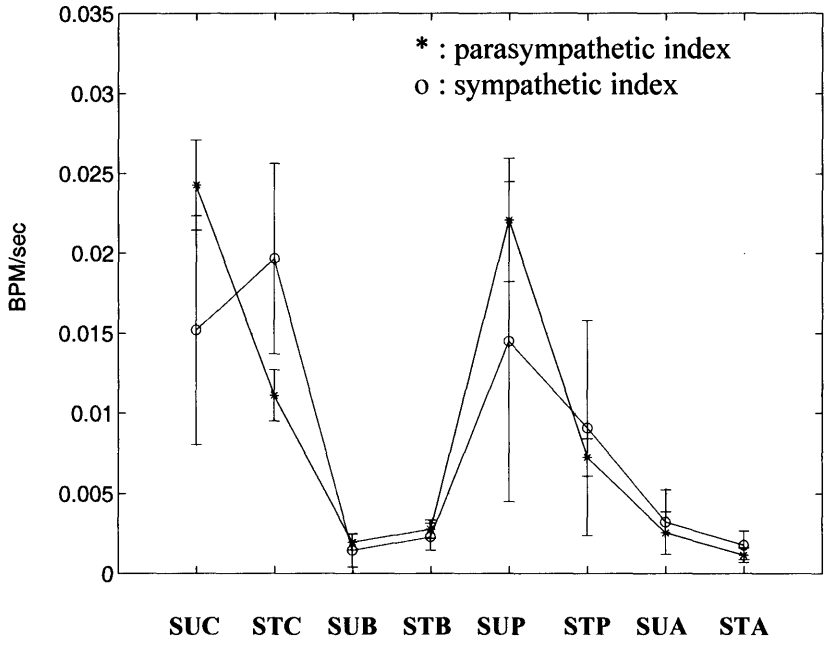

Figure 3-17 Autonomic function quantification results (mean ± SE) using the Area method – CRC data (SUC: supine control; STC: standing control; SUB: supine double blockade; STB: standing double blockade; SUP: supine propranolol; STP: standing propranolol; SUA: supine atropine; STA: standing atropine)

Table 3-1 *P* values of paired T tests (for 14-subject comparisons) and Wilcoxon's signrank tests (for 7-subject comparisons) of the autonomic indexes identified by the Area method – CRC data

(a) Parasympathetic index

Supine *vs.* standing	SUC *vs.* STC	SUB *vs.* STB	SUP *vs.* STP	SUA *vs.* STA		
	3.67e-4	0.11	0.016	0.58		
Control *vs.* blockade	SUC *vs.* SUB	STC *vs.* STB	SUC *vs.* SUP	STC *vs.* STP	SUC *vs.* SUA	STC *vs.* STA
	2.0e-6	5.88e-5	0.58	0.38	0.016	0.016

(b) Sympathetic index

Supine *vs.* standing	SUC *vs.* STC	SUB *vs.* STB	SUP *vs.* STP	SUA *vs.* STA		
	0.46	0.40	0.22	0.94		
Control *vs.* blockade	SUC *vs.* SUB	STC *vs.* STB	SUC *vs.* SUP	STC *vs.* STP	SUC *vs.* SUA	STC *vs.* STA
	0.054	0.0085	0.58	0.031	0.16	0.016

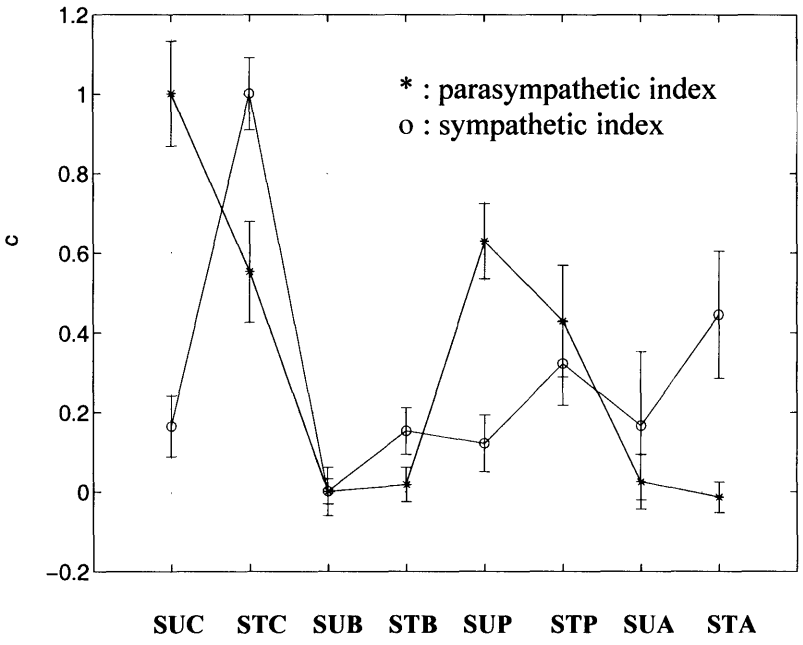

Figure 3-18 Autonomic function quantification results (mean ± SE) using the SD method – CRC data (SUC: supine control; STC: standing control; SUB: supine double blockade; STB: standing double blockade; SUP: supine propranolol; STP: standing propranolol; SUA: supine atropine; STA: standing atropine).

Table 3-2 *P* values of paired T tests (for 14-subject comparisons) and Wilcoxon's signrank tests (for 7-subject comparisons) of the autonomic indexes identified by the SD method – CRC data

(a) Parasympathetic index

Supine *vs.* standing	SUC *vs.* STC	SUB *vs.* STB	SUP *vs.* STP	SUA *vs.* STA		
	6.22e-4	0.79	0.11	0.81		
Control *vs.* blockade	SUC *vs.* SUB	STC *vs.* STB	SUC *vs.* SUP	STC *vs.* STP	SUC *vs.* SUA	STC *vs.* STA
	1.51e-6	2.27e-4	0.38	0.58	0.016	0.016

(b) Sympathetic index

Supine *vs.* standing	SUC *vs.* STC	SUB *vs.* STB	SUP *vs.* STP	SUA *vs.* STA		
	4.37e-7	0.0039	0.38	0.22		
Control *vs.* blockade	SUC *vs.* SUB	STC *vs.* STB	SUC *vs.* SUP	STC *vs.* STP	SUC *vs.* SUA	STC *vs.* STA
	0.0025	1.55e-7	0.45	0.016	0.81	0.031

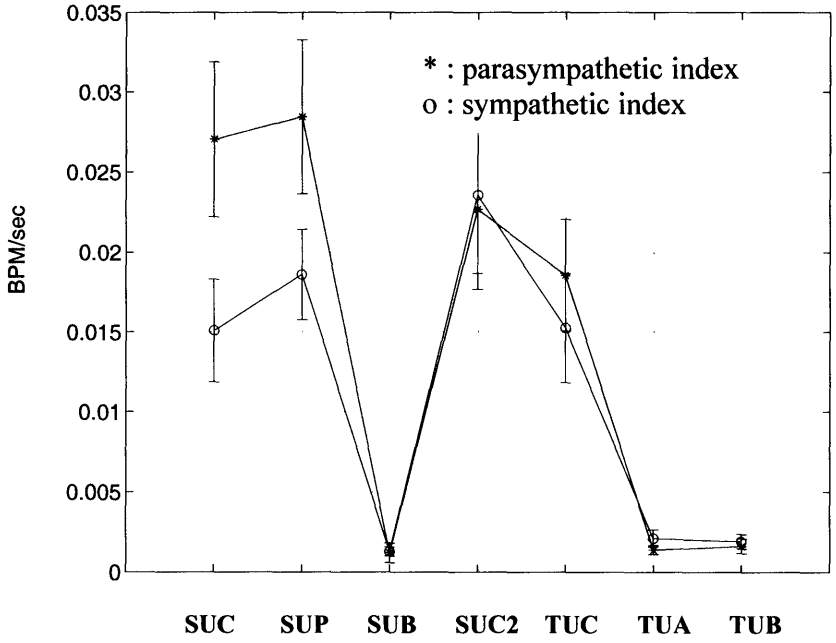

Figure 3-19 Autonomic quantification results (mean ± SE) using the Area method – TDR data (SUC: supine control; SUP: supine propranolol; SUB: supine double blockade; SUC2: supine control on the tilt day; TUC: 30° tilt-up, control; TUA: 30° tilt-up, atropine; TUB: 30° tilt-up, double blockade)

Table 3-3 *P* values of paired T tests of the autonomic indexes identified by the Area method – TDR data

(a) Parasympathetic index

SUC2 *vs.* TUC	SUC *vs.* SUP	SUC *vs.* SUB	TUC *vs.* TUA	TUC *vs.* TUB
0.079	0.75	6.1e-4	0.0024	6.4e-4

(b) Sympathetic index

SUC2 *vs.* TUC	SUC *vs.* SUP	SUC *vs.* SUB	TUC *vs.* TUA	TUC *vs.* TUB
0.20	0.36	0.0024	0.0059	0.0045

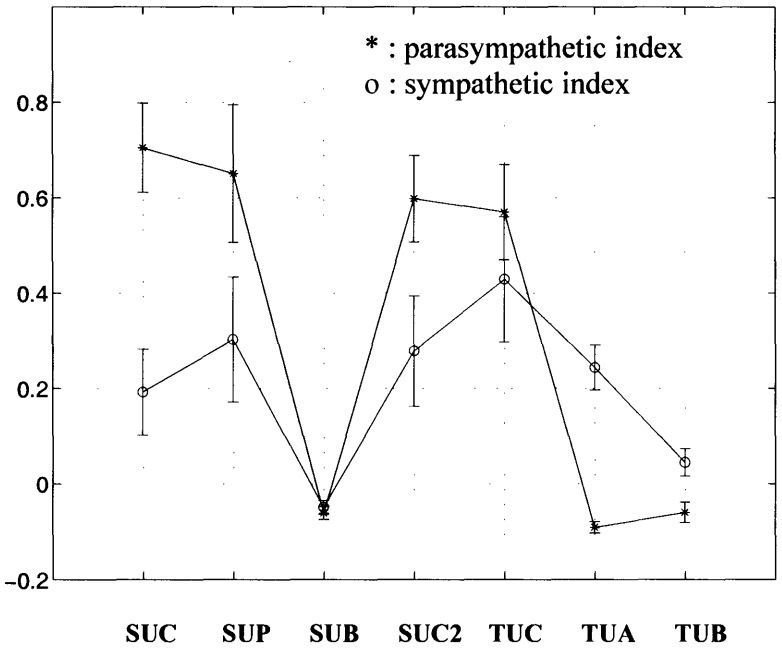

Figure 3-20 Autonomic function quantification results (mean ± SE) using the SD method – TDR data (SUC: supine control; SUP: supine propranolol; SUB: supine double blockade; SUC2: supine control on the tilt day; TUC: 30° tilt-up, control; TUA: 30° tilt-up, atropine; TUB: 30° tilt-up, double blockade)

Table 3-4 *P* values of paired T tests of the autonomic indexes identified by the SD method – TDR data

(a) Parasympathetic index

SUC2 *vs.* TUC	SUC *vs.* SUP	SUC *vs.* SUB	TUC *vs.* TUA	TUC *vs.* TUB
0.68	0.60	2.55e-5	2.41e-4	1.06e-4

(b) Sympathetic index

SUC2 *vs.* TUC	SUC *vs.* SUP	SUC *vs.* SUB	TUC *vs.* TUA	TUC *vs.* TUB
0.058	0.72	0.025	0.16	0.0096

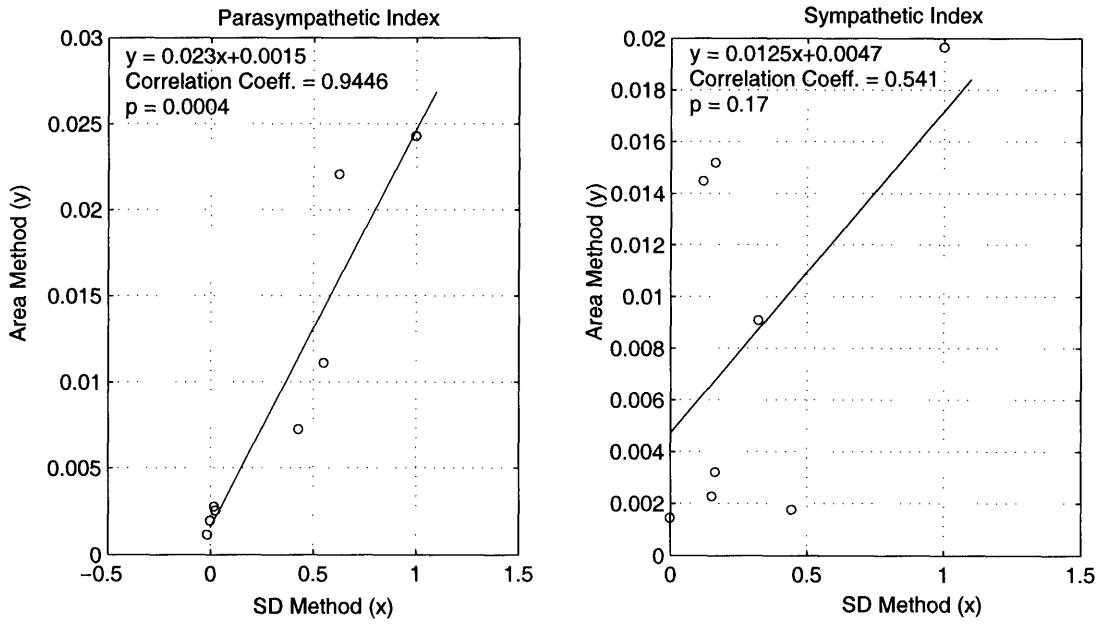

Figure 3-21 Correlation analysis of the averaged results obtained by the SD method and the Area method – CRC data

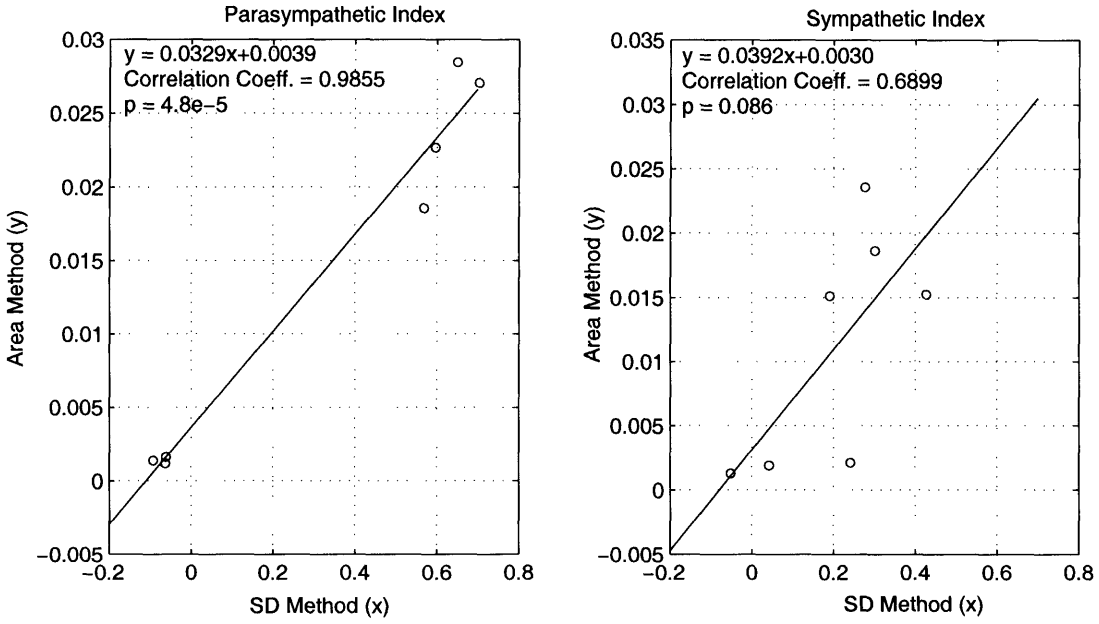

Figure 3-22 Correlation analysis of the averaged results obtained by the SD method and the Area method – TDR data

3.4.3 Spontaneous Breathing Data

In this section, we apply the SD method to analyze spontaneous ILV and HR data in two databases. The first database involves the same subjects and experimental protocol as the TDR database except that the data were obtained during spontaneous breathing. We name it the TDS database.

Figure 3-23 and Table 3-5 demonstrate the identification results of the TDS data using the SD method. The changes in parasympathetic function due to autonomic blockade are identified significantly and are consistent with the *a priori* knowledge. Note that the parasympathetic index decreased significantly after administration of propranolol which may be the result of compensation due to the ensuing drop in HR. A decrease in parasympathetic function due to the 30° tilt is also identified. The sympathetic index decreased significantly during autonomic double blockade, while no significant change was detected after injection of propranolol. An increase in sympathetic function due to the 30° tilt is also identified.

Since the TDR and TDS data were obtained from the same subjects under the same experimental conditions, it is expected that the respective autonomic indices identified be closely correlated. Figure 3-24 shows the correlation analysis results relevant to the two data sets. The correlation coefficients are acceptably high to indicate that the SD method applies to both the random breathing data and the spontaneous breathing data. In Section 3.5, we will further discuss the identification results for data with different respiratory patterns.

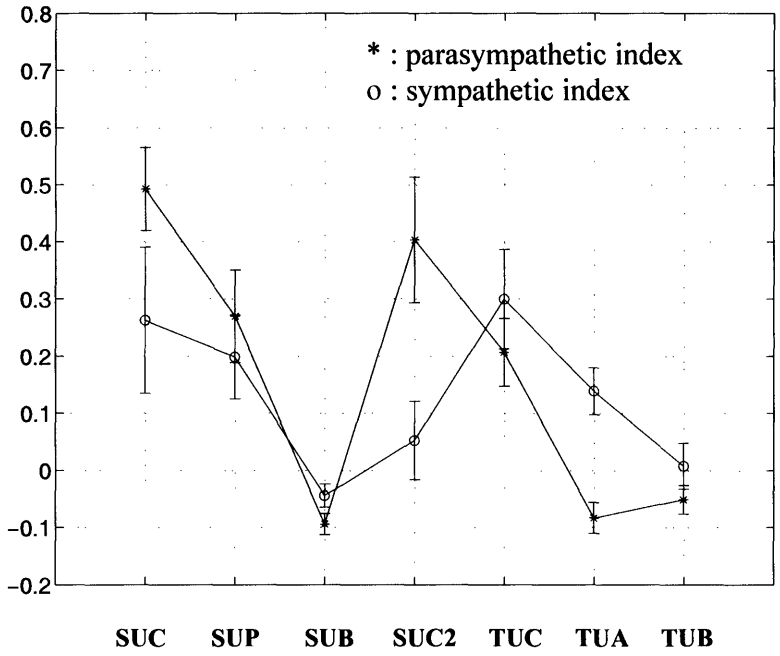

Figure 3-23 Autonomic function quantification results (mean ± SE) using the SD method – TDS data (SUC: supine control; SUP: supine propranolol; SUB: supine double blockade; SUC2: supine control on the tilt day; TUC: 30° tilt-up, control; TUA: 30° tilt-up, atropine; TUB: 30° tilt-up, double blockade)

Table 3-5 *P* values of paired T tests of the autonomic indexes identified by the SD method – TDS data

(a) Parasympathetic index

SUC2 *vs.* TUC	SUC *vs.* SUP	SUC *vs.* SUB	TUC *vs.* TUA	TUC *vs.* TUB
0.048	0.014	4.91e-5	0.0019	0.0050

(b) Sympathetic index

SUC2 *vs.* TUC	SUC *vs.* SUP	SUC *vs.* SUB	TUC *vs.* TUA	TUC *vs.* TUB
0.041	0.65	0.047	0.15	0.025

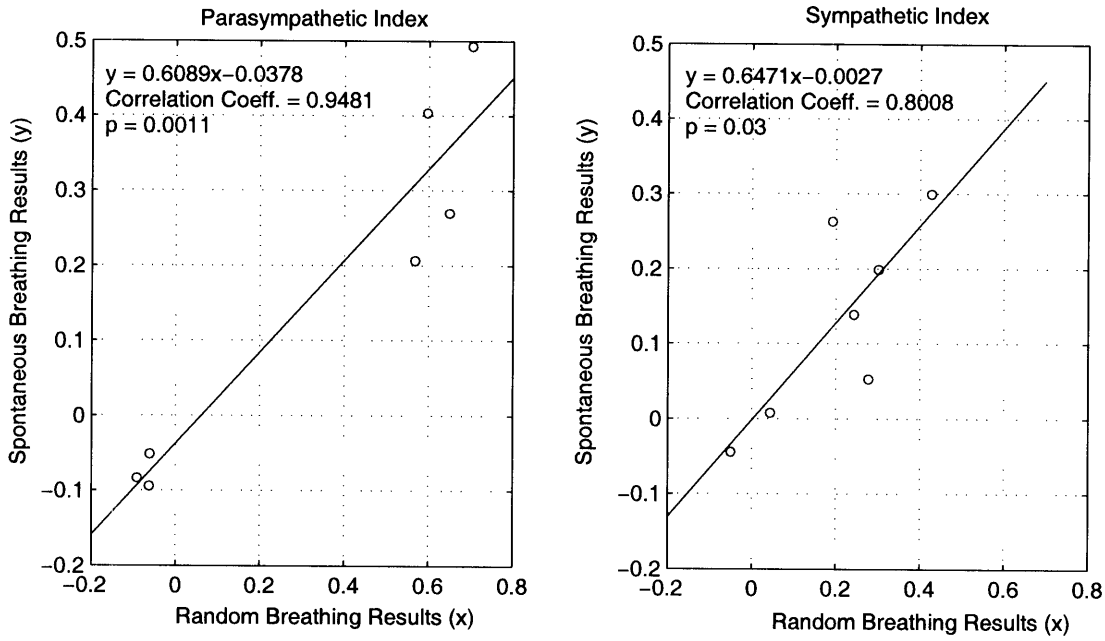

Figure 3-24 Correlation analysis of the averaged results utilizing random breathing data and spontaneous breathing data, SD method – TDR and TDS data

Another set of data is also analyzed using the SD method. This data set is part of the HMS-MIT-FFMS database [159]. It was originally obtained to study autonomic function in different age groups. For our purpose, we take the nine healthy volunteers who are younger than 50 yrs (two males, seven females, age: 30.6 ± 9.6 (SD) yr). We refer to this data set as the AGE database. In this database, approximately 6 minutes of ILV and ECG signals with a sample frequency of 360 Hz were collected during spontaneous breathing in supine and standing postures. The data were downsampled to 1.5 Hz for the purpose of system identification.

Table 3-6 shows the autonomic indices identified using the SD method. Significant changes upon standing in both parasympathetic index and sympathetic index were identified illustrating the effectiveness of the SD method in analyzing this data set.

Table 3-6 Identification results of the AGE database using the SD method

	Parasympathetic Index (BPM/sec)		Sympathetic Index (BPM/sec)	
	Supine	Standing	Supine	Standing
Mean ± SE	0.46 ± 0.10	0.24 ±0.047	0.075 ±0.046	0.93 ±0.20
P value		0.023		0.005

3.4.4 Metronomic Breathing Data

To validate the SD_m method, we employ experimental data (referred to as the AM database) from 11 healthy volunteers (three males, eight females, age: 30.0 ± 8.5 (SD) yr) (also part of the HMS-MIT-FFMS database [159]). The ECG and ILV signals were collected during metronomic breathing at a rate of 14 breaths/min with a sample frequency of 360 Hz. Table 3-7 shows the identification results. A significant decrease in the parasympathetic index and a significant increase in the sympathetic index are detected upon standing, which is consistent with the *a priori* knowledge on autonomic function changes relative to postural shift.

Table 3-7 Identification results of the AM database using the SD_m method

	Parasympathetic Index (BPM/sec)		Sympathetic Index (BPM/sec)	
	Supine	Standing	Supine	Standing
Mean ± SE	1.09 ± 0.25	0.36 ±0.09	-0.63 ±0.17	0.26 ±0.10
P value		0.0095		0.00033

3.5 Discussion

In this chapter, we presented three methods for autonomic function quantification. The Area method requires measurements of second-to-second ECG, ILV and ABP signals during random breathing. The other two methods (SD and SD_m) only necessitate ECG measurement. The SD method is applicable to data collected during either random breathing or spontaneous breathing, while its modified version, the SD_m method, is suitable for data collected during metronomic breathing. All three methods are built based on linear time-invariant system identification and *a priori* knowledge about HR variability in the time/frequency domain. The linearity assumption in system identification is valid if variation in the signals is relatively small, as is the case when the subjects are in a resting condition.

3.5.1 Validation of the Methods on Random Breathing Data

For both random breathing databases, the Area method was capable of tracking all the parasympathetic changes resulted from autonomic blockade or postural shift except for the 30° tilt in the TDR database which is not essentially a very significant postural change. However, for the sympathetic alterations, the Area method only identified changes due to autonomic double blockade, not those associated with postural shift.

In comparison, the SD method performed equally well in terms of the parasympathetic function quantification. For the CRC database, the SD method accurately identified sympathetic changes due to both postural shift and autonomic blockade. Note that the model coefficients (Equation (2.54)) utilized by the SD method were computed based on a subset of the CRC database. Hence, it is expected that the SD method performs the best on this training data set. For the TDR database which was not employed to train the SD model, the SD method detected sympathetic changes due to autonomic double blockade, similar to the Area method. In addition, it indicates a trend (P = 0.058) of increase in sympathetic function upon 30° tilt.

The parasympathetic indices based on the Area method and the SD method correlate closely with each other. However, the sympathetic indices of the two methods correlate poorly for the CRC database and more closely for the TDR database. This observation may be explained as follows. Since it is expected that the SD method performs the best on its training data, there may exist much disparity between the results of the Area method and those of the SD method on this database if the former performs only moderately well. For the TDR database, the disparity is reduced because the accuracy of the SD method is not as high as that for the training data set. Thus, the correlation coefficient of the results based on the two methods is higher for the TDR database.

Based on the above discussion, the overall performance of the Area method and the SD method is equivalent in terms of parasympathetic function quantification, while the SD method may perform slightly better than the Area method in identifying the sympathetic index given a new data set. One limitation of the Area method is the possible overlap between the parasympathetic and sympathetic components in the ILV→HR impulse response. We assumed this overlap to be negligible which may cause some error due to inter-subject variability. Another inherent source of error lies in the WPCR system identification procedure on which the Area method relies, since no system identification technique is error-free in analyzing experimental data. On the other hand, one advantage of the Area method is the standardization of the results because the autonomic indices are both derived from an *impulse* response which enables a high consistency among subjects. Therefore, the Area method may be more appropriate for population-based study. In comparison, the SD method may be more suitable for individualized patient monitoring. Before further assessing the SD method, we now discuss its performance on the spontaneous and metronomic breathing data.

3.5.2 The SD Method on Spontaneous/Metronomic Breathing Data

From the results presented in Sections 3.4.3 and 3.4.4, the SD method is capable of tracking the changes in both parasympathetic and sympathetic function due to 30° (TDS data-

base) or 90° (AGE and AM databases) postural shift and autonomic blockade (TDS database). The only change it failed to identify was the expected decrease in sympathetic index after administration of propranolol in the supine posture (TDS database). Note that such a significant change was neither detected in the CRC or TDR databases. This may be because of the already low sympathetic level in the supine control state.

Results of the SD method on random breathing and spontaneous breathing data of the same subject group (TDR and TDS databases) correlates closely, which proves, to some extent, the effectiveness of the method to analyze spontaneous breathing data. Note that although Figure 3-11 and Figure 3-12 demonstrated that the peak amplitudes of the ILV⇒HR impulse responses of spontaneous and random breathing data have similar values, the corresponding parasympathetic indices should not be the same. This is because in the SD method, the ILV data is normalized by its standard deviation as previously mentioned (Section 3.3.2). Since the standard deviation of ILV during spontaneous breathing is usually less than that during random breathing, a smaller spontaneous breathing parasympathetic index resulted. Furthermore, because the ILV signal is an external excitation to the closed-loop coupling between HR and ABP, the reduced energy in ILV during spontaneous breathing (especially in the low frequency range) leads to a smaller variability in HR compared to the case of random breathing. Consequently, the spontaneous breathing sympathetic index is usually smaller than that of random breathing, as can be appreciated from Figure 3-24.

3.5.3 Respiratory Pattern and Autonomic Indices

Based on the above discussion, identified values of the autonomic indices by the SD method are related to the respiratory pattern of the subject. Thus, they are comparable only within data of the same breathing pattern. In general, the interference of respiratory effect in the identification of autonomic function is a common issue in many techniques. For patient monitoring purpose, the controlled breathing modes (random or metronomic) seem to be more desirable because a fairly consistent respiratory signal can be obtained in different measurements. However, it is more practical and realistic to collect data during spontaneous

breathing at resting conditions. The SD method possesses some advantages in analyzing such data. For the sympathetic index, since the SD method only utilizes HR information in the low frequency range in which the spontaneous ILV signal usually contains little energy, it is robust to the disparities present in the spontaneous breathing pattern of different subjects and of the same subject at different times. For the parasympathetic index, note that it is not technically necessary to normalize the ILV signal in the calculation. This procedure is performed to account for differences in size and respiration need among subjects in order to achieve a better inter-subject consistency. Without the normalization, the parasympathetic index is not affected by respiration pattern because it is derived from the impulse response, namely, the HR response to an impulse ILV, a stimulator that is identical for all subjects.

3.5.4 Limitations and Improvement

A further discussion is necessary about the assumption of linearity in the relationship of parasympathetic or sympathetic indices with respect to HR variability (Equation (2.54)). We assumed that α and β are constant since they are unitless proportional coefficients representing the value of $\Delta(HR_\omega)$ that is equivalent to a unit P_I or S_I. In theory, since $\Delta(HR_\omega)$, P_I and S_I reflect the variation relative to their associated mean level, α and β, as proportional coefficients, should not vary for different autonomic *states*. In reality, α and β may differ among significantly distinct pathophysiologic conditions which are associated with abnormal parasympathetic-sympathetic interaction or balance.

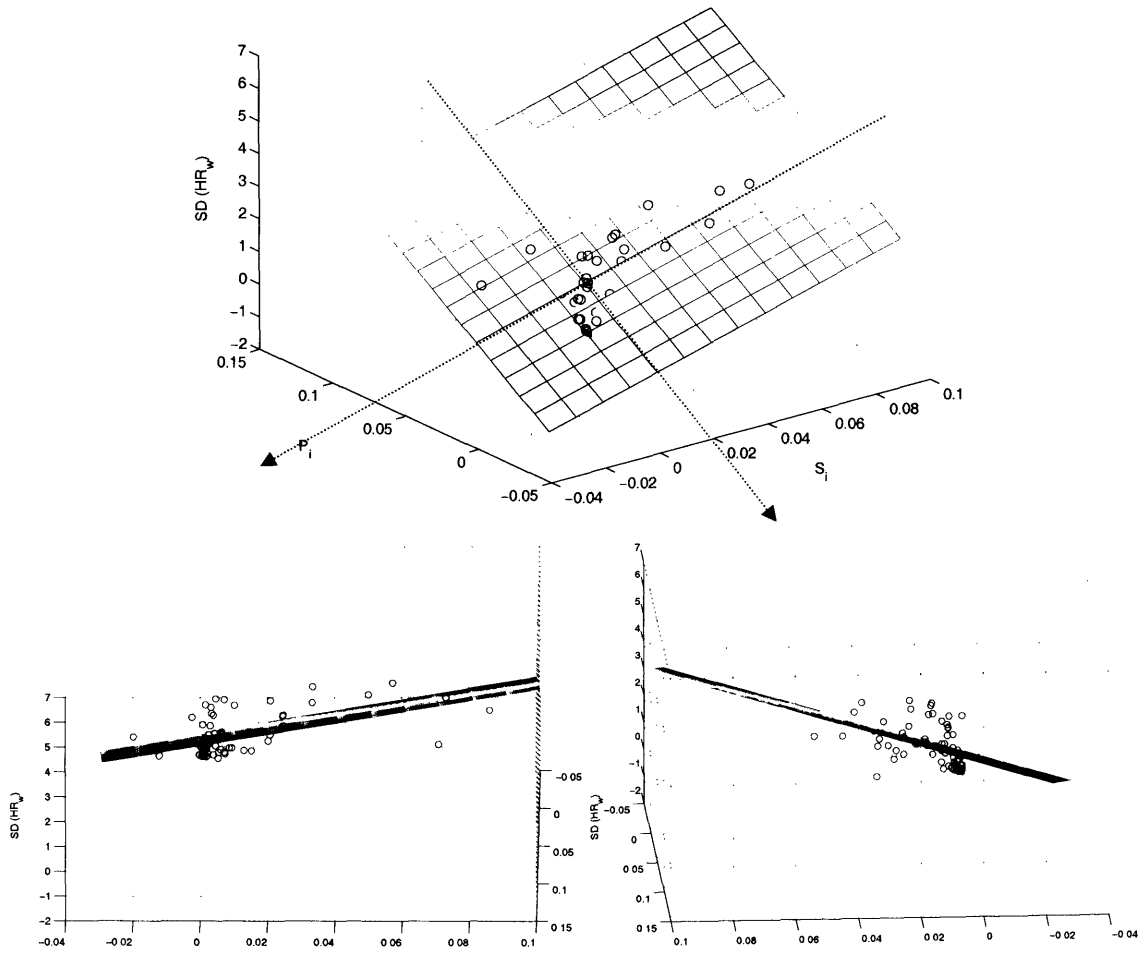

Figure 3-25 3-D scatter plots and linear regression of the standard deviation of HR in the [0.05 0.15] Hz range versus the autonomic indexes of the CRC subjects identified by the Area method; The two plots in the lower panel are the rotated version of the original 3-D plot (upper panel). The rotations were performed for views parallel to the arrows.

Nevertheless, based on our experimental validation (Figure 3-13), the linear assumption is realistic and enables a simple, concise model. To further test this assumption, we generated Figure 3-25 to display the scatter plot of the $\Delta(HR_\omega)$ (ω = 0.05~0.15 Hz) value versus the parasympathetic area and sympathetic area of the CRC subjects identified by the Area method under all interventions. The plane results from linear regression of the data. The correlation coefficient (R^2) is 0.75, the P value for this regression is 1.56e-12 and the F-observed statistic (38.9) is much greater than the F-critical value (~3.1). These statistical

analyses indicate that the linear relationship fits the data reasonably well. Although the Area method may lead to some error in estimating autonomic indices, this result corroborates the linear assumption in the SD method. However, it is safe to keep in mind that when a more sensitive quantification of autonomic function is desired, a model with a complicated structure may be necessary.

It should be pointed out that there are still potentials of improvement in the application of the SD method. First, the training data set of 14 subjects is a fairly small database. Second, the training data were obtained from relatively young male subjects only. In reality, it is known that baseline sympathetic and parasympathetic balance may be different in females from that in males and it also changes with age. Although our results on the TDR, TDS, AGE and AM databases (mixture of male and female subjects, and older subjects in AGE and AM data sets) showed the effectiveness of the SD method trained by the small, unisexual database, it would be more precise to group the general population according to sex and age and apply different model coefficients to different groups.

3.6 Conclusion

In this chapter, we presented three techniques for autonomic function quantification applicable to different respiration modes. Experimental data were employed to evaluate the validity of each technique. Both the Area method and the SD method are suitable to data collected during random breathing. The Area method has a good inter-subject comparability, while the SD method only necessitates measurement of ECG tracings and it is readily applicable to spontaneous breathing data. Its modified version, the SD_m method, was demonstrated to work effectively on metronomic breathing data. The SD method may be easily applied in clinical settings for general patient monitoring and diagnosis in the future.

Chapter 4

Effects of Simulated Microgravity on Cardiac Autonomic Control and Orthostatic Intolerance[7]

In previous chapters, we presented a new system identification method named weighted principal component regression (WPCR) based on which techniques for quantitative characterizations of autonomic responsiveness were developed. In this chapter, we apply these techniques to study the effects of simulated microgravity (prolonged bed rest) on cardiac autonomic control and the association between orthostatic intolerance (OI) and alterations in autonomic function. We begin with a brief introduction on microgravity-related cardiovascular problems, followed by a review of previous studies on autonomic function and OI after microgravity exposure. We then delineate the experimental protocol for OI testing and microgravity simulation. Subsequently, results of autonomic function identification using the Area and the SD methods are presented, followed by discussions and conclusion.

4.1 Introduction

Microgravity exposure during spaceflight may impact many aspects of human physiology. Alterations in the cardiovascular system [160, 161], the immune system [162, 163], the

[7] Part of the content in this chapter has been published in the Journal of Applied Physiology [106]

neurovestibular system [164, 165], and the psychological system [166, 167], etc, have been studied intensively in recent years. Possible changes with regard to the cardiovascular system consist of variations in the autonomic nervous control [111, 168, 169], vascular compliance [170, 171], blood volume regulation [172-174], cardiac electrical stability [175, 176], cardiac pump function [177-179], *et al.* An often-studied phenomenon, microgravity-induced orthostatic intolerance (OI), is thought to be at least partially related to cardiovascular deconditioning. It affects up to 83% of astronauts and cosmonauts depending on the duration of exposure to the weightless environment [180]. OI may be defined as the development of some or all of the following symptoms while standing or sitting upright [181]: lightheadedness, dizziness, tiredness, blurred vision, palpitations, chest discomfort, throbbing of the head, tremulousness during standing and occasionally syncope (fainting). The fundamental etiology of microgravity-induced OI remains unclear and therefore the development of effective countermeasures has been hindered. Previous in-flight and ground-based experimental studies have focused on a variety of factors which may contribute to OI, such as reduced blood volume [160, 172, 182, 183], cardiac atrophy [179, 184-186], and peripheral blood pooling associated with increased venous compliance [187-189]. The autonomic system may also be closely involved in inducing OI in view of its critical role in regulating heart rate, blood pressure and other hemodynamic parameters. In the following sections, we concentrate on the investigation of the effect of simulated microgravity on cardiac autonomic control and its association with OI. Note that simulation of microgravity is realized through prolonged head-down-tilt bed rest (HDBR) which is a widely accepted model for this purpose [160].

4.1.1 Previous Studies on Autonomic Function and Microgravity

Different techniques have been utilized to evaluate the functioning of the autonomic system during and/or after (simulated) microgravity exposure. Heart rate variability (HRV) analysis is widely practiced for this purpose due to its noninvasive nature and simplicity. As discussed in Chapter 3, the high frequency (HF, > 0.15 Hz) power in R-R interval or HR spectrum (often normalized by the total frequency power) is usually employed as a para-

sympathetic index. Note that definition of the upper bound of this frequency range may differ in various studies, for example, 0.25, 0.4 and 0.5 Hz have been utilized in the literature. Sympathetic activity is often quantified by normalized low frequency (LF, < 0.15 Hz) power or the ratio of LF and HF power. Table 4-1 displays a few examples of HRV analysis in bed rest studies. Although only a small portion of the vast previous publications is listed here, it can be appreciated that there is a lack of consensus about changes in the autonomic function, especially the sympathetic one, after HDBR. Besides possible disparities in sample size, protocol, the number of subjects who had pre-syncopal episodes and the fact that only a small number of subjects are involved in some of the studies, another important factor causing the inconsistent results may be the inherent limitation of HRV analysis as discussed previously (Section 3.1).

Another technique for direct evaluation of sympathetic function, muscle sympathetic nerve activity (MSNA) measurement, is also utilized in (simulated) microgravity studies. Table 4-2 summarizes some of the publications to demonstrate the diversity in the findings about changes in MSNA relative to microgravity exposure. Both reduction and augmentation in MSNA have been observed after bed rest or spaceflight. Alteration in MSNA in response to external stimulus, such as head-up-tilt, was reported to be unchanged, increased or decreased after microgravity exposure. Evidently, these disparities may be due to the difference in sample size, protocol and other underlying factors. However, they may also be contributed by the inherent complexity of the technique. The level of MSNA reflects the balanced effect of different factors contributing to metabolic need of the muscle and blood supply available. In addition, the perfusion process and the chemosensitive muscle afferent pathway may also affect MSNA level [190]. Hence, it may not be a direct indicator of the effective sympathetic tone regulating the body's hemodynamics in general. Moreover, the accuracy and consistency of the MSNA measurement may be confounded by other factors. In a typical laboratory setting, the MSNA recordings are likely to be clouded by frequent baseline shifts, significant noise spikes, and muscle twitches [191], all of which may induce an inaccurate quantification of MSNA. Furthermore, the dependence of visual identification of sympathetic bursts by a trained microneurographer poses questions in the consistency of the MSNA interpretation.

Other studies considered the alteration in baroreflex sensitivity after microgravity exposure. Sundblad *et al.* [192] defined arterial-cardiac-chronotropic baroreflex sensitivity (ABS) as the ratio between tilt-induced heart rate transients and the preceding (and reciprocal) transient in arterial pressure. No significant change in ABS was observed after 42 days of 6° HDBR in seven healthy male subjects [192]. Pagani *et al.* [193] defined a similar spontaneous baroreceptor reflex sensitivity based on the changes in systolic arterial pressure and in R-R interval. It was found that this measure was decreased significantly after 42 days of 6° HDBR in seven healthy male subjects [193]. Convertino *et al.* [194] studied the baroreflex response provoked with ramped neck pressure-suction sequences in 11 healthy men before and after 30 days of 6° HDBR and concluded that the responsiveness and buffer capacity of vagal baroreflex-cardiac reflexes were impaired after HDBR. Fritsch-Yelle *et al.* [168] measured responses to Valsalva maneuvers and carotid baroreceptor-cardiac reflex responses with neck chamber suction in 16 astronauts before and after shuttle missions lasting 8-14 days. They found a reduction in parasympathetic and an increase in sympathetic influences on arterial pressure control after spaceflight [168]. Note that the above techniques for quantification of baroreflex sensitivity are limited in that they are affected by factors other than alterations in autonomic tone (e.g. respiration).

Table 4-1 Effect of simulated microgravity on cardiovascular autonomic function identified by heart rate variability analysis

Study	Protocol	Subjects	Total	LFno	HFno	LF/HF	Other
Patwardhan *et al.* [195]	20 h -6° BR	9 M			↓		
Lacolley *et al.* [196]	24 h -5° BR	6 M	=	=	=		
Sigaudo *et al.* [197]	4 d -6° BR	8 M	=		↓	=	
Pavy-Le Traon *et al.* [198]	4 d -6° BR	8 M	↓	↓	↓	=	
Pavy-Le Traon *et al.* [199]	14 d -6° BR	6 M	=		=	=	
Iwasaki *et al.* [200]	14 d -6° BR	9 M			↓	=	
Sigaudo *et al.* [135]	42 d -6° BR	7 M	↓	=	↓	↑	↓ UC
Pavy-Le Traon *et al.* [201]	42 d -6° BR	7 M	↓	= (stand) ↑ LBNP	↓		

↓: decrease after bed rest; ↑: increase after bed rest; =: no significant change; h: hour; d: day; BR: bed rest; M: male; Total: total frequency power of the R-R interval; LFno: normalized low frequency power; HFno: normalized high frequency power; LF/HF: the ratio of the low and high frequency power; UC: urinary catecholamines; Stand: changes associated with stand test; LBNP: changes associated with lower body negative pressure test.

Table 4-2 Effects of simulated microgravity on muscle sympathetic nerve activity (MSNA)

Study	Protocol	Subjects	Resting MSNA	ΔMSNA/Stimulation
Khan *et al.* [202]	24 h -6° BR	13 (9F, 4M)		↓ / LBNP
Kamiya *et al.* [203]	14 d -6° BR	16 M	↑	↓ / PHMI
Levine *et al.* [204]	16 d SF	5 M	↑	= / 60° HUT
Shoemaker *et al.* [205]	16 d -6° BR	16 M	↓	
Cox *et al.* [206]	16 d SF	4 M		↑ / Valsalva
Pawelczyk *et al.* [207]	18 d -6° BR	7 M		= / PCWP
Kamiya *et al.* [208]	60, 120 d SF	6 M	↑	= / 60° HUT

↓: decrease after bed rest or spaceflight; ↑: increase after bed rest or spaceflight; =: no significant change; h: hour; d: day; BR: bed rest; SF: spaceflight; M: male; F: female; LBNP: lower body negative pressure; PHMI: post-handgrip muscle ischemia; Valsalva: valsalva straining; HUT: head-up-tilt; PCWP: pulmonary capillary wedge pressure;

4.1.2 Previous Studies on Orthostatic Intolerance and Microgravity

In exploring the mechanisms responsible for reduced orthostatic tolerance after microgravity exposure, it is often hypothesized that multiple contributing factors are involved, e.g., decreased blood volume, increased peripheral pooling in the legs (and perhaps abdomen), altered cardiovascular neurohumoral regulation, abnormal regulation of cerebral perfusion *et al.* [110, 209]. Buckey and coworkers [110] studied 14 individuals before and after space shuttle missions of 9-14 days. After spaceflight, 9 of the 14 (64%) subjects failed a 10-min stand test that all completed preflight. They observed, between the finishers and nonfinishers, a similar cardiac output, postural reduction in stroke volume and increase in hear rate upon standing [110]. However, the finishers had a higher total peripheral resistance during standing [110]. Pavy-Le Traon *et al.* [201] observed no significant difference in the parasympathetic and sympathetic indicators derived from heart rate variability analysis between subjects who tolerated the stand test after HDBR and those who did not tolerate the test. In contrast, another study on ten subjects after long-term spaceflight (90 to 198

days) reported higher indicators of parasympathetic activity in HR spectrum when supine, both pre and post-flight in the nonfinisher group [209]. Fritsch-Yelle *et al.* [169] carried out an extensive study of cardiovascular responses to upright posture in 40 astronauts before and after spaceflights lasting up to 16 days. Astronauts who could not remain standing for 10 min on landing day (nonfinishers) had significantly smaller increases in plasma norepinephrine levels while standing than the finishers [169]. In addition, they had significantly lower standing peripheral vascular resistance and greater decreases in systolic and diastolic pressures after spaceflight [169]. Based on the above studies, although a unanimous conclusion has not been established about the mechanisms of increased incidence of OI after microgravity exposure, there are significant evidence that changes in autonomic control of the cardiovascular system may play an important role in this phenomenon.

In the remainder of this chapter, we will apply the techniques proposed in Chapter 2 to quantitatively study cardiac autonomic responsiveness of subjects who underwent a 16-day HDBR experiment. Changes in the autonomic indices after bed rest and their association with tilt-tolerance will be explored.

4.2 Methods

Subjects

Twenty-nine male subjects (age: 35.7±11.5 (SD) years, height: 70.3±2.5 (SD) inches, weight: 79.6±10.4 (SD) kilograms) were recruited for this study. All subjects were in excellent health and passed the screening test for physical and psychological fitness. The Brigham and Women's Hospital (Boston, MA) Research Committee approved the protocol and all subjects provided written, informed consent.

Bed rest study protocol

Subjects were admitted into the hospital for a 3-day (subjects 1-4) or 5-day (subjects 5-29) pre-bed rest ambulatory period at which time baseline testing was done and an isocaloric diet was maintained (200 mEq sodium, 100 mEq potassium and 2500 ml fluid). Then subjects underwent 9 (subject 1), 14 (subjects 2-4), or 16 (subjects 5-29) days of 4-degree head-down-tilt bed rest with the same diet. Lastly, 2 (subjects 1-4) or 3 (subjects 5-29) days of post-bed rest period were scheduled for the recovery when they were allowed ad lib activity but continued the constant diet.

Throughout the in-patient course, the subjects maintained a constant light/dark cycle. Subjects 1-21 participated in a non-sleep deprivation protocol (16-hour light/8-hour dark) while subjects 22-29 participated in a sleep deprivation protocol with a shorter dark time (17.9-hour light/6.1-hour dark). In addition, routine vital signs were monitored every eight hours and daily weights were recorded.

At the end of bed rest (*end-bed rest*), midodrine was given to seven subjects in a randomized blinded fashion before the tilt/stand test (see *Orthostatic Tolerance Testing*) as part of a parallel study on countermeasures of OI [210]. It was hypothesized that midodrine causes venous and arteriolar constriction thus increasing venous return and ABP. Since administration of midodrine may modify the hemodynamic response to the tilt/stand testing, end-bed rest standing data from these subjects were excluded from analysis here.

Orthostatic Tolerance Testing

On the last day of the pre-bed rest phase, last day of the bed rest phase (*end-bed rest day*) and last day of the post-bed rest phase, a tilt/stand test was used to determine orthostatic tolerance. After recording baseline data in the supine position, the subjects were then tilted upright on a tilt table to thirty degrees for about ten minutes. The angle of tilt was then increased to sixty degrees for about ten minutes. Finally the subjects were tilted to an upright posture. After each posture was attained and a hemodynamically steady state was reached, data for CSI analysis were collected (see Data collection for CSI). The test was immediately terminated and the subject was returned to the supine position if there was evidence of a

sudden drop in blood pressure and/or he had difficulty appropriately responding to questions, i.e., manifested mental status changes consistent with presyncopal symptoms. After the CSI testing in the upright posture, the subjects were allowed to move their legs or walk as needed while maintaining the upright posture for approximately 120 minutes and being closely monitored for presyncopal symptoms.

Data collection for CSI As discussed in Chapter 2 (Section 2.10)

Data Analysis

System identification of the ILV→HR impulse response involving ILV, ABP and HR signals using the WPCR method has been described in detail in Section 2.10. Subsequently, the Area method (Section 3.3.1) can be employed to compute sympathetic and parasympathetic indicators of each subject. We refer to this method as the Area-WPCR method in the following sections.

On the other hand, utilizing the ILV and HR signals, we can also compute autonomic indices via the SD method (Section 3.3.2). Approximately 6 minutes of data were downsampled to 1.25 Hz. System identification of the ILV⇒HR impulse response was carried out through the WPCR-ARX algorithm with a maximum AR or MA order of 10 and the preweighting scheme as proposed previously (Section 2.9). A parasympathetic index was then computed based on the peak amplitude of the ILV⇒HR impulse response and a sympathetic index was obtained through Equation (2.54).

4.3 Results

Statistical comparison between sleep-deprived and non-sleep-deprived subgroups of subjects demonstrated no significant difference in terms of impulse response parameters or noise

source power spectra. In addition, there is no significant difference in the incidence of end-bed rest orthostatic tolerance between the two groups. Therefore, in the results presented below, we did not differentiate subjects in terms of sleep-awake patterns.

4.3.1 Supine vs. Tilt

It is generally accepted that postural change from supine to standing is accompanied by a reduction in the parasympathetic activity and an enhancement in the sympathetic activity. Autonomic indices calculated from data obtained in supine and in standing postures were compared (see Table 4-3 and Table 4-4 for results using the Area-WPCR method and Table 4-7 and Table 4-8 for results using the SD method). Parasympathetic indices of both the Area-WPCR method and the SD method demonstrate statistically significant changes upon tilt-up from the supine posture. While the SD method tracks alterations in the sympathetic function at all tilt angles significantly, the Area-WPCR method does not show any significance in this respect. These results will be discussed in detail in Section 4.4.

4.3.2 Pre-bed Rest vs. End/Post-bed Rest

Autonomic indices obtained from data collected in all postures on the end-bed rest day and on the post-bed rest day were compared respectively with those obtained from the pre-bed rest data. In addition, the end-bed rest and post-bed rest autonomic indices were also compared (see Table 4-3 and Table 4-4 for results using the Area-WPCR method and Table 4-7 and Table 4-8 for results using the SD method). The parasympathetic indices of both methods demonstrated significant reduction at end-bed rest compared with those at pre-bed rest. The post-bed rest parasympathetic index is also smaller than the pre-bed rest one, which indicates that the three-day post-bed rest recovery period is not long enough for the parasympathetic index to return to its baseline level, although a trend of increase compared to end-bed rest indices is demonstrated (Table 4-7). Sympathetic indices of both the Area-WPCR and the SD methods demonstrate statistically smaller values after bed rest compared to pre-

bed rest. The Area-WPCR method also shows smaller post-bed rest sympathetic indices compared to the baseline values although there is a trend of recovery reflected in the end-bed rest and post-bed rest comparison.

Table 4-11 lists the number of subjects who tolerated (T) the tilt/stand testing and those who had a presyncopal event (NT) on each test day. Sixty-six percent of patients tolerated tilt/stand testing before bed rest, 36% tolerated the test at end-bed rest, while 83% tolerated the test after the recovery period. Fisher's Exact categorical test [211] was performed with the following hypotheses: the proportion of subjects having presyncopal episode during tilt/stand testing at end-bed rest is higher than those at pre or post-bed rest respectively and the proportion of subjects having presyncopal episode at post-bed rest is the same as that at pre-bed rest (complete recovery). If a P value less than 0.05 is considered significant, then the statistical tests conclude that more subjects failed the tilt/stand testing at end-bed rest compared to both pre and post-bed rest while post-bed rest tilt tolerance is not statistically different from pre-bed rest tolerance. Note that those seven subjects who received midodrine (see Section 4.2) were excluded from the statistical analysis of tilt tolerance at end-bed rest.

4.3.3 Toleration of Tilt/Stand Testing

Although monitoring of presyncopal symptoms lasted more than two hours for each subject, presyncope always occurred during either the tilting or the early standing period. The time to presyncope was: pre-bed rest: 25.5 ± 10.8 (SD) min; end-bed rest: 22.2 ± 6.9 (SD); post-bed rest: 30.8 ± 12.2 min. Therefore, we categorize the subjects in this section as tilt-tolerant or tilt-intolerant without a more detailed differentiation according to their presyncope-free survival times.

At pre-bed rest, 10/29 subjects were tilt-intolerant. Eight subjects displayed a vasovagal pattern of tilt intolerance (an abrupt drop in arterial blood pressure and heart rate), while two followed a dysautonomic pattern of tilt intolerance with a gradual drop in arterial blood

pressure and gradual increase or little change in heart rate. At end-bed rest, 14/22 subjects were tilt-intolerant (excluding the 7 subjects who received midodrine at the end of bed rest). Twelve subjects had a vasovagal pattern and two had a dysautonomic pattern of tilt intolerance. At post-bed rest, 5/29 subjects were tilt-intolerant. All of them had a vasovagal pattern of presyncope. The patterns of presyncope and syncope will be discussed further in Section 4.4.4.

Autonomic indices were compared between the subject group who tolerated (T) the tilt/stand testing and the group who experienced presyncopal episodes (F) on each test day using data collected on the same day (see Table 4-5, Table 4-6, Table 4-9 and Table 4-10 for the results of the Area-WPCR and the SD methods). The parasympathetic responsiveness was higher for the F group while sympathetic responsiveness was lower for this group. We also compared autonomic indices of subjects who tolerated (T) the tilt/stand testing with those who experienced a presyncopal episode (F) on the *end-bed rest* day using data collected on the *pre-bed rest* day. Therefore, this is an attempt to associate tilt tolerance after bed rest with baseline measures. Based on both the Area-WPCR and the SD methods, those subjects who experienced a presyncopal event after bed rest had a higher parasympathetic responsiveness ($P < 0.1$) and a lower sympathetic responsiveness prior to bed rest (at baseline).

Table 4-3 Group average comparisons of parasympathetic responsiveness results of the Area-WPCR method: supine (Su) vs. tilt; pre-bed rest (Pre) vs. end-bed rest (End) or post-bed rest (Post); End vs. Post; (29 subjects for Pre vs. End in supine posture, Supine vs. Tilt at pre-bed rest, Pre vs. Post and End vs. Post in supine posture; 22 subjects for Pre vs. End at Tilt postures and Supine vs. Tilt at end-bed rest – subjects treated with midodrine are excluded; Values are means ± SE.).

		Parasympathetic Area (mean ± SE)	*P* value Su vs. Tilt	*P* value Pre vs. End/Post	*P* value End vs. Post
Pre-bed rest	Su	0.016±0.0017			
	30°	0.015±0.0024	0.60		
	60°	0.010±0.0014	0.0017		
	90°	0.009±0.0012	0.0007		
End-bed rest	Su	0.013±0.0018		0.039	
	30°	0.009±0.0014	0.045	0.022	
	60°	0.008±0.0019	0.058	0.25	
	90°	0.005±0.0009	0.010	0.029	
Post-bed rest	Su	0.012±0.0013		0.006	0.44
	30°	0.010±0.0013	0.078	0.027	0.32
	60°	0.007±0.0014	0.0011	0.0096	0.65
	90°	0.006±0.0010	0.0002	0.080	0.85

Table 4-4 Group average comparisons of sympathetic responsiveness results of the Area-WPCR method: supine (Su) vs. tilt; pre-bed rest (Pre) vs. end-bed rest (End) or post-bed rest (Post); End vs. Post; (see the caption of Table 4-3 for the number of subjects in each category).

		Sympathetic Area (mean ± SE)	*P* value Su vs. Tilt	*P* value Pre vs. End/Post	*P* value End vs. Post
Pre-bed rest	Su	0.018±0.0033			
	30°	0.015±0.0021	0.15		
	60°	0.014±0.0028	0.28		
	90°	0.015±0.0039	0.27		
End-bed rest	Su	0.007±0.0011		0.0019	
	30°	0.008±0.0014	0.37	0.002	
	60°	0.010±0.0017	0.11	0.18	
	90°	0.007±0.0020	0.94	0.15	
Post-bed rest	Su	0.010±0.0015		0.014	0.022
	30°	0.007±0.0015	0.10	0.001	0.30
	60°	0.009±0.0018	0.62	0.083	0.79
	90°	0.006±0.0012	0.59	0.047	0.13

Table 4-5 Group average comparisons of parasympathetic responsiveness results of the Area-WPCR method: Subjects who tolerated (T) the orthostatic tolerance testing vs. those who failed (F); same day: the orthostatic tolerance testing and data collection for system identification were performed on the same day; End: the orthostatic tolerance testing was performed at end-bed rest. (Su: supine; Values are means ± SE; see Table 4-11 for the number of subjects in each category)

		Parasympathetic Area (mean ± SE)			Parasympathetic Area (mean ± SE)		
		T-same day	F-same day	P value	T-End	F-End	P value
Pre-bed rest	Su	0.014±0.001	0.025±0.004	0.002	0.012±0.002	0.019±0.003	0.076
	30°	0.015±0.003	0.015±0.005	0.97	0.011±0.002	0.018±0.005	0.32
	60°	0.009±0.001	0.011±0.004	0.61	0.008±0.002	0.010±0.003	0.61
	90°	0.009±0.001	0.007±0.002	0.62	0.008±0.002	0.008±0.002	0.90
End-bed rest	Su	0.010±0.002	0.015±0.003	0.25			
	30°	0.008±0.001	0.009±0.002	0.86			
	60°	0.006±0.001	0.009±0.003	0.35			
	90°	0.005±0.001	0.005±0.001	0.90			
Post-bed rest	Su	0.011±0.001	0.019±0.006	0.032			
	30°	0.009±0.001	0.023±0.004	5e-5			
	60°	0.006±0.001	0.018±0.007	0.001			
	90°	0.006±0.001	0.008±0.004	0.33			

Table 4-6 Group average comparisons of sympathetic responsiveness results of the Area-WPCR method: Subjects who tolerated (T) the orthostatic tolerance testing vs. those who failed (F); (see the caption of Table 4-5 for more details)

		Sympathetic Area (mean ± SE)			Sympathetic Area (mean ± SE)		
		T-same day	F-same day	P value	T-End	F-End	P value
Pre-bed rest	Su.	0.018±0.005	0.014±0.003	0.50	0.012±0.004	0.018±0.006	0.42
	30°	0.016±0.003	0.010±0.002	0.19	0.015±0.003	0.014±0.003	0.91
	60°	0.018±0.004	0.005±0.002	0.033	0.017±0.005	0.012±0.005	0.42
	90°	0.018±0.005	0.004±0.002	0.11	0.018±0.003	0.005±0.002	0.001
End-bed rest	Su.	0.009±0.002	0.006±0.001	0.069			
	30°	0.007±0.001	0.008±0.002	0.89			
	60°	0.014±0.003	0.006±0.002	0.035			
	90°	0.009±0.003	0.006±0.003	0.43			
Post-bed rest	Su.	0.01±0.002	0.008±0.004	0.66			
	30°	0.006±0.001	0.013±0.007	0.15			
	60°	0.009±0.002	0.009±0.009	0.91			
	90°	0.006±0.001	0.007±0.005	0.92			

Table 4-7 Group average comparisons of parasympathetic responsiveness results of the SD method: supine (Su) vs. tilt; pre-bed rest (Pre) vs. end-bed rest (End) or post-bed rest (Post); End vs. Post; (see the caption of Table 4-3 for the number of subjects in each category).

		Parasympathetic Index (mean ± SE)	*P* value Su. vs. Tilt	*P* value Pre vs. End/Post	*P* value End vs. Post
Pre-bed rest	Su.	0.76±0.094			
	30°	0.53±0.091	0.0026		
	60°	0.38±0.059	0.0002		
	90°	0.34±0.061	8.2e-5		
End-bed rest	Su.	0.49±0.070		0.0013	
	30°	0.35±0.059	0.018	0.0064	
	60°	0.19±0.066	0.0004	0.0039	
	90°	0.031±0.003	5.3e-5	3.6e-5	
Post-bed rest	Su.	0.54±0.072		0.0018	0.40
	30°	0.36±0.057	0.0008	0.0026	0.52
	60°	0.27±0.047	7.9e-5	0.034	0.062
	90°	0.15±0.035	1.5e-5	0.0021	0.05

Table 4-8 Group average comparisons of sympathetic responsiveness results of the SD method: supine (Su) vs. tilt; pre-bed rest (Pre) vs. end-bed rest (End) or post-bed rest (Post); End vs. Post; (see the caption of Table 4-3 for the number of subjects in each category).

		Sympathetic Index (mean ± SE)	*P* value Su. vs. Tilt	*P* value Pre vs. End/Post	*P* value End vs. Post
Pre-bed rest	Su.	0.63±0.11			
	30°	0.95±0.12	0.0047		
	60°	1.63±0.20	0.00017		
	90°	1.40±0.16	0.00029		
End-bed rest	Su.	0.52±0.07		0.14	
	30°	0.90±0.16	0.012	0.72	
	60°	1.51±0.21	0.00017	0.17	
	90°	1.14±0.20	0.014	0.019	
Post-bed rest	Su.	0.55±0.08		0.47	0.34
	30°	1.00±0.12	1.3e-5	0.73	0.12
	60°	1.49±0.17	3.6e-6	0.16	0.83
	90°	1.24±0.14	3.1e-5	0.17	0.057

Table 4-9 Group average comparisons of parasympathetic responsiveness results of the SD method: Subjects who tolerated (T) the orthostatic tolerance testing vs. those who failed (F); (see the caption of Table 4-5 for more details)

		Parasympathetic Index (mean ± SE)			Parasympathetic Index (mean ± SE)		
		T-same day	F-same day	P value	T-End	F-End	P value
Pre-bed rest	Su.	0.65±0.08	1.04±0.20	0.051	0.50±0.11	0.82±0.11	0.079
	30°	0.49±0.10	0.56±0.15	0.69	0.40±0.08	0.50±0.09	0.47
	60°	0.39±0.06	0.35±0.11	0.75	0.38±0.09	0.47±0.08	0.48
	90°	0.33±0.073	0.36±0.12	0.82	0.32±0.057	0.35±0.12	0.84
End-bed rest	Su.	0.45±0.08	0.49±0.10	0.76			
	30°	0.34±0.06	0.35±0.07	0.93			
	60°	0.14±0.06	0.25±0.09	0.36			
	90°	0.074±0.03	-0.019±0.03	0.075			
Post-bed rest	Su.	0.45±0.06	0.97±0.25	0.006			
	30°	0.29±0.04	0.86±0.12	0.0001			
	60°	0.19±0.03	0.65±0.14	0.0003			
	90°	0.15±0.03	0.28±0.09	0.21			

Table 4-10 Group average comparisons of sympathetic responsiveness results of the SD method: Subjects who tolerated (T) the orthostatic tolerance testing vs. those who failed (F); (see the caption of Table 4-5 for more details)

		Sympathetic Index (mean ± SE)			Sympathetic Index (mean ± SE)		
		T-same day	F-same day	P value	T-End	F-End	P value
Pre-bed rest	Su.	0.73±0.13	0.32±0.11	0.07	0.64±0.08	0.57±0.13	0.69
	30°	0.99±0.14	0.91±0.21	0.74	0.85±0.12	1.00±0.21	0.61
	60°	1.76±0.25	1.48±0.28	0.54	1.81±0.36	1.43±0.27	0.41
	90°	1.50±0.17	1.13±0.36	0.32	1.87±0.24	1.08±0.21	0.026
End-bed rest	Su.	0.60±0.11	0.46±0.08	0.33			
	30°	0.92±0.23	0.93±0.19	0.98			
	60°	1.56±0.37	1.49±0.20	0.87			
	90°	1.26±0.27	0.99±0.29	0.51			
Post-bed rest	Su.	0.61±0.08	0.31±0.18	0.16			
	30°	1.06±0.13	0.59±0.12	0.19			
	60°	1.55±0.19	1.09±0.11	0.36			
	90°	1.32±0.14	0.61±0.11	0.09			

Table 4-11 Number of subjects in the two groups: tilt-tolerant group (T) and tilt-intolerant group (F) at pre-bed rest, end-bed rest and post-bed rest respectively. The *P* values were obtained using Fisher's Exact categorical test (see text for details).

Number of subjects	Pre-bed rest	End-bed rest	Post-bed rest
T	19	8	24
F	10	14	5
Percent Tolerant	65.5%	36.4%	82.8%
P value, pre vs. end/post		0.037	0.23
P value, end vs. post			8.7e-4

4.4 Discussion

This study employs the autonomic function identification techniques developed in Chapter 3 to analyze data obtained in a 16-day head-down tilt bed rest study. We may make three observations based on the data presented here. First, prolonged bed rest may impair autonomic control of heart rate. Second, orthostatic intolerance after bed rest is associated with impaired autonomic responsiveness. Third, there may be a pre-bed rest predisposition to the development of orthostatic intolerance after bed rest.

For comparison purpose, we included in Appendix C the identification results using the Area-APR method on the same data set. This method was previously employed in [106]. It implements the same Area method to compute sympathetic and parasympathetic responsiveness, but system identification was carried out through an ARX parameter reduction algorithm (APR) [55] instead of the WPCR method.

4.4.1 Supine vs. Tilt

It is well accepted that postural change from supine to standing results in a relative shift from parasympathetic-dominant to sympathetic-dominant cardiovascular control [45]. Results of the SD method conform very well with this general notion. However, the Area-

WPCR method demonstrated the expected changes upon tilt only in the parasympathetic indices. Its sympathetic index does not show any significant difference upon postural shift. In contrast, the Area-APR method (see Appendix C, Table C - 2) detected some of the changes in the sympathetic index upon tilt.

The difference of the APR and the WPCR methods have been discussed in Chapter 2 (Section 2.10). We observed that characteristic times of the HR baroreflex and the ILV→HR impulse responses computed by the APR method were seemingly larger than those computed by the WPCR method. A detailed investigation on the two methods indicated that the APR method leads to a noisy estimation of the impulse response, especially for the sympathetic component. In the results presented in this chapter, it can also be appreciated that the WPCR method gives a much smaller group-averaged standard error in sympathetic index than the APR method does. Therefore, the two methods displayed different properties in dealing with noise-corrupted data. The APR method attempts to retain more noisy components to model the underlying system dynamics, while the WPCR method imposes a stringent restraint to retain less noisy components and enable a succinct estimate of the impulse response.

Data collected in tilt-up postures may have more inherent noise/instability than in the supine posture. In addition, the ILV→HR impulse response in tilt-up postures may be complicated by the resistance baroreflex more than in the supine posture. We postulate that the WPCR method estimates the impulse response conservatively in tilt-up postures to reduce the effect of noise. Therefore, it may underestimate the sympathetic area and lead to insignificant comparisons between supine and tilt-up results. On the other hand, the APR method retains more noisy components which induce a larger standard error for tilt-up data. Although compromised by the uncertainties in the estimated impulse responses, significant changes in sympathetic area are still detected upon tilt. The stringent estimation of the WPCR method may prove advantageous in statistical comparisons involving data collected in the same posture (see discussions below).

4.4.2 Effect of Bed Rest

Both the SD and the Area-WPCR methods demonstrated that parasympathetic and sympathetic responsiveness decreased significantly after bed rest. The SD method showed statistical significance in parasympathetic change upon every posture assumed, while the sympathetic index was significantly reduced after bed rest only in the standing posture. In addition, the SD method did not demonstrate significant changes at post-bed rest compared to both pre and end-bed rest. As discussed in Chapter 3, theoretical values of the SD model coefficients (Equation (2.54)) may not change dramatically among subjects and among physiological conditions. However, it is not clear if prolonged bed rest changes the *state* of autonomic functioning and, therefore, requires modifications in the model parameter values (for detailed discussion about the SD method, see Section 3.5.4). The Area methods detected more significant changes with respect to sympathetic quantification than the SD method. Furthermore, considering both Pre vs. End and Pre vs. Post analyses, the Area-WPCR method resulted in smaller P values and more significant comparisons compared to the Area-APR method, especially in terms of the sympathetic index. The WPCR method is more effective in these scenarios than the APR method maybe due to its ability to reduce the effect of noise in the estimated impulse response, as discussed previously.

Many researchers have shown that parasympathetic activity is impaired following simulated or actual microgravity exposure using different techniques, such as, by analyzing R-R interval of HR or by performing Valsalva's maneuver [111, 168, 194]. However, there remains a lack of consensus about the changes in sympathetic activity. For example, some [205] showed a reduction in muscle sympathetic nerve activity (MSNA) after 14 days of bed rest, while others reported an increase [207, 208] in MSNA reflex control after bed rest (see also Table 4-1 and Table 4-2). In another study [135], HR power spectrum and urinary catecholamine response were both analyzed. However, the two techniques resulted in different conclusions regarding changes in sympathetic activity following bed rest. Fritsch-Yelle and coworkers [169] found that after 16 days of spaceflight, returning astronauts had subnormal increases in plasma norepinephrine level on the assumption of upright posture. Note that this indicates a functional change in the neurogenic feedback loop, which includes

arterial baroreceptors, brainstem, spinal tracts and sympathetic nerves. One of the advantages of our methods is that they estimate the modulation of the efferent autonomic activity on the sinoatrial node directly without involving a reflex mechanism, thereby simplifying the interpretation of the results.

In addition, our analyses (especially through the Area-WPCR method) showed that post-bed rest autonomic indices are lower than the pre-bed rest measures. Therefore, the three-day post-bed rest phase did not enable a complete recovery to the baseline level in cardiac autonomic control. Results presented by Spaak *et al.* [212] demonstrated that the longer the duration of microgravity exposure is, the longer it takes to reach a complete recovery of the cardiovascular response to sustained handgrip exercise. Convertino *et al.* [194] studied 11 healthy men before and after 30 days of 6° HDBR. They showed that the baroreflex function was impaired after bed rest and did not recover to the baseline level after five days post-bed rest. However, Fritsch-Yelle *et al.* showed that carotid baroreceptor-cardiac reflex response returned to the baseline level on and after the 3rd day post-space flight in 16 astronauts finishing shuttle missions lasting 8-14 days [168]. The above inconsistency in the results of different studies may be due to the difference in the HDBR/space flight duration or in the protocols for the recovery period because the activities of the subjects after HDBR or space flight are usually less strictly regulated or monitored than those before and during microgravity exposure.

4.4.3 Toleration of Tilt/Stand Testing

Our results suggest that those who tolerated the tilt/stand test had a lower parasympathetic responsiveness and a higher sympathetic responsiveness measured on the day of the test than those who did not tolerate the test. The SD method failed to detect statistically significant difference in the sympathetic index (although having P values less than 0.1), the Area-APR method failed to detect the difference in the parasympathetic index, while the Area-WPCR method identified both types of significance. Note that the difference in parasympathetic responsiveness between the two groups is statistically significant or nearly significant often

in the supine posture, while that of sympathetic responsiveness is significant in the 60 or 90-degree posture. This may be due to the fact that supine posture is a parasympathetic-dominant state while upright posture is a sympathetic-dominant state. The above results show that autonomic responsiveness is associated with tilt/stand test tolerance. Furthermore, combining this result and the fact that more subjects failed the tilt/stand test (Table 4-11) after bed rest and the result that bed rest impaired both parasympathetic and sympathetic responsiveness, one may speculate that autonomic control, sympathetic responsiveness in particular, may be mechanistically involved in determining tilt tolerance. The relation between OI and various factors directly or indirectly related to autonomic function have been studied [110, 194, 201, 213]. However, a general consensus has not been reached. Our results are consistent with those of Fritsch-Yelle *et al.* [169, 214] who also showed that the tilt-tolerant group on landing day had a greater sympathetic response upon standing than the tilt-intolerant group.

At post-bed rest, a significantly higher proportion of subjects tolerated the tilt/stand testing than at end-bed rest (Table 4-11). However, the autonomic indices at post-bed rest almost do not demonstrate any significant changes from those at end-bed rest. This apparent disagreement with the pre vs. end comparisons may imply the intrinsic nature of complexity in the underlying mechanisms of tilt tolerance. Given the evidences we have thus far, we postulate that psychological factors may play an important role in inducing a better tolerance of tilt/stand testing post-bed rest when the subjects' mental stress is lessened near the completion of the bed rest study. In addition, the previous two tilt/stand testings (at pre and end-bed rest) may have served as a learning process for the subjects to psychologically adapt to this test.

4.4.4 Prediction of Orthostatic Intolerance

The Area methods and the SD method all demonstrated that subjects with a relatively higher sympathetic responsiveness pre-bed rest tended to tolerate the tilt/stand test after bed rest. The Area-WPCR method gives the smallest P values in this comparison. The Area-APR

method also indicates a significantly smaller pre-bed rest parasympathetic area in subjects who tolerated the tilt/stand test after bed rest, while the *P* values induced by the SD and the Area-WPCR methods for this comparison are nearly significant. Since we showed that parasympathetic responsiveness was impaired after bed rest and more subjects failed the tilt/stand test after bed rest, it is unlikely that reduced parasympathetic responsiveness contributes mechanistically to orthostatic tolerance. Hence, the finding of a smaller parasympathetic responsiveness in tilt-tolerant subjects may simply be a manifestation of the inhibitory effect between sympathetic and parasympathetic control [45].

The above results suggest that an altered sympathetic function might be related mechanistically to a predisposition to end-bed rest orthostatic intolerance, and they also raise the possibility of predicting end-bed rest OI using pre-bed rest measures. Few studies demonstrated similar statistical significance in this aspect. Fritsch-Yelle *et al.* [169, 214] was the first to suggest the possibility of predicting which individuals would be susceptible to OI post-space flight. They found that baseline peripheral vascular resistances, systolic and diastolic pressures before flight were significantly lower in the after-flight presyncopal group than in the other group. Since autonomic function plays a major role in regulating these hemodynamic variables, one might infer from their results a preflight intergroup difference in autonomic responsiveness. Although various factors may be involved in the development of OI following microgravity exposure, our results suggest that autonomic function might specifically play a role in this process.

Most of our tilt-intolerant subjects followed a vasovagal syncope pattern [210], while only two subjects showed a dysautonomic pattern. Both patterns have been documented after spaceflight [110, 180]. In addition, the above results may have relevance to the development of vasovagal syncope upon adopting an upright posture in Earth-bound patients. During vasovagal syncope, the efferent responses are increased vagal activity, especially to the heart, and decreased sympathetic activity. Experimental evidence indicated that the precipitous fall in blood pressure in vasovagal syncope is preceded by both vagally mediated bradycardia and inhibition of peripheral sympathetic nerve activity which causes vasodilatation [215]. The most widely held explanation for this paradoxic response of blood pressure

and heart rate is the Bezold-Jarish reflex [216, 217] mechanism – sensory receptors in the left ventricular myocardium mediate vagomimetic and sympathoinhibitory effects when activated by mechanical stretch or chemical stimulations [215, 216]. It has been hypothesized that during orthostatsis, hypovolemic hypotension leads to augmented ventricular contraction resulting in a nearly empty chamber, thereby producing mechanical deformation of these receptors and the ensuing paradoxic response [215, 216]. Our results also suggest that patients with lower sympathetic responsiveness and higher parasympathetic responsiveness at baseline may be predisposed to vasovagal syncope. However, a more specific study needs to be conducted to further validate this hypothesis.

4.4.5 Limitations

When subjects in this study became presyncopal before finishing the CSI data collection in the upright position, they were returned to the supine position for recovery thus only data collected before the onset of presyncopal symptoms could be analyzed. The reduced length of available data may adversely affect the accuracy of system identification. Since a significant number of subjects became presyncopal during the tilt/stand test after bed rest, this limitation affects end-bed rest results more seriously than pre-bed rest ones.

4.5 Conclusions

In summary, we studied cardiovascular autonomic function in healthy subjects before and after 16 days of head-down-tilt bed rest. We found that bed rest impaired both parasympathetic and sympathetic responsiveness. Higher parasympathetic and lower sympathetic responsiveness pre-bed rest identified individuals more susceptible to OI both before and after bed rest. Our findings may have significance for studying Earth-bound orthostatic hypotension as well as for designing effective countermeasures to post-flight OI.

In this study, we applied two methods, the Area method and the SD method, to quantify sympathetic and parasympathetic responsiveness. Furthermore, two system identification algorithms, the WPCR and the APR algorithms, were employed to compute the ILV→HR impulse response which is needed by the Area method. Although the SD method is capable of tracking changes due to postural shift, it is limited in studying the effect of bed rest on sympathetic control and orthostatic intolerance due to a possible change of autonomic state after bed rest. The Area-WPCR method outperforms the Area-APR method in this study except for detecting changes in sympathetic control related to postural shift, which may be a result of the stringency of the WPCR method in handling noise-corrupted data.

Chapter 5

Conclusions

5.1 Summary of Contributions

The research presented in this thesis focuses on the development of an LTI system identification method based on which new techniques for quantification of cardiac autonomic responsiveness are proposed, evaluated and applied to investigate practical biomedical problems. In this section, we summarize the major results of this research.

In Chapter 2, the new system identification method based on Weighted-Principal Component Regression (WPCR) was introduced. This method was presented in conjunction with both moving average (MA) and autoregressive exogenous input (ARX) model structures. We investigated in detail the frequency domain interpretation of the WPCR-MA and WPCR-ARX methods. It was demonstrated that the WPCR methods enable construction and selection of candidate models in the frequency domain. In addition, the estimated model parameters are weighted such that those associated with dominant frequency components of the data are more accurately identified than those corresponding to the insignificant components. By excluding the frequency components weakly-represented in the data, the WPCR method reduces the variance of estimated model parameters when the input is a colored signal. Furthermore, since the WPCR method builds data-specific candidate models in the frequency domain, it is able to cope with systems with input delays and multiple inputs.

To practically implement the WPCR method, we proposed and validated weighting schemes for the MA and the ARX structures respectively. We evaluated the performance of

the WPCR methods through both simulated and experimental data. Both open-loop and closed-loop systems were simulated whose dynamics resemble that of physiologic systems. We incorporated a pre-whitening procedure into the WPCR-MA method for closed-loop system identification. Compared to conventional ARX (open-loop) or GLS (closed-loop) methods, the WPCR method demonstrated its advantage in terms of impulse response estimation. In addition, we showed that the WPCR method is potentially effective when the input signal is not persistently exciting relative to the system dynamics. Lastly, we evaluated the performance of the WPCR methods via experimental data where open-loop, closed-loop, multiple-inputs single-output and noncausal systems are involved. The effectiveness of the WPCR methods in handling this complicated set of systems is confirmed through comparisons with the previously exploited Arma Parameter Reduction (APR) method.

In Chapter 3, we applied the WPCR system identification method to study cardiovascular autonomic control, which demonstrated the effectiveness of engineering methodologies in tackling biomedical problems. Specifically, we proposed three techniques to quantify cardiac autonomic responsiveness. The Area method was built based on the WPCR system identification involving arterial blood pressure (ABP), instantaneous lung volume (ILV) and heart rate (HR). The derivation of a parasympathetic quantification and a sympathetic one from the ILV$\rightarrow$HR impulse response was based on solid experimental evidence. The Area method requires data collected during random breathing to generate persistently exciting input signals. In contrast, the SD method is suitable for both spontaneous and random breathing data. The advantage of the WPCR method accredited to its frequency selective property was well appreciated in dealing with spontaneous breathing data because the ILV signal is not persistently exciting for the identification of ILV$\Rightarrow$HR impulse response. The SD_m technique, a modified version of the SD method, utilizes a straightforward nonparametric system identification procedure. It is specifically designed to analyze ILV and HR data when the respiratory activity is metronomic. The SD and SD_m methods only necessitate measurements of surface ECG signals.

We validated the above three techniques using experimental data. Both the Area and the SD methods were applied to analyze random breathing data. Corresponding to different in-

terventions involved in the databases, results consistent with expected physiologic changes were obtained for both methods. Values of the parasympathetic and sympathetic indices based on the two methods were fairly closely correlated. The SD method was also applied to analyze spontaneous breathing data. Identified parasympathetic and sympathetic indices of the same subject group during spontaneous breathing and during random breathing were compared, through which applicability of the SD method to spontaneous breathing data was confirmed. The SD_m method was applied to one set of metronomic breathing data and it enabled a statistically significant differentiation of the autonomic responsiveness associated with supine and standing postures.

In Chapter 4, we applied the Area and the SD methods to investigate one specific topic – the effect of simulated microgravity on cardiac autonomic control and orthostatic intolerance. We concluded that both the parasympathetic and sympathetic responsiveness were diminished after prolonged head-down-tilt bed rest. We found that more subjects failed the tilt/stand test at end-bed rest than at pre-bed rest and that those subjects who tolerated the test had a higher sympathetic index and a lower parasympathetic index on the tilt/stand test day than those who failed the test. These findings indicate that impaired sympathetic responsiveness may be closely associated with orthostatic intolerance. Moreover, we found that subjects who tolerated the tilt/stand test on end-bed rest day had a higher sympathetic responsiveness and a lower parasympathetic responsiveness pre-bed rest. This result raised the possibility of predicting end-bed rest orthostatic intolerance using pre-bed rest measures. Lastly, values of post-bed rest autonomic indices are statistically different from the pre-bed rest values suggesting that the autonomic control system did not completely recover to baseline three days after bed rest. The above application of the Area and the SD methods also validated the techniques themselves and provided a better understanding of their applicability. The Area method is suitable for population-based studies since it considers an impulse response function which is intrinsically standardized, while the SD method is better suited for patient monitoring because computation of the sympathetic impulse response depends on some empirically-derived proportional constants.

5.2 Future Directions for Research

There are a few potential areas of future research that could expand upon the work in this thesis.

1. An important element of the WPCR method is the weighting scheme on the data matrix which is a reflection of the *a priori* knowledge that current output is more closely correlated with recent inputs/outputs and less with remote ones. This weighting scheme proved very effective in both MA and ARX structures. It would be an interesting attempt to investigate the applicability of a similar weighting scheme in total least-squares (TLS) estimation or parametric spectral estimation problems. In addition, the concept of WPCR may also be incorporated into nonlinear system identification settings such as those based on Volterra series.

2. Pertaining to the WPCR-ARX structure, there is one question remaining unresolved. Due to the nonlinearity involved in the mapping between model parameters and the impulse response function, it is unclear how the pre-weighting factors affect the basis function of the impulse response. Since in physiologic system identification, pre-knowledge about the shape of the impulse response is usually available which was gained through past experience, it would be helpful to incorporate such knowledge in the designing of the weighting function. To determine the basis function of the weighted ARX impulse response, approximations based on linearization theory may be required or another more involved weighting scheme may need to be developed.

3. As mentioned in Chapter 3, there is still much potential to improve the SD method. One direction is to increase the size of the training data and categorize the subjects according to their age and sex. In this way, different model parameters may be derived for subjects in different categories which could enable a more accurate identification of autonomic responsiveness for specific subjects. The other potentially interesting work is to correct the model parameters based on some information derived from cuff blood pressure, e.g., the pulse pressure. Because low frequency components in HR variability are mainly contributed by blood pressure fluctuation, such

correction may prove useful in improving the accuracy of the estimated model parameters.

4. The study of effects of microgravity on cardiac autonomic control and orthostatic intolerance presented in this thesis is merely a first step in investigating this highly complicated topic. Continuing studies may involve an in-depth examination of similar problems in female subjects and subjects with older ages. It is also desirable to analyze data directly collected from astronauts at baseline and after spaceflight of varying durations. Importantly, countermeasures may be designed and tested based on the study on autonomic function and its association with orthostatic intolerance.

We hope that the presented work will stimulate further research into the application of system identification techniques in studying cardiovascular dynamics and its neural control. It is also desired that the methodologies developed in this thesis may inspire development of novel techniques in probing other physiologic mechanisms.

Appendix A

Proof of the Asymptotic Property of the Covariance Matrix of a Stationary Time Series [85, 104]

It is well-known that the covariance matrix of a stationary time series is a symmetric Toeplitz matrix. If the covariance function of a time series is absolutely summable, we proof in the following that the eigenvectors and eigenvalues of the covariance matrix have certain special forms asymptotically. (This section mainly follows that of Ref. [104].)

Definition: Consider a T x T matrix $C = [C_{jk}]$, if C_{jk} , the element residing in the j^{th} row and the k^{th} column, depends only on j-k, that is, $C_{jk} = c(j-k)$ for some function $c(.)$, then the matrix C is defined as a finite Toeplitz matrix.

Asymptotic Property: Let F be the matrix whose columns are the asymptotic eigenvectors of the T x T covariance matrix of a stationary time series with absolutely summable covariance function $\gamma(h)$. If T is odd, assume $T = 2m+1$, then the first column F_1 has constant elements $1/\sqrt{T}$, the $(2j)^{\text{th}}$ column F_{2j} has elements $\sqrt{2/T}\cos(2\pi jt/T)$, and the $(2j+1)^{\text{th}}$ column F_{2j+1} has elements $\sqrt{2/T}\sin(2\pi jt/T)$, for $t = 1, 2, \quad , T$ and $j = 1, 2, \quad , m$, where $T = 2m+1$. The orthogonal matrix F is called Fourier matrix. The eigenvalues are asymptotically:

$$d_1 = \frac{1}{2\pi}\sum_{h=-\infty}^{\infty}\gamma(h),$$

$$d_{2j} = d_{2j+1} = \frac{1}{2\pi}\sum_{h=-\infty}^{\infty}\gamma(h)e^{-i2\pi hj/T}$$

If T is even, assume $T = 2m+2$, the first $2m+1$ eigenvectors are the same as above, there is an extra eigenvector $1/\sqrt{T}\,[1,-1,1,...,-1]$ associated with $j = m+1$, and a corresponding eigenvalue:

$$d_T = \frac{1}{2\pi}\sum_{h=-\infty}^{\infty}\gamma(h)\cos\pi h$$

To prove the above property, we first consider the following theorem:

Theorem A-1: Let $Z = [z(k\text{-}j)]$ be a T x T circulant matrix, then its eigenvalues are given by:

$$\sum_{j=0}^{T-1} z(j)\exp\{-i2\pi jk/T\},\ k = 0,\ 1,\quad ,\ T\text{-}1,$$

and the corresponding eigenvectors by:

$$1/\sqrt{T}\,[\exp(-i2\pi jk/T);\ j = 0,...,T-1],\ k = 0,\quad ,\ T\text{-}1.$$

Proof:

A circulant matrix Z is defined as:

$$Z = \begin{bmatrix} z(0) & z(1) & \dots & z(T-1) \\ z(T-1) & z(0) & \dots & Z(T-2) \\ \vdots & \vdots & \dots & \vdots \\ z(1) & z(2) & \dots & z(0) \end{bmatrix}$$

That is: in matrix Z, there are T independent elements: $z(0)$, $z(1)$, , $z(T\text{-}1)$. They appear in the 1st row, and the elements in successive rows are the successive cyclic permutations of the first row.

Since the eigenvalues λ_j and eigenvectors x_j of Z satisfies:

$$Zx_j = \lambda_j x_j, j = 1, 2, \quad , T \tag{A.1}$$

We have:

$$\begin{cases} z(0)x_{1j} + z(1)x_{2j} + \cdots + z(T-2)x_{T-1,j} + z(T-1)x_{T,j} = \lambda_j x_{1j} \\ z(T-1)x_{1j} + z(0)x_{2j} + \cdots + z(T-3)x_{T-1,j} + z(T-2)x_{T,j} = \lambda_j x_{2j} \\ \vdots \\ z(1)x_{1j} + z(2)x_{2j} + \cdots + z(T-1)x_{T-1,j} + z(0)x_{T,j} = \lambda_j x_{Tj} \end{cases} \tag{A.2}$$

where x_{kj} is the k^{th} element of the j^{th} eigenvector. Let r_j be a root of the scalar equation $r^T=1$ and set $x_{kj} = r_j^k$, the above equation becomes:

$$\begin{cases} z(0)r_j + z(1)r_j^2 + \cdots + z(T-2)r_j^{T-1} + z(T-1)r_j^T = \lambda_j r_j \\ z(T-1)r_j + z(0)r_j^2 + \cdots + z(T-3)r_j^{T-1} + z(T-2)r_j^T = \lambda_j r_j^2 \\ \vdots \\ z(1)r_j + z(2)r_j^2 + \cdots + z(T-1)r_j^{T-1} + z(0)r_j^T = \lambda_j r_j^T \end{cases} \tag{A.3}$$

If multiply the 1st equation by r_j^{T-1}, the 2nd by r_j^{T-2}, and so forth, using $r_j^{T+k} = r_j^k$, we see that the equality will be obtained for each equation if:

$$\lambda_j = \sum_{h=0}^{T-1} z(h) r_j^h \tag{A.4}$$

The equation $r^T=1$ has T distinct roots: $\exp(i2\pi j/T), j = 1, 2, \quad , T$, which may also be expressed as: $r_j = \exp(-i2\pi j/T), j = 0, 1, \quad , T\text{-}1$. Therefore, the eigenvalues of Z are:

$$\sum_{j=0}^{T-1} z(j)\exp\{-i2\pi jk/T\}, k = 0, \quad , T\text{-}1,$$

The eigenvectors are:

$$x_j = 1/\sqrt{T}\left[1, e^{-i2\pi j/T}, e^{-i2\pi 2j/T}, \cdots, e^{-i2\pi(T-1)j/T}\right]', j = 0, 1, \quad , T\text{-}1$$

Note that the scale factor $1/\sqrt{T}$ is to have unit norm for the eigenvectors.

End of Proof

Next, we construct a T x T circular symmetric matrix by replacing $z(T\text{-}1)$ by $z(1)$, $z(T\text{-}2)$ by $z(2)$ in matrix Z.

$$Z_s = \begin{bmatrix} z(0) & z(1) & z(2) & \cdots & z(2) & z(1) \\ z(1) & z(0) & z(1) & \cdots & z(3) & z(2) \\ z(2) & z(1) & z(0) & \cdots & z(4) & z(3) \\ \vdots & \vdots & \vdots & & \vdots & \vdots \\ z(1) & z(2) & z(3) & \cdots & z(1) & z(0) \end{bmatrix} \tag{A.5}$$

Substituting into Equation(A.4), we obtain for the eigenvalues of Z_s:

$$\lambda_j = \begin{cases} \sum_{h=-(T-1)/2}^{(T-1)/2} z(h)e^{-i2\pi hj/T}, T \ \ odd \\ \sum_{h=-T/2+1}^{T/2} z(h)e^{-i2\pi hj/T}, T \ \ even \end{cases} \tag{A.6}$$

For the case of T being odd, Equation (A.6) may also be written as:

$$\lambda_j = \sum_{h=-(n-1)/2}^{(n-1)/2} z(h)\cos\frac{2\pi}{T}hj, j = 0, 1, \quad , T\text{-}1 \tag{A.7}$$

Since, for $0 \le m \le 2\pi$, $\cos m = \cos(2\pi\text{-}m)$, the eigenvalues associated with $j = 1, 2, \quad , (T\text{-}1)/2$ have multiplicity of two. For each of the repeated eigenvalues, we can find two real orthogonal eigenvectors. These are chosen to be:

$$\sqrt{2/T}\left[1, \cos 2\pi\frac{j}{T}, \cos 2\pi\frac{2j}{T}, \ldots, \cos 2\pi\frac{(T-1)j}{T}\right]'$$

and (A.8)

$$\sqrt{2/T}\left[0, \sin 2\pi\frac{j}{T}, \sin 2\pi\frac{2j}{T}, \ldots, \sin 2\pi\frac{(T-1)j}{T}\right]'$$

Much the same pattern holds for the roots of a circular symmetric matrix of dimension T x T where T is even. There is an eigenvector $1/\sqrt{T}[1,1,...,1]$ associated with $j = 0$ and a vector $1/\sqrt{T}[1,-1,1,...,-1]$ associated with $j = T/2$. The remaining $(T/2)$-2 roots have multiplicity two and the eigenvalues are given by Equation (A.6).

Now, consider the case of T being odd, define the orthogonal matrix Q by setting $T^{1/2}2^{-1/2}Q'$ equal to:

$$\begin{bmatrix} 2^{-1/2} & 2^{-1/2} & 2^{-1/2} & \cdots & 2^{-1/2} \\ 1 & \cos 2\pi\frac{1}{T} & \cos 2\pi\frac{2}{T} & \cdots & \cos 2\pi\frac{T-1}{T} \\ 0 & \sin 2\pi\frac{1}{T} & \sin 2\pi\frac{2}{T} & \cdots & \sin 2\pi\frac{T-1}{T} \\ 1 & \cos 4\pi\frac{1}{T} & \cos 4\pi\frac{2}{T} & \cdots & \cos 4\pi\frac{T-1}{T} \\ \vdots & \vdots & \vdots & & \vdots \\ 0 & \sin\frac{T-1}{T}2\pi\frac{1}{T} & \sin\frac{T-1}{T}2\pi\frac{2}{T} & \cdots & \sin\frac{T-1}{T}2\pi\frac{T-1}{T} \end{bmatrix} \tag{A.9}$$

Note that Q is the matrix composed of the T characteristic vectors defined by Equation (A.8). Define the T x T diagonal matrix D by

$$D = diag(d_1, d_2, ..., d_n) \tag{A.10}$$

where

$$\begin{aligned} d_1 &= \frac{1}{2\pi}\sum_{h=-\infty}^{\infty} z(h), \\ d_{2j} &= d_{2j+1} = \frac{1}{2\pi}\sum_{h=-\infty}^{\infty} z(h)e^{-i2\pi hj/T} \end{aligned} \tag{A.11}$$

It is evident that for Z_s defined in Equation (A.5), the matrix $Q'Z_sQ$ is a diagonal matrix whose elements converge to $2\pi D$ as T increases. This also holds for even T if the definition of Q is slightly modified. An additional row,

$$T^{-1/2}[1, -1, 1, ..., 1, -1]$$

which is the eigenvector associated with $j = T/2$, is added to the Q' of Equation (A.9) when T is even. The last entry in D for even T is

$$d_T = \frac{1}{2\pi}\sum_{h=-\infty}^{\infty} z(h)\cos\pi h$$

Now, we construct a symmetric Toeplitz matrix C using the elements $z(j)$, j = 0, 1, , T-1, which can represent the covariance matrix of a stationary time series:

$$C = \begin{bmatrix} z(0) & z(1) & \cdots & z(T-1) \\ z(1) & z(0) & \cdots & z(T-2) \\ \vdots & \vdots & & \vdots \\ z(T-1) & z(T-2) & \cdots & z(0) \end{bmatrix} \tag{A.12}$$

We next demonstrate that $Q'CQ'$ also converges to $2\pi D$. Let $q_i = [q_{1i}, q_{2i}, \ldots, q_{Ti}]'$ be the i^{th} column of Q. We have:

$$\begin{aligned} \left| q_i' Z_s q_j - q_i' C q_j \right| = \Bigg| & \sum_{m=1}^{M} [z(m) - z(T-m)] \\ & \times \sum_{k=1}^{m} [q_{ki} q_{T-m+k,j} + q_{T-m+k,i} q_{kj}] \Bigg| \end{aligned} \tag{A.13}$$

where $M = (T\text{-}1)/2$ if T is odd and $M = (T/2)\text{-}1$ if T is even. It is evident that Equation (A.13) is less than

$$\begin{aligned} & \frac{4}{T} \left\{ \sum_{m=1}^{M} m |z(m)| + \sum_{m=1}^{M} m |z(T-m)| \right\} \\ & \leq \frac{4}{T} \left\{ \sum_{m=1}^{M} m |z(m)| + \sum_{h=M+1}^{T} M |z(h)| \right\} \end{aligned} \tag{A.14}$$

since $q_{ki} q_{rj} \leq 2/T$ for all $k, i, r, j \in (1, 2, \ldots, T)$. As T increases, the limit of the first term is zero by Lemma A-1 (see below) and the limit of the second term is zero if $z(h)$ is absolutely summable. Therefore, the elements of $Q'CQ'$ converges to $2\pi D$.

In summary, the asymptotic property of a stationary time series with absolutely summable covariance function stated in the beginning of this section is proved.

Lemma A-1 (Kronecker's lemma): If the sequence $\{a_j\}$ is such that $\lim_{n\to\infty}\sum_{j=0}^{n}|a_j| = A < \infty$, then $\lim_{n\to\infty}\sum_{j=0}^{n}\frac{j}{n}|a_j| = 0$.

Proof:[8] By assumption, give $\varepsilon > 0$, there exists an N such that

$$\sum_{j=N+1}^{\infty}|a_j| < \varepsilon$$

Therefore, for $n > N$, we have

$$\sum_{j=0}^{n}\frac{j}{n}|a_j| < \frac{1}{n}\sum_{j=0}^{N} j|a_j| + \varepsilon$$

Clearly, for fixed N,

$$\lim_{n\to\infty}\frac{1}{n}\sum_{j=0}^{N} j|a_j| = 0$$

and since ε was arbitrary, the result follows.

End of Proof

Finally, note that for any Toeplitz matrix (not necessary symmetric), its eigenvectors are asymptotically:

$$1/\sqrt{T}[\exp\{-i2\pi jk/T\}; j = 0,...,T-1], k = 0,...,T-1 \qquad \text{(A.15)}$$

and the corresponding eigenvalues are asymptotically:

$$\sum_{u=-T+1}^{T-1} c(u)\exp(i2\pi uk/T), k = 0,...,T-1 \qquad \text{(A.16)}$$

The proof for this property is presented in [85].

[8] This proof is adapted from [104]

Appendix B

Identification of the ILV⇒HR Impulse Response from Spontaneous Breathing Data

In the SD method for autonomic function quantification (Section 3.3.2), the peak amplitude of the ILV⇒HR impulse response is utilized to derive a parasympathetic index. If data collection is carried out during spontaneous breathing, the ILV signal normally does not contain adequate frequency components to encompass the entire spectrum of the ILV⇒HR frequency response (see Figure 3-10 and Figure 3-7). This presents a problem for system identification since it is generally required that the input signal be persistently exciting so as to all the modes in the system are identifiable. A closer study at the features of the ILV⇒HR impulse response is necessary to solve this problem.

Based on the identification results on random breathing data (e.g. Figure 3-8), a normal ILV⇒HR impulse response contains two prominent components. One is the initial upright wave whose shape resembles a symmetric triangle. The second one is the delayed slower wave which is low-frequency dominant. Hence, the relatively high frequency power in the ILV⇒HR spectrum is mainly contributed by the first component. Since spontaneous breathing ILV signal has significant energy in this frequency range, heuristically, the first component, especially the peak amplitude of the impulse response based on which the parasympathetic index is derived, is more identifiable than the second one. However, given that there are still inherent low frequency factors in the first component, it needs to be evaluated how much the lack of low frequencies in the input signal would affect the estimation accuracy of the peak amplitude, the parameter we are mainly interested in.

We constructed an impulse response analogous to the previously identified ILV⇒HR impulse response and the input signal was band-limited that mimics the frequency ranges of spontaneous breathing ILV data (Figure B - 1). Low and high frequency noise disturbances were simulated respectively. Figure B - 2 shows the estimation error of the peak amplitude of the impulse response using the WPCR-MA, WPCR-ARX and the conventional ARX method. 30 input delays were included in the WPCR-MA structure and 15 AR and 15 MA terms were included in both the ARX and the WPCR-ARX maximum models. The weighting schemes as discussed in Chapter 2 were employed for the WPCR methods.

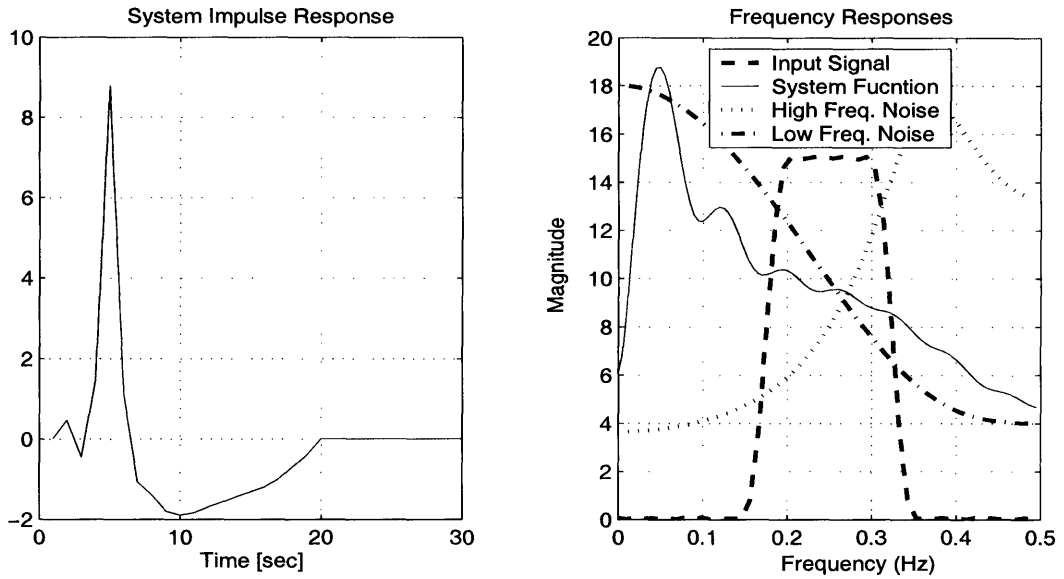

(a) (b)

Figure B - 1 (a) the simulated impulse response of the system; (b) the frequency responses of the system, the band-limited input signal and the noise terms

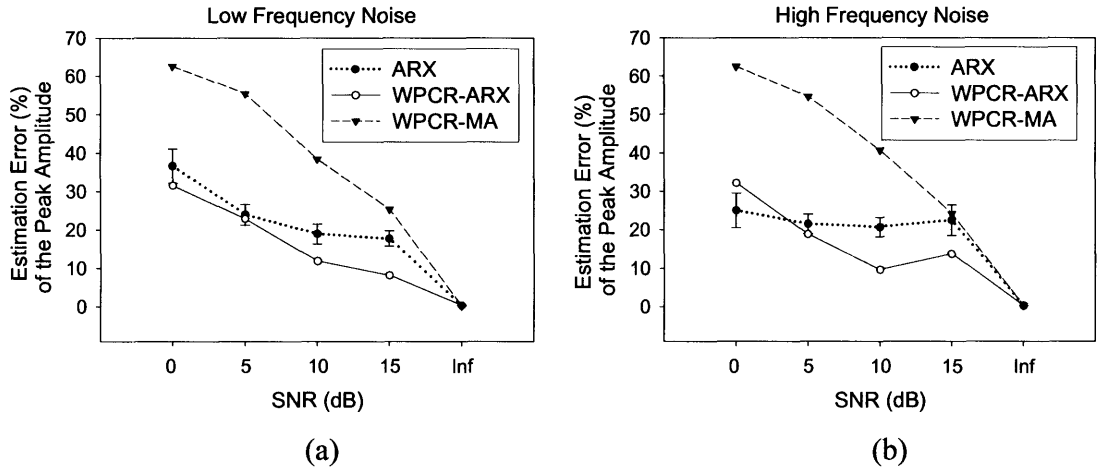

Figure B - 2 Estimation error of the peak amplitude of the ILV⇒HR impulse response (a) low frequency noise; (b) high frequency noise (values are mean ± 1.96*SE, 100 noise realizations)

The simulation results showed that the WPCR-ARX method outperforms the conventional ARX method for both types of noise disturbances, which is expected since the frequency selective property of the WPCR method renders it advantage when coping with colored signals, as discussed in detail in Chapter 2. However, the WPCR-MA method performs poorly in this application. It may be explained by the fact that inclusion of the AR terms (in the ARX structures) enables a better estimation of the noise disturbance. In case of inpersistently exciting input, there exist noise components that are out-of-band with the input but in-band with the system function. Such noise disturbances may corrupt the estimation results significantly. Therefore, an ARX structure which provides room for an explicit noise model is more desirable. Interestingly, when the simulated noise level is zero (SNR = ∞), all methods reached a nearly zero estimation error which implies that the band-limited input contains adequate information for the identification of the peak amplitude.

Based on the above simulations, we propose to employ the WPCR-ARX method in the ILV⇒HR system identification in this thesis.

Appendix C

Autonomic Indices of Subjects in the Bed Rest Study Computed by the APR Method

In using the Area method to compute autonomic indices based on heart rate (HR), arterial blood pressure (ABP) and instantaneous lung volume (ILV) collected during random breathing, the ILV→HR impulse response needs to be identified first. A method previously used in our lab for this purpose is the ARX Parameter Reduction (APR) method [55]. This algorithm estimates the signal-to-noise ratio (SNR) of each moving average (MA) or autoregressive (AR) parameter in the maximum ARX model. Candidate models are then constructed according to the SNR value associated with each MA or AR term. Model parameters with higher SNR values are considered first based on the hypothesis that such parameters have a larger likelihood of being "true". A model selection criterion (e.g. MDL) is then utilized to choose the best performing "minimal" model from the set of candidate models.

We employed the Area-APR method to analyze the bed rest data in order to compare with the proposed Area-WPCR method. The identification results are shown in Table C - 1, Table C - 2, Table C - 3 and Table C - 4. A detailed discussion on these results is provided in Chapter 4 (Section 4.4).

Table C - 1 Group average comparisons of parasympathetic responsiveness results of the Area-APR method: supine (Su) vs. tilt; pre-bed rest (Pre) vs. end-bed rest (End) or post-bed rest (Post); End vs. Post; (29 subjects for Pre vs. End in supine posture, Supine vs. Tilt at pre-bed rest, Pre vs. Post and End vs. Post in supine posture; 22 subjects for Pre vs. End at Tilt postures and Supine vs. Tilt at end-bed rest – subjects treated with midodrine are excluded; Values are means ± SE.).

		Parasympathetic Area (mean ± SE)	*P* value Su. vs. Tilt	*P* value Pre vs. End/Post	*P* value End vs. Post
Pre-bed rest	Su.	0.020±0.002			
	30°	0.013±0.002	0.036		
	60°	0.011±0.002	0.003		
	90°	0.012±0.002	0.026		
End-bed rest	Su.	0.014±0.001		0.015	
	30°	0.008±0.001	0.001	0.003	
	60°	0.008±0.002	0.012	0.30	
	90°	0.006±0.001	0.031	0.03	
Post-bed rest	Su.	0.016±0.002		0.25	0.72
	30°	0.014±0.002	0.14	0.43	0.14
	60°	0.012±0.002	0.008	0.88	0.80
	90°	0.007±0.001	0.0005	0.002	0.50

Table C - 2 Group average comparisons of sympathetic responsiveness results of the Area-APR method: supine (Su) vs. tilt; pre-bed rest (Pre) vs. end-bed rest (End) or post-bed rest (Post); End vs. Post; (see the caption of Table 4-3 for the number of subjects in each category).

		Sympathetic Area (mean ± SE)	*P* value Su. vs. Tilt	*P* value Pre vs. End/Post	*P* value End vs. Post
Pre-bed rest	Su.	0.027±0.007			
	30°	0.030±0.010	0.79		
	60°	0.010±0.012	0.48		
	90°	0.028±0.012	0.54		
End-bed rest	Su.	-0.002±0.005		0.019	
	30°	0.001±0.009	0.15	0.032	
	60°	0.020±0.009	0.016	0.46	
	90°	0.031±0.007	0.025	0.43	
Post-bed rest	Su.	0.006±0.007		0.054	0.19
	30°	0.012±0.008	0.33	0.27	0.41
	60°	0.037±0.011	0.011	0.51	0.19
	90°	0.025±0.010	0.11	0.31	0.56

Table C - 3 Group average comparisons of parasympathetic responsiveness results of the Area-APR method: Subjects who tolerated (T) the orthostatic tolerance testing vs. those who failed (F); same day: the orthostatic tolerance testing and data collection for system identification were performed on the same day; End: the orthostatic tolerance testing was performed at end-bed rest. (Su: supine; Values are means ± SE; see Table 4-11 for the number of subjects in each category)

		Parasympathetic Area (mean ± SE)			Parasympathetic Area (mean ± SE)		
		T-same day	F-same day	P value	T-End	F-End	P value
Pre-bed rest	Su.	0.017±0.003	0.026±0.004	0.07	0.010±0.002	0.024±0.003	0.004
	30°	0.013±0.001	0.013±0.003	0.89	0.013±0.002	0.012±0.002	0.77
	60°	0.010±0.002	0.010±0.003	0.99	0.006±0.002	0.014±0.003	0.054
	90°	0.010±0.001	0.017±0.005	0.092	0.009±0.002	0.015±0.004	0.26
End-bed rest	Su.	0.014±0.002	0.014±0.002	0.99			
	30°	0.007±0.001	0.009±0.002	0.58			
	60°	0.007±0.001	0.008±0.004	0.70			
	90°	0.006±0.002	0.006±0.003	0.78			
Post-bed rest	Su.	0.014±0.002	0.018±0.003	0.30			
	30°	0.011±0.002	0.018±0.004	0.14			
	60°	0.010±0.003	0.014±0.004	0.34			
	90°	0.007±0.001	0.007±0.002	0.89			

Table C - 4 Group average comparisons of sympathetic responsiveness results of the Area-APR method: Subjects who tolerated (T) the orthostatic tolerance testing vs. those who failed (F); (see the caption of Table 4-5 for more details)

		Sympathetic Area (mean ± SE)			Sympathetic Area (mean ± SE)		
		T-same day	F-same day	P value	T-End	F-End	P value
Pre-bed rest	Su.	0.030±0.010	0.021±0.010	0.58	0.027±0.015	0.025±0.008	0.93
	30°	0.026±0.010	0.031±0.020	0.81	0.034±0.013	0.026±0.015	0.74
	60°	0.007±0.013	0.023±0.011	0.39	0.032±0.015	-0.005±0.02	0.12
	90°	0.034±0.011	-0.018±0.010	0.029	0.058±0.020	0.001±0.008	0.013
End-bed rest	Su.	0.013±0.008	-0.011±0.010	0.10			
	30°	0.021±0.014	-0.010±0.10	0.09			
	60°	0.029±0.011	0.014±0.013	0.42			
	90°	0.027±0.012	0.035±0.006	0.59			
Post-bed rest	Su.	0.008±0.007	-0.005±0.02	0.48			
	30°	0.014±0.008	0.001±0.024	0.53			
	60°	0.047±0.012	-0.007±0.023	0.063			
	90°	0.034±0.011	-0.018±0.010	0.043			

Bibliography

[1] T. Soderstrom and P. Stoica, *System Identification*. Englewood Cliffs, NJ: Prentice Hall, 1988.

[2] L. Ljung, *System identification, theory for the user*: Prentice Hall, Inc, 1999.

[3] K. AbedMeraim, W. Z. Qui, and Y. B. Hua, "Blind system identification," *Proc. IEEE*, vol. 85, pp. 1310-1322, 1997.

[4] Y. Zhong, H. Wang, K. Ju, K. M. Jan, and K. H. Chon, "Nonlinear analysis of the separate contributions of autonomic nervous systems to heart rate variability using principal dynamic modes," *IEEE Trans Biomed Eng*, pp. In press, 2004.

[5] R. Haber, *Nonlinear system identification : input-output modeling approach*. Dordrecht ; Boston: Kluwer Academic Publishers, 1999.

[6] K. H. Chon and R. J. Cohen, "Linear and nonlinear ARMA model parameter estimation using an artificial neural network," *IEEE Trans Biomed Eng*, vol. 44, pp. 168-74, 1997.

[7] K. H. Chon, T. J. Mullen, and R. J. Cohen, "A dual-input nonlinear system analysis of autonomic modulation of heart rate," *IEEE Trans Biomed Eng*, vol. 43, pp. 530-44, 1996.

[8] J. Allen and A. Murray, "Modelling the relationship between peripheral blood pressure and blood volume pulses using linear and neural network system identification techniques," *Physiol Meas*, vol. 20, pp. 287-301, 1999.

[9] K. H. Chon, Y. M. Chen, N. H. Holstein-Rathlou, D. J. Marsh, and V. Z. Marmarelis, "On the efficacy of linear system analysis of renal autoregulation in rats," *IEEE Trans Biomed Eng*, vol. 40, pp. 8-20, 1993.

[10] R. D. Berger, J. P. Saul, and R. J. Cohen, "Transfer function analysis of autonomic regulation. I. Canine atrial rate response," *Am J Physiol*, vol. 256, pp. H142-52, 1989.

[11] Y. Zhu, *Multivariable system identification for process control*. Oxford, UK: Elsevier Science Ltd, 2001.

[12] J. B. Moore, M. Niedzwiechi, and L. Xia, "Identification/prediction algorithms for armax models with relaxed positive real conditions," *International Journal of Adaptive Control and Signal Processing*, vol. 4, pp. 49-67, 1990.

[13] J. Durbin, "Efficient estimators of parameters in moving average models," *Biometrica*, vol. 46, pp. 306-316, 1959.

[14] K. J. Astrom and P. Eykhoff, "System identification - a survey," *Automatica*, vol. 7, pp. 123-167, 1971.

[15] D. W. Clarke, "Generalized-least-squares estimation of the parameters of a dynamic model," presented at 1st IFAC Symp. Identification Automat. Contr. Syst., 1967.

[16] L. Ljung and B. Wahlberg, "Asymptotic Properties of the Least-Squares Method for Estimating Transfer-Functions and Disturbance Spectra," *Advances in Applied Probability*, vol. 24, pp. 412-440, 1992.

[17] B. Wahlberg, "System-Identification Using Laguerre Models," *Ieee Transactions on Automatic Control*, vol. 36, pp. 551-562, 1991.

[18] B. Wahlberg, "System-Identification Using Kautz Models," *Ieee Transactions on Automatic Control*, vol. 39, pp. 1276-1282, 1994.

[19] P. S. C. Heuberger, P. M. J. Vandenhof, and O. H. Bosgra, "A Generalized Orthonormal Basis for Linear Dynamical-Systems," *Ieee Transactions on Automatic Control*, vol. 40, pp. 451-465, 1995.

[20] P. Van Overschee and B. De Moor, *Subspace identification for linear systems : theory, implementation, applications*. Norwell, MA: Kluwer Academic, 1996.

[21] E. W. Jensen, P. Lindholm, and S. W. Henneberg, "Autoregressive modeling with exogenous input of middle-latency auditory-evoked potentials to measure rapid changes in depth of anesthesia," *Methods Inf Med*, vol. 35, pp. 256-60, 1996.

[22] D. Liberati, L. Bedarida, P. Brandazza, and S. Cerutti, "A model for the cortico-cortical neural interaction in multisensory-evoked potentials," *IEEE Trans Biomed Eng*, vol. 38, pp. 879-90, 1991.

[23] T. J. Mullen, M. L. Appel, R. Mukkamala, J. M. Mathias, and R. J. Cohen, "System identification of closed-loop cardiovascular control: effects of posture and autonomic blockade," *Am J Physiol*, vol. 272, pp. H448-61, 1997.

[24] P. Bodin, L. F. Villemoes, and B. Wahlberg, "Selection of best orthonormal rational basis," *Siam Journal on Control and Optimization*, vol. 38, pp. 995-1032, 2000.

[25] J. Shao, "Linear-Model Selection by Cross-Validation," *Journal of the American Statistical Association*, vol. 88, pp. 486-494, 1993.

[26] F. Gustafsson and H. Hjalmarsson, "Twenty-one ML estimators for model selection," *Automatica*, vol. 31, pp. 1377-1392, 1995.

[27] H. Akaike, "Fitting autoregressive models for prediction," *Ann Inst Statist Math*, vol. 21, pp. 243-247, 1969.

[28] C. L. Mallows, "Some comments on cp," *Technometrics*, vol. 15, pp. 661-675, 1973.

[29] P. Craven and G. Wahba, "Smoothing Noisy Data with Spline Functions - Estimating the Correct Degree of Smoothing by the Method of Generalized Cross-Validation," *Numerische Mathematik*, vol. 31, pp. 377-403, 1979.

[30] R. Shibata, "An Optimal Selection of Regression Variables," *Biometrika*, vol. 68, pp. 45-54, 1981.

[31] V. Cherkassky, X. H. Shao, F. M. Mulier, and V. N. Vapnik, "Model complexity control for regression using VC generalization bounds," *Ieee Transactions on Neural Networks*, vol. 10, pp. 1075-1089, 1999.

[32] X. Xiao, Y. Li, and R. Mukkamala, "A Model Order Selection Criterion with

Applications to Physiologic Systems," *To apprear in IEEE T Biomed Eng*, 2004.

[33] O. Chapelle, V. Vapnik, and Y. Bengio, "Model selection for small sample regression," *Machine Learning*, vol. 48, pp. 9-23, 2002.

[34] H. Akaike, "Information theory and an extension of the maximum likelihood principle," presented at Proc. 2nd Int. Symp. on Information Theory, Tsahkadsor, USSR, 1971.

[35] H. Akaike, "On entropy maximization principle," in *Proc. Symp. on Applications of Statistics*, P. R. Krishnaiah, Ed. Amsterdam, Neitherlands: North-Holland, 1977, pp. 27-41.

[36] G. Schwarz, "Estimating the dimension of a model," *The Annals of Statistica*, vol. 6, pp. 461-464, 1978.

[37] E. J. Hannan and B. G. Quinn, "Determination of the Order of an Autoregression," *Journal of the Royal Statistical Society Series B-Methodological*, vol. 41, pp. 190-195, 1979.

[38] C. M. Hurvich and C. L. Tsai, "Regression and time series model selection in small samples," *Biometrika*, vol. 76, pp. 297-307, 1989.

[39] A. McQuarrie, R. Shumway, and C. L. Tsai, "The model selection criterion AICu," *Statistics & Probability Letters*, vol. 34, pp. 285-292, 1997.

[40] J. Rissanen, "Modelling by shortest data description," *Automatica*, vol. 14, pp. 465-471, 1978.

[41] S. Beheshti and M. A. Dahleh, "A new minimum description length," presented at IEEE Conf. on American Control Conference, 2003.

[42] M. Qi and G. P. Zhang, "An investigation of model selection criteria for neural network time series forecasting," *European Journal of Operational Research*, vol. 132, pp. 666-680, 2001.

[43] C. W. J. Granger, "Strategies for Modeling Nonlinear Time-Series Relationships," *Economic Record*, vol. 69, pp. 233-238, 1993.

[44] J. Yen and L. Wang, "Application of statistical information criteria for optimal fuzzy model construction," *Ieee Transactions on Fuzzy Systems*, vol. 6, pp. 362-372, 1998.

[45] A. C. Guyton and J. E. Hall, *Textbook of medical physiology*: WB Saunders, 1994.

[46] A. Selman, A. McDonald, R. Kitney, and D. Linkens, "The interaction between heart rate and respiration: part I - experimental studies in man," *Automedica*, vol. 4, pp. 131-139, 1982.

[47] J. P. Saul, R. D. Berger, M. H. Chen, and R. J. Cohen, "Transfer function analysis of autonomic regulation. II. Respiratory sinus arrhythmia," *Am J Physiol*, vol. 256, pp. H153-61, 1989.

[48] R. D. Berger, J. P. Saul, and R. J. Cohen, "Assessment of autonomic response by broad-band respiration," *IEEE Trans Biomed Eng*, vol. 36, pp. 1061-5, 1989.

[49] R. D. Berger, M. Fogaca, J. P. Saul, and R. J. Cohen, "Transfer function analysis of cardiovascular regulation in an open-loop animal model," *Computers in Cardiology*, pp. 331-335, 1989.

[50] G. Stanley, D. Verotta, N. Craft, R. A. Siegel, and J. B. Schwartz, "Age and autonomic effects on interrelationships between lung volume and heart rate," *Am J Physiol*, vol. 270, pp. H1833-40, 1996.

[51] C. Julien, B. Chapuis, Y. Cheng, and C. Barráes, "Dynamic interactions between arterial pressure and sympathetic nerve activity: role of arterial baroreceptors," *Am J Physiol Regul Integr Comp Physiol*, vol. 285, pp. R834-41, 2003.

[52] T. Kawada, T. Miyamoto, K. Uemura, K. Kashihara, A. Kamiya, M. Sugimachi, and K. Sunagawa, "Effects of neuronal norepinephrine uptake blockade on baroreflex neural and peripheral arc transfer characteristics," *Am J Physiol Regul Integr Comp Physiol*, vol. Epub ahead of print, Feb 12, 2004.

[53] J. P. Saul, R. D. Berger, and R. J. Cohen, "A simple analytical model mimics complex physiological behavior," *Computers in Cardiology*, pp. 335-338, 1990.

[54] M. L. Appel, J. P. Saul, R. D. Berger, and R. J. Cohen, "Closed-loop identification of blood pressure variability mechanisms," in *Blood Pressure and Heart Rate Variability*, M. D. R. e. al., Ed.: IOS Press, 1992, pp. 68-74.

[55] M. H. Perrott and R. J. Cohen, "An efficient approach to ARMA modeling of biological systems with multiple inputs and delays," *IEEE Trans Biomed Eng*, vol. 43, pp. 1-14, 1996.

[56] R. Mukkamala, J. M. Mathias, T. J. Mullen, R. J. Cohen, and R. Freeman, "System identification of closed-loop cardiovascular control mechanisms: diabetic autonomic neuropathy," *Am J Physiol*, vol. 276, pp. R905-12, 1999.

[57] R. Mukkamala, "A forward model-based analysis of cardiovascular system identification methods," in *Electrical Engineering and Computer Science*. Cambridge, MA: Massachusetts Institute of Technology, 2000, pp. 112-113.

[58] V. Di Virgilio, R. Barbieri, L. Mainardi, S. Strano, and S. Cerutti, "A multivariate time-variant AR method for the analysis of heart rate and arterial blood pressure," *Med Eng Phys*, vol. 19, pp. 109-24, 1997.

[59] K. Yamada, H. Asanoi, J. Takagawa, S. Joho, T. Kameyama, T. Hirai, T. Nozawa, and H. Inoue, "Parametric system identification of arterial baroreflex with random perturbation of blood pressure in normal subjects," *J Cardiovasc Pharmacol*, vol. 42, pp. S11-3, 2003.

[60] R. Kosaka, Y. Sankai, T. Jikuya, T. Yamane, and T. Tsutsui, "Online parameter identification of second-order systemic circulation model using the delta operator," *Artif Organs*, vol. 26, pp. 967-70, 2002.

[61] R. Mukkamala, K. Toska, and R. J. Cohen, "Noninvasive identification of the total peripheral resistance baroreflex," *Am J Physiol Heart Circ Physiol*, vol. 284, pp. H947-59, 2003.

[62] X. Xiao, R. Mukkamala, N. Sheynberg, G. H. Williams, and R. J. Cohen, "Effects of Prolonged Bed Rest on the Total Peripheral Resistance Baroreflex," *Computers in Cardiology*, vol. 29, pp. 53-56, 2002.

[63] A. K. Ahmed, S. Y. Fakhouri, J. B. Harness, and A. J. Mearns, "Modelling of the control of heart rate by breathing using a kernel method," *J Theor Biol*, vol. 119, pp. 67-79, 1986.

[64] J. P. Saul, D. Kaplan, and R. Kitney, "Nonlinear interactions between respiration and heart rate: clinical physiology or entrained nonlinear oscillators," *Computers in Cardiology*, pp. 299-302, 1988.

[65] K. Pearson, "On lines and planes of closest fit to systems of points in space.," *Phil. Mag.*, vol. 6, pp. 559-572, 1901.

[66] H. Hotelling, "Analysis of a complex of statistical variables into principal components," *J. Educ. Psychol.*, vol. 24, pp. 417-441, 498-520, 1933.

[67] I. T. Jolliffe, *Principal component analysis*. New York: Springer-Verlag, 1986.

[68] J. Mandel, "Use of the singular value decomposition in regression analysis," *AM STAT*, vol. 36, pp. 15-24, 1982.

[69] B. Pilgram and W. Schappacher, "Estimation of the dominant singular values for svd based noise reduction methods," *International Journal of Bifurcation and Chaos*, vol. 8, pp. 571-580, 1998.

[70] K. Shin, J. K. Hammond, and P. R. White, "Iterative svd method for noise reduction of low-dimensional, chaotic time series," *Mechanical Systems and Signal Processing*, vol. 13, pp. 115-124, 1999.

[71] K. Konstantinides, B. Natarajan, and G. S. Yovanof, "Noise estimation and filtering using block-based singular value decomposition," *Ieee Transactions on Image Processing*, vol. 6, pp. 479-483, 1997.

[72] J. J. Wei, C. J. Chang, N. K. Chou, and G. J. Jan, "ECG data compression using truncated singular value decomposition," *Ieee Transactions on Information Technology in Biomedicine*, vol. 5, pp. 290-299, 2001.

[73] R. Swiniarski and A. Swiniarska, "Comparison of feature extraction and selection methods in mammogram recognition," in *Techniques in Bioinformatics and Medical Informatics*, vol. 980, *Annals of the New York Academy of Sciences*. New York: NEW YORK ACAD SCIENCES, 2002, pp. 116-124.

[74] P. P. Kanjilal and S. Palit, "The Singular-Value Decomposition - Applied in the Modeling and Prediction of Quasi-Periodic Processes," *Signal Processing*, vol. 35, pp. 257-267, 1994.

[75] D. W. Tufts and R. Kumaresan, "Singular Value Decomposition and Improved Frequency Estimation Using Linear Prediction," *Ieee Transactions on Acoustics Speech and Signal Processing*, vol. 30, pp. 671-675, 1982.

[76] M. Uike, T. Uchiyama, and H. Minamitani, "Comparison of Linear Prediction Methods Based on Singular Value Decomposition," *Journal of Magnetic Resonance*, vol. 99, pp. 363-371, 1992.

[77] R. D. Prony, "Essai Experimentale et analytique," *J. Ecole Polytechnique (Paris)*, pp. 24-76, 1795.

[78] F. B. Hildebrand, *Introduction to Numerical Analysis*. New York: McGraw-Hill, 1956.

[79] R. Kumaresan, D. W. Tufts, and L. L. Scharf, "A Prony Method for Noisy Data - Choosing the Signal Components and Selecting the Order in Exponential Signal Models," *Proceedings of the Ieee*, vol. 72, pp. 230-232, 1984.

[80] J. A. Cadzow, B. Baseghi, and T. Hsu, "Singular-Value Decomposition Approach to Time-Series Modeling," *Iee Proceedings-F Radar and Signal Processing*, vol. 130, pp. 202-210, 1983.

[81] J. A. Cadzow, "Spectral estimation: an overdetermined rational model equation approach," *Proc. IEEE*, vol. 70, pp. 907-939, 1982.

[82] D. W. Tufts and R. Kumaresan, "Estimation of Frequencies of Multiple Sinusoids - Making Linear Prediction Perform Like Maximum-Likelihood," *Proceedings of the Ieee*, vol. 70, pp. 975-989, 1982.

[83] A. Cantoni and L. C. Godara, "Resolving the Directions of Sources in a Correlated Field Incident on an Array," *Journal of the Acoustical Society of America*, vol. 67, pp. 1247-1255, 1980.

[84] S. S. Reddi, "Multiple Source Location a Digital Approach," *Ieee Transactions on Aerospace and Electronic Systems*, vol. 15, pp. 95-105, 1979.

[85] D. Brillinger, *Time series, data analysis and theory*: Holden-Day, Inc, 1981.

[86] M. B. Priestley, T. Subba Rao, and H. Tong, "Applications of principal component analysis and factor analysis in the identification of multivariable systems," *IEEE Transactions on Automatic Control*, vol. AC-19, pp. 730-734, 1974.

[87] R. RicoMartinez, J. S. Anderson, and I. G. Kevrekidis, "Self-consistency in neural network-based NLPC analysis with applications to time-series processing," *Computers & Chemical Engineering*, vol. 20, pp. S1089-S1094, 1996.

[88] G. Castellano and A. M. Fanelli, "Variable selection using neural-network models," *Neurocomputing*, vol. 31, pp. 1-13, 2000.

[89] P. V. Overschee and B. De Moor, *Subspace identification for linear systems : theory, implementation, applications*. Norwell, MA: Kluwer Academic, 1996.

[90] D. Z. Feng, Z. Bao, and L. C. Jiao, "Total least mean squares algorithm," *IEEE T. Signal Proces.*, vol. 46, pp. 2122-2130, 1998.

[91] B. Ho and R. Kalman, "Efficient construction of linear state variable models from input/output functions," *Regelungstechnik*, vol. 14, pp. 545-548, 1966.

[92] S. Kung, "A new identification and model reduction algorithm via singular value decompositions," presented at Conference Record of the Twelfth Asilomar Conference on Circuits, Systems and Computers, 6-8 Nov. 1978, Pacific Grove, CA, USA, 1978.

[93] M. Viberg, "Subspace-based methods for the identification of linear time-invariant systems," *Automatica*, vol. 31, pp. 1835-1851, 1995.

[94] J.-N. Juang and R. S. Pappa, "An eigensystem realization algorithm for modal parameter identification and model reduction," *Journal of Guidance, Control, and Dynamics*, vol. 8, pp. 620-7, 1985.

[95] K. Glover, "All optimal Hankel-norm approximations of linear multivariable systems and their L/sup infinity /-error bounds," *International Journal of Control*, vol. 39, pp. 1115-93, 1984.

[96] A. M. King, U. B. Desai, and R. E. Skelton, "A generalized approach to q-Markov covariance equivalent realizations for discrete systems," *Automatica*, vol. 24, pp. 507-15, 1988.

[97] M. Verhaegen, "Identification of the determinstic part of MIMO state spae models, given in innovations form from input-output data," *Automatica*, vol. 30, pp. 61-74, 1994.

[98] P. Van Overschee and B. De Moor, "N4SID: subspace algorithms for the identification of combined deterministic-stochastic systems," *Automatica*, vol. 30, pp. 75-93, 1994.

[99] W. E. Larimore, "Canonical variate analysis in identification, filtering, and adaptive control," presented at Proceedings of the 29th IEEE Conference on Decision and Control (Cat. No.90CH2917-3), 5-7 Dec. 1990, Honolulu, HI, USA, 1990.

[100] G. H. Golub and C. F. Van Loan, "An analysis of the total least squares problem," *SIAM J. Numer Anal*, vol. 17, pp. 883-893, 1980.

[101] F. Deprettere, "SVD and signal processing, algorithms, applications and architecture." Amsterdam: The Netherlands: North Holland, 1988.

[102] J. A. Cadzow and O. M. Solomon, "Algebraic approach to system identification," *IEEE T Acoustics, Speech, and Signal Processing*, vol. ASSP-34, pp. 462-469, 1986.

[103] J. Durbin, "Present positiona dn potential developments: some personal views, time series analysis," *J R statist Soc A*, vol. 147, pp. 161-173, 1984.

[104] W. A. Fuller, *Introduction to Statistical Time Series*. New York: J. Wiley, 1996.

[105] P. E. Wellstead and J. M. Edmunds, "Least-squares identification of closed-loop systems," *Int. J. Contr.*, vol. 21, pp. 689-699, 1975.

[106] X. Xiao, R. Mukkamala, N. Sheynberg, S. M. Grenon, M. D. Ehrman, T. J. Mullen, C. D. Ramsdell, G. H. Williams, and R. J. Cohen, "Effects of Simulated Microgravity on Closed-loop Cardiovascular Regulation and Orthostatic Intolerance: Analysis by Means of System Identification," *J Appl Physiol*, vol. 96, pp. 489-497, 2003.

[107] D. P. Zipes, M. N. Levy, L. A. Cobb, S. Julius, P. G. Kaufman, N. E. Miller, and R. L. Verrier, "Task Force-2 - Sudden Cardiac Death - Neural-Cardiac Interactions," *Circulation*, vol. 76, pp. 202-207, 1987.

[108] R. L. Verrier and B. D. Nearing, "Method and apparatus for prediction of sudden cardiac death by simultaneous assessment of autonomic function and cardiac electrical stability." USA: Georgetown University (Washington, DC), 1993.

[109] K. E. J. Airaksinen, "Autonomic mechanisms and sudden death after abrupt coronary occlusion," *Annals of Medicine*, vol. 31, pp. 240-245, 1999.

[110] J. C. Buckey, Jr., L. D. Lane, B. D. Levine, D. E. Watenpaugh, S. J. Wright, W. E. Moore, F. A. Gaffney, and C. G. Blomqvist, "Orthostatic intolerance after spaceflight," *J Appl Physiol*, vol. 81, pp. 7-18, 1996.

[111] W. H. Cooke, J. I. Ames, A. A. Crossman, J. F. Cox, T. A. Kuusela, K. U. Tahvanainen, L. B. Moon, J. Drescher, F. J. Baisch, T. Mano, B. D. Levine, C. G. Blomqvist, and D. L. Eckberg, "Nine months in space: effects on human autonomic cardiovascular regulation," *J Appl Physiol*, vol. 89, pp. 1039-45, 2000.

[112] D. J. Ewing, J. M. M. Neilson, C. M. Shapiro, J. A. Stewart, and W. Reid, "24 Hour Heart-Rate-Variability - Effects of Posture, Sleep, and Time of Day in Healthy Controls and Comparison with Bedside Tests of Autonomic Function in Diabetic-Patients," *British Heart Journal*, vol. 65, pp. 239-244, 1991.

[113] D. J. Ewing, C. N. Martyn, R. J. Young, and B. F. Clarke, "The value of cardiovascular autonomic function tests: 10 years experience in diabetes," *Diabetes Care*, vol. 8, pp. 491-8, 1985.

[114] D. Ziegler, "Diabetic cardiovascular autonomic neuropathy: prognosis, diagnosis and treatment," *Diabetes Metab Rev*, vol. 10, pp. 339-83, 1994.

[115] G. Vita, R. Dattola, R. Calabráo, L. Manna, C. Venuto, A. Toscano, V. Savica, and G. Bellinghieri, "Comparative analysis of autonomic and somatic dysfunction in chronic uraemia," *Eur Neurol*, vol. 28, pp. 335-40, 1988.

[116] A. Rèockel, H. Hennemann, A. Sternagel-Haase, and A. Heidland, "Uraemic sympathetic neuropathy after haemodialysis and transplantation," *Eur J Clin Invest*, vol. 9, pp. 23-7, 1979.

[117] D. R. Grimm, "Neurally mediated syncope: a review of cardiac and arterial receptors," *J Clin Neurophysiol*, vol. 14, pp. 170-82, 1997.

[118] H. Kaufmann, "Neurally mediated syncope and syncope due to autonomic failure: differences and similarities," *J Clin Neurophysiol*, vol. 14, pp. 183-96, 1997.

[119] P. A. Kelly, J. Nolan, J. I. Wilson, and E. J. Perrins, "Preservation of autonomic function following successful reperfusion with streptokinase within 12 hours of the onset of acute myocardial infarction," *Am J Cardiol*, vol. 79, pp. 203-5, 1997.

[120] A. D. Flapan, R. A. Wright, J. Nolan, J. M. Neilson, and D. J. Ewing, "Differing patterns of cardiac parasympathetic activity and their evolution in selected patients with a first myocardial infarction," *J Am Coll Cardiol*, vol. 21, pp. 926-31, 1993.

[121] J. Nolan, A. D. Flapan, S. Capewell, T. M. MacDonald, J. M. Neilson, and D. J. Ewing, "Decreased cardiac parasympathetic activity in chronic heart failure and its relation to left ventricular function," *Br Heart J*, vol. 67, pp. 482-5, 1992.

[122] J. Nolan, P. D. Batin, R. Andrews, S. J. Lindsay, P. Brooksby, M. Mullen, W. Baig, A. D. Flapan, A. Cowley, R. J. Prescott, J. M. Neilson, and K. A. Fox, "Prospective study of heart rate variability and mortality in chronic heart failure: results of the United Kingdom heart failure evaluation and assessment of risk trial (UK-heart)," *Circulation*, vol. 98, pp. 1510-6, 1998.

[123] J. P. Singh, M. G. Larson, H. Tsuji, J. C. Evans, C. J. O'Donnell, and D. Levy, "Reduced heart rate variability and new-onset hypertension: insights into pathogenesis of hypertension: the Framingham Heart Study," *Hypertension*, vol. 32, pp. 293-7, 1998.

[124] S. Akselrod, O. Oz, M. Grinberg, and L. Keselbrenner, "Dynamic autonomic response to change of posture investigated by time-dependent heart rate variability among normal and mild-hypertensive adults," *J Auton Nerv Syst*, vol. 64, pp. 33-43, 1997.

[125] J. McClain, C. Hardy, B. Enders, M. Smith, and L. I. Sinoway, "Limb congestion and sympathoexcitation during exercise: implications for congestive heart failure," *J Clin Invest*, vol. 92, pp. 2353-2359, 1993.

[126] M. J. Brown, "The measurement of autonomic function in clinical practice," *J R Coll Physicians Lond*, vol. 21, pp. 206-9, 1987.

[127] T. Wheeler and P. J. Watkins, "Cardiac denervation in diabetes," *Br Med J*, vol. 4, pp. 584-6, 1973.

[128] D. J. Ewing, I. W. Campbell, A. Murray, J. M. Neilson, and B. F. Clarke, "Immediate heart-rate response to standing: simple test for autonomic neuropathy in diabetes," *Br Med J*, vol. 1, pp. 145-7, 1978.

[129] A. B. Levin, "A simple test of cardiac function based upon the heart rate changes induced by the Valsalva maneuver," *Am J Cardiol*, vol. 18, pp. 90-9, 1966.

[130] G. Sundkvist, B. Lilja, and L. O. Almer, "Abnormal diastolic blood pressure and heart rate reactions to tilting in diabetes mellitus," *Diabetologia*, vol. 19, pp. 433-8, 1980.

[131] E. A. Hines and G. E. Brown, "The cold pressor test for measuring the reactibility of the blood pressure: data concerning 571 normal and hypertensive subjects," *Am Heart J*, vol. 11, pp. 1-9, 1936.

[132] D. J. Ewing, J. B. Irving, F. Kerr, J. A. Wildsmith, and B. F. Clarke, "Cardiovascular responses to sustained handgrip in normal subjects and in patients with diabetes mellitus: a test of autonomic function," *Clin Sci Mol Med*, vol. 46, pp. 295-306, 1974.

[133] J. Pumprla, K. Howorka, D. Groves, M. Chester, and J. Nolan, "Functional assessment of heart rate variability: physiological basis and practical applications," *Int J Cardiol*, vol. 84, pp. 1-14, 2002.

[134] S. Akselrod, D. Gordon, F. A. Ubel, D. C. Shannon, A. C. Berger, and R. J. Cohen, "Power spectrum analysis of heart rate fluctuation: a quantitative probe of beat-to-beat cardiovascular control," *Science*, vol. 213, pp. 220-2, 1981.

[135] D. Sigaudo, J. O. Fortrat, A. M. Allevard, A. Maillet, J. M. Cottet-Emard, A. Vouillarmet, R. L. Hughson, G. Gauquelin-Koch, and C. Gharib, "Changes in the sympathetic nervous system induced by 42 days of head-down bed rest," *Am J Physiol*, vol. 274, pp. H1875-84, 1998.

[136] E. Toledo, O. Gurevitz, H. Hod, M. Eldar, and S. Akselrod, "Wavelet analysis of instantaneous heart rate: a study of autonomic control during thrombolysis," *Am J Physiol Regul Integr Comp Physiol*, vol. 284, pp. R1079-91, 2003.

[137] S. J. Shin, W. N. Tapp, S. S. Reisman, and B. H. Natelson, "Assessment of autonomic regulation of heart rate variability by the method of complex demodulation," *IEEE Trans Biomed Eng*, vol. 36, pp. 274-83, 1989.

[138] V. L. Schechtman, K. A. Kluge, and R. M. Harper, "Time domain systems for assessing variation in heart rate," *Med Biol Eng Comput*, vol. 26, pp. 367-373, 1988.

[139] P. Coumel, J. S. Hermida, B. Wennerblom, A. Leenhardt, P. Maisonblanche, and B. Cauchemez, "Heart-Rate-Variability in Left-Ventricular Hypertrophy and Heart-Failure, and the Effects of Beta-Blockade - a Non-Spectral Analysis of Heart-Rate-Variability in the Frequency-Domain and in the Time Domain," *European Heart Journal*, vol. 12, pp. 412-422, 1991.

[140] R. Vetter, J. M. Vesin, P. Celka, and U. Scherrer, "Observer of the human cardiac sympathetic nerve activity using noncausal blind source separation," *IEEE Trans Biomed Eng*, vol. 46, pp. 322-30, 1999.

[141] M. Kollai and K. Koizumi, "Reciprocal and non-reciprocal action of the vagal and sympathetic nerves innervating the heart," *J Auton Nerv Syst*, vol. 1, pp. 33-52, 1979.

[142] R. Vetter, N. Virag, J. M. Vesin, P. Celka, and U. Scherrer, "Observer of autonomic cardiac outflow based on blind source separation of ECG parameters," *IEEE Trans Biomed Eng*, vol. 47, pp. 578-82, 2000.

[143] T. A. Buckingham, Z. R. Bhutto, E. A. Telfer, and J. Zbilut, "Differences in Corrected Qt Intervals at Minimal and Maximal Heart-Rate May Identify Patients at Risk for Torsades-De-Pointes During Treatment with Antiarrhythmic Drugs," *Journal of Cardiovascular Electrophysiology*, vol. 5, pp. 408-411, 1994.

[144] S. Guzzetti, S. Mezzetti, R. Magatelli, A. Porta, G. De Angelis, G. Rovelli, and A. Malliani, "Linear and non-linear 24 h heart rate variability in chronic heart failure," *Auton Neurosci*, vol. 86, pp. 114-9, 2000.

[145] S. Kagiyama, A. Tsukashima, I. Abe, S. Fujishima, S. Ohmori, U. Onaka, Y. Ohya, K. Fujii, T. Tsuchihashi, and M. Fujishima, "Chaos and spectral analyses of heart rate variability during head-up tilting in essential hypertension," *Journal of the Autonomic Nervous System*, vol. 76, pp. 153-158, 1999.

[146] V. Z. Marmarelis, K. H. Chon, N. H. Holstein-Rathlou, and D. J. Marsh, "Nonlinear analysis of renal autoregulation in rats using principal dynamic modes," *Ann Biomed Eng*, vol. 27, pp. 23-31, 1999.

[147] V. Z. Marmarelis, "Modeling methodology for nonlinear physiological systems," *Ann Biomed Eng*, vol. 25, pp. 239-51, 1997.

[148] J. K. Triedman, M. H. Perrott, R. J. Cohen, and J. P. Saul, "Respiratory sinus arrhythmia: time domain characterization using autoregressive moving average analysis," *Am J Physiol*, vol. 268, pp. H2232-8, 1995.

[149] G. B. Moody, R. G. Mark, A. Zoccola, and S. Mantero, "Derivation of respiratory signals from multi-lead ECGs," *Computers in Cardiology*, vol. 12, pp. 113-116, 1985.

[150] J. Felblinger and C. Boesch, "Amplitude demodulation of the electrocardiogram signal (ECG) for respiration monitoring and compensation during MR examinations," *Magn Reson Med*, vol. 38, pp. 129-36, 1997.

[151] A. M. Bianchi, G. D. Pinna, M. Croce, R. Maestri, M. T. La Rovere, and S. Cerutti, "Estimation of the respiratory activity from orthogonal ECG leads," *Computers in Cardiology*, vol. 30, pp. 85-88, 2003.

[152] B. W. Hyndman and R. K. Mohn, "A model of the cardiac pacemaker and its use in decoding the information content of cardiac intervals," *Automedica*, vol. 1, pp. 239-252, 1975.

[153] E. Pyetan and S. Akselrod, "Do the high-frequency indexes of HRV provide a faithful assessment of cardiac vagal tone? A critical theoretical evaluation," *IEEE Trans Biomed Eng*, vol. 50, pp. 777-83, 2003.

[154] H. W. Chiu and T. Kao, "A mathematical model for autonomic control of heart rate variation," *IEEE Eng Med Biol Mag*, vol. 20, pp. 69-76, 2001.

[155] E. Pyetan, E. Toledo, O. Zoran, and S. Akselrod, "Parametric description of cardiac vagal control," *Auton Neurosci*, vol. 109, pp. 42-52, 2003.

[156] G. B. Moody and R. G. Mark, "A database to support development and evaluation of intelligent intensive care monitoring," *Computers in Cardiology*, vol. 23, pp. 657-660, 1996.

[157] A. L. Goldberger, L. A. Amaral, L. Glass, J. M. Hausdorff, P. C. Ivanov, R. G. Mark, J. E. Mietus, G. B. Moody, C. K. Peng, and H. E. Stanley, "PhysioBank, PhysioToolkit, and PhysioNet: components of a new research resource for complex physiologic signals," *Circulation*, vol. 101, pp. E215-20, 2000.

[158] M. Elstad, K. Toska, K. H. Chon, E. A. Raeder, and R. J. Cohen, "Respiratory sinus arrhythmia: opposite effects on systolic and mean arterial pressure in supine humans," *J Physiol*, vol. 536, pp. 251-9, 2001.

[159] J. F. Sobh, R. M., R. Barbieri, and J. P. Saul, "Database for ECG, arterial blood pressure, and respiration signal analysis: feature extraction, spectral estimation, and parameter quantification," *IEEE-EMBC and CMBEC, Theme4: Signal Processing*, pp. 955-956, 1995.

[160] C. G. Blomqvist and H. L. Stone, "Cardiovascular adjustments to gravitational stress," in *Handbook of Physiology. The Cardiovascular System Peripheral Circulation and Organ Blood Flow*, vol. III. Bethesda, MD: Am. Physiol. Soc, 1983, pp. 1025-1063.

[161] J. B. Charles and C. M. Lathers, "Cardiovascular adaptation to spaceflight," *J Clin Pharmacol*, vol. 31, pp. 1010-23, 1991.

[162] G. Sonnenfeld, "Space flight, microgravity, stress, and immune responses," *Adv Space Res*, vol. 23, pp. 1945-53, 1999.

[163] G. Sonnenfeld, "The immune system in space and microgravity," *Med Sci Sports Exerc*, vol. 34, pp. 2021-7, 2002.

[164] "Vestibular function in microgravity," *Lancet*, vol. 2, pp. 561, 1984.

[165] H. Scherer, U. Brandt, A. H. Clarke, U. Merbold, and R. Parker, "European vestibular experiments on the Spacelab-1 mission: 3. Caloric nystagmus in microgravity," *Exp Brain Res*, vol. 64, pp. 255-63, 1986.

[166] Q. J. Zhang and Y. Q. Bai, "[Psychological issues in manned spaceflight]," *Space Med Med Eng (Beijing)*, vol. 12, pp. 144-8, 1999.

[167] V. I. Gushin, "Problems of psychological control in prolonged spaceflight," *Earth Space Rev*, vol. 4, pp. 28-31, 1995.

[168] J. M. Fritsch-Yelle, J. B. Charles, M. M. Jones, L. A. Beightol, and D. L. Eckberg, "Spaceflight alters autonomic regulation of arterial pressure in humans," *J Appl Physiol*, vol. 77, pp. 1776-83, 1994.

[169] J. M. Fritsch-Yelle, P. A. Whitson, R. L. Bondar, and T. E. Brown, "Subnormal norepinephrine release relates to presyncope in astronauts after spaceflight," *J Appl Physiol*, vol. 81, pp. 2134-41, 1996.

[170] W. E. Thornton, T. P. Moore, and S. L. Pool, "Fluid shifts in weightlessness," *Aviat Space Environ Med*, vol. 58, pp. A86-90, 1987.

[171] D. E. Watenpaugh, J. C. Buckey, L. D. Lane, F. A. Gaffney, B. D. Levine, W. E. Moore, S. J. Wright, and C. G. Blomqvist, "Effects of spaceflight on human calf hemodynamics," *J Appl Physiol*, vol. 90, pp. 1552-8, 2001.

[172] P. C. Johnson, T. B. Driscoll, and A. D. LeBlanc, "Blood volume changes," in *Biomedical Results from Skylab*. Washington, DC: NASA, 1977, pp. 235-241.

[173] C. Drummer, C. Hesse, F. Baisch, P. Norsk, B. Elmann-Larsen, R. Gerzer, and M. Heer, "Water and sodium balances and their relation to body mass changes in microgravity," *Eur J Clin Invest*, vol. 30, pp. 1066-75, 2000.

[174] A. I. Grigoriev, I. A. Popova, and A. S. Ushakov, "Metabolic and hormonal status of crewmembers in short-term spaceflights," *Aviat Space Environ Med*, vol. 58, pp. A121-5, 1987.

[175] J. M. Fritsch-Yelle, U. A. Leuenberger, D. S. D'Aunno, A. C. Rossum, T. E. Brown, M. L. Wood, M. E. Josephson, and A. L. Goldberger, "An episode of ventricular tachycardia during long-duration spaceflight," *Am J Cardiol*, vol. 81, pp. 1391-2, 1998.

[176] D. S. D'Aunno, A. H. Dougherty, H. F. DeBlock, and J. V. Meck, "Effect of short- and long-duration spaceflight on QTc intervals in healthy astronauts," *Am J Cardiol*, vol. 91, pp. 494-7, 2003.

[177] M. W. Bungo, D. J. Goldwater, R. L. Popp, and H. Sandler, "Echocardiographic evaluation of space shuttle crewmembers," *J Appl Physiol*, vol. 62, pp. 278-83, 1987.

[178] D. S. Martin, D. A. South, M. L. Wood, M. W. Bungo, and J. V. Meck, "Comparison of echocardiographic changes after short- and long-duration spaceflight," *Aviat Space Environ Med*, vol. 73, pp. 532-6, 2002.

[179] M. A. Perhonen, F. Franco, L. D. Lane, J. C. Buckey, C. G. Blomqvist, J. E. Zerwekh, R. M. Peshock, P. T. Weatherall, and B. D. Levine, "Cardiac atrophy after bed rest and spaceflight," *J Appl Physiol*, vol. 91, pp. 645-53, 2001.

[180] J. V. Meck, C. J. Reyes, S. A. Perez, A. L. Goldberger, and M. G. Ziegler, "Marked exacerbation of orthostatic intolerance after long- vs. short-duration spaceflight in veteran astronauts," *Psychosom Med*, vol. 63, pp. 865-73, 2001.

[181] P. A. Low, T. L. Opfer-Gehrking, S. C. Textor, E. E. Benarroch, W. K. Shen, R. Schondorf, G. A. Suarez, and T. A. Rummans, "Postural tachycardia syndrome (POTS)," *Neurology*, vol. 45, pp. S19-25, 1995.

[182] D. E. Watenpaugh and A. L. Hargens, "The cardiovascular system in microgravity," in *Handbook of Physiolgoy Environmental Physiology*, vol. I. Bethesda, MD: Am. Physiol. Soc, 1996, pp. 631-674.

[183] C. L. Fischer, P. C. Johnson, and C. A. Berry, "Red blood cell mass and plasma volume changes in manned space flight," *Jama*, vol. 200, pp. 579-83, 1967.

[184] B. D. Levine, J. H. Zuckerman, and J. A. Pawelczyk, "Cardiac atrophy after bed-rest deconditioning: a nonneural mechanism for orthostatic intolerance," *Circulation*, vol. 96, pp. 517-25, 1997.

[185] W. L. Henry, S. E. Epstein, J. M. Griffith, R. E. Goldstein, and D. R. Redwood, "Effect of prolonged space flight on cardiac functions and dimensions," in *Biomedical Results from Skylab*. Greenbelt, MD: NASA, 1977, pp. 366-371.

[186] S. M. Fortney, V. S. Schneider, and J. E. Greenleaf, "The physiology of bed rest," in *Handbook of physiology. Environmental Physiology*, vol. II. Bethesda, MD: Am. Physiol. Soc, 1996, pp. 889-939.

[187] V. A. Convertino, D. F. Doerr, and S. L. Stein, "Changes in size and compliance of the calf after 30 days of simulated microgravity," *J Appl Physiol*, vol. 66, pp. 1509-12, 1989.

[188] J. C. Buckey, L. D. Lane, G. Plath, F. A. Gaffney, F. Baisch, and C. G. Blomqvist, "Effects of head-down tilt for 10 days on the compliance of the leg," *Acta Physiol Scand Suppl*, vol. 144, pp. 53-60, 1992.

[189] L. Beck, F. Baisch, F. A. Gaffney, J. C. Buckey, P. Arbeille, F. Patat, A. D. J. Tenharkel, A. Hillebrecht, H. Schulz, J. M. Karemaker, M. Meyer, and C. G. Blomqvist, "Cardiovascular response to lower body negative pressure before, during, and after ten days head-down tilt bedrest," *Acta Physiol Scand Suppl*, vol. 604, pp. 43-52, 1992.

[190] D. Michikami, A. Kamiya, Q. Fu, J. Cui, H. Usui, S. Atsuta, Y. Niimi, S. Iwase, and T. Mano, "Responses of muscle sympathetic nerve activity to static handgrip exercise after 14 days of exposure to simulated microgravity," *J Gravit Physiol*, vol. 7, pp. P175-6, 2000.

[191] J. W. Hamner and J. A. Taylor, "Automated quantification of sympathetic beat-by-beat activity, independent of signal quality," *J Appl Physiol*, vol. 91, pp. 1199-206, 2001.

[192] P. Sundblad, J. Spaak, and D. Linnarsson, "Haemodynamic and baroreflex responses to whole-body tilting in exercising men before and after 6 weeks of bedrest," *Eur J Appl Physiol*, vol. 82, pp. 397-406, 2000.

[193] M. Pagani, F. Iellamo, D. Lucini, M. Cerchiello, F. Castrucci, P. Pizzinelli, A. Porta, and A. Malliani, "Selective impairment of excitatory pressor responses after prolonged simulated microgravity in humans," *Auton Neurosci*, vol. 91, pp. 85-95, 2001.

[194] V. A. Convertino, D. F. Doerr, D. L. Eckberg, J. M. Fritsch, and J. Vernikos-Danellis, "Head-down bed rest impairs vagal baroreflex responses and provokes orthostatic hypotension," *J Appl Physiol*, vol. 68, pp. 1458-64, 1990.

[195] A. R. Patwardhan, J. M. Evans, M. Berk, K. J. Grande, J. B. Charles, and C. F. Knapp, "Spectral indices of cardiovascular adaptations to short-term simulated microgravity exposure," *Integr Physiol Behav Sci*, vol. 30, pp. 201-14, 1995.

[196] P. J. Lacolley, B. M. Pannier, J. L. Cuche, J. S. Hermida, S. Laurent, P. Maisonblanche, J. L. Duchier, B. I. Levy, and M. E. Safar, "Microgravity and orthostatic intolerance: carotid hemodynamics and peripheral responses," *Am J Physiol*, vol. 264, pp. H588-94, 1993.

[197] D. Sigaudo, J. O. Fortrat, A. Maillet, A. M. Allevard, A. Pavy-Le Traon, R. L. Hughson, A. Guell, C. Gharib, and G. Gauquelin, "Comparison of a 4-day confinement and head-down tilt on endocrine response and cardiovascular variability in humans," *Eur J Appl Physiol Occup Physiol*, vol. 73, pp. 28-37, 1996.

[198] A. Pavy-Le Traon, D. Sigaudo, P. Vasseur, J. O. Fortrat, A. Gèuell, R. L. Hughson, and C. Gharib, "Orthostatic tests after a 4-day confinement or simulated weightlessness," *Clin Physiol*, vol. 17, pp. 41-55, 1997.

[199] A. Pavy-Le Traon, A. M. Allevard, J. O. Fortrat, P. Vasseur, G. Gauquelin, A. Guell, A. Bes, and C. Gharib, "Cardiovascular and hormonal changes induced by a simulation of a lunar mission," *Aviat Space Environ Med*, vol. 68, pp. 829-37, 1997.

[200] K. I. Iwasaki, R. Zhang, J. H. Zuckerman, J. A. Pawelczyk, and B. D. Levine, "Effect of head-down-tilt bed rest and hypovolemia on dynamic regulation of heart rate and blood pressure," *Am J Physiol Regul Integr Comp Physiol*, vol. 279, pp. R2189-99, 2000.

[201] A. P. Traon, D. Sigaudo, P. Vasseur, A. Maillet, J. O. Fortrat, R. L. Hughson, G. Gauquelin-Koch, and C. Gharib, "Cardiovascular responses to orthostatic tests after a 42-day head-down bed-rest," *Eur J Appl Physiol Occup Physiol*, vol. 77, pp. 50-9, 1998.

[202] M. H. Khan, A. R. Kunselman, U. A. Leuenberger, W. R. Davidson, Jr., C. A. Ray, K. S. Gray, C. S. Hogeman, and L. I. Sinoway, "Attenuated sympathetic nerve responses after 24 hours of bed rest," *Am J Physiol Heart Circ Physiol*, vol. 282, pp. H2210-5, 2002.

[203] A. Kamiya, S. Iwase, D. Michikamia, Q. Fua, and T. Mano, "Muscle sympathetic nerve activity during handgrip and post-handgrip muscle ischemia after exposure to simulated microgravity in humans," *Neurosci Lett*, vol. 280, pp. 49-52, 2000.

[204] B. D. Levine, J. A. Pawelczyk, A. C. Ertl, J. F. Cox, J. H. Zuckerman, A. Diedrich, I. Biaggioni, C. A. Ray, M. L. Smith, S. Iwase, M. Saito, Y. Sugiyama, T. Mano, R. Zhang, K. Iwasaki, L. D. Lane, J. C. Buckey, Jr., W. H. Cooke, F. J. Baisch, D. L. Eckberg, and C. G. Blomqvist, "Human muscle sympathetic neural and haemodynamic responses to tilt following spaceflight," *J Physiol*, vol. 538, pp. 331-40, 2002.

[205] J. K. Shoemaker, C. S. Hogeman, U. A. Leuenberger, M. D. Herr, K. Gray, D. H. Silber, and L. I. Sinoway, "Sympathetic discharge and vascular resistance after bed rest," *J Appl Physiol*, vol. 84, pp. 612-7, 1998.

[206] J. F. Cox, K. U. Tahvanainen, T. A. Kuusela, B. D. Levine, W. H. Cooke, T. Mano, S. Iwase, M. Saito, Y. Sugiyama, A. C. Ertl, I. Biaggioni, A. Diedrich, R. M. Robertson, J. H. Zuckerman, L. D. Lane, C. A. Ray, R. J. White, J. A. Pawelczyk, J. C. Buckey, Jr., F. J. Baisch, C. G. Blomqvist, D. Robertson, and D. L. Eckberg, "Influence of microgravity on astronauts' sympathetic and vagal responses to Valsalva's manoeuvre," *J Physiol*, vol. 538, pp. 309-20, 2002.

[207] J. A. Pawelczyk, J. H. Zuckerman, C. G. Blomqvist, and B. D. Levine, "Regulation of muscle sympathetic nerve activity after bed rest deconditioning," *Am J Physiol Heart Circ Physiol*, vol. 280, pp. H2230-9, 2001.

[208] A. Kamiya, S. Iwase, H. Kitazawa, T. Mano, O. L. Vinogradova, and I. B. Kharchenko, "Baroreflex control of muscle sympathetic nerve activity after 120 days of 6 degrees head-down bed rest," *Am J Physiol Regul Integr Comp Physiol*, vol. 278, pp. R445-52, 2000.

[209] D. Sigaudo-Roussel, M. A. Custaud, A. Maillet, A. Gèuell, R. Kaspranski, R. L. Hughson, C. Gharib, and J. O. Fortrat, "Heart rate variability after prolonged spaceflights," *Eur J Appl Physiol*, vol. 86, pp. 258-65, 2002.

[210] C. D. Ramsdell, T. J. Mullen, G. H. Sundby, S. Rostoft, N. Sheynberg, N. Aljuri, M. Maa, R. Mukkamala, D. Sherman, K. Toska, J. Yelle, D. Bloomfield, G. H. Williams, and R. J. Cohen, "Midodrine prevents orthostatic intolerance associated with simulated spaceflight," *J Appl Physiol*, vol. 90, pp. 2245-8, 2001.

[211] B. Rosner, *Fundamentals of Biostatistics*: Duxbury Press, 1995.

[212] J. Spaak, P. Sundblad, and D. Linnarsson, "Impaired pressor response after spaceflight and bed rest: evidence for cardiovascular dysfunction," *Eur J Appl Physiol*, vol. 85, pp. 49-55, 2001.

[213] D. A. Ludwig and V. A. Convertino, "Predicting orthostatic intolerance: physics or physiology?," *Aviat Space Environ Med*, vol. 65, pp. 404-11, 1994.

[214] W. W. Waters, M. G. Ziegler, and J. V. Meck, "Postspaceflight orthostatic hypotension occurs mostly in women and is predicted by low vascular resistance," *J Appl Physiol*, vol. 92, pp. 586-94, 2002.

[215] M. L. Smith, "Mechanisms of vasovagal syncope: relevance to postflight orthostatic intolerance," *J Clin Pharmacol*, vol. 34, pp. 460-5, 1994.

[216] A. L. Mark, "The Bezold-Jarisch reflex revisited: clinical implications of inhibitory reflexes originating in the heart," *J Am Coll Cardiol*, vol. 1, pp. 90-102, 1983.

[217] A. Jarisch and Y. Zotterman, "Depressor reflexes from the heart," *Acta Physiol Scand*, vol. 16, pp. 31-51, 1949.